RESEARCH ON HALIDE SUPERALLOY WINDOWS

Perry A. Miles, et al

Raytheon Company

Prepared for:

Air Force Cambridge Research Laboratories

November 1973

ARPA Order Number

2014

Program Code Number

2D10

Contractor

Raytheon Company

Effective Date of Contract

April 20, 1972

Contract Number

F19628-72-C-0367

Principal Investigator and Phone Number

Dr. Perry A. Miles
(617) 899-8400, Ext. 3765

AFCRL Project Scientist and Phone Number

Dr. John J. Larkin
(617) 861-4956

Contract Expiration Date

October 19, 1973

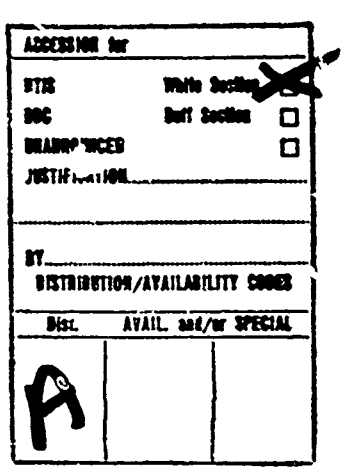

Unclassified
Security Classification

AD-778108

DOCUMENT CONTROL DATA - R&D

(Security classification of title, body of abstract and indexing annotation must be entered when the overall report is classified)

1. ORIGINATING ACTIVITY *(Corporate author)*
Raytheon Research Division
Waltham, Massachusetts 02154

2a. REPORT SECURITY CLASSIFICATION
Unclassified

2b. GROUP

3. REPORT TITLE
RESEARCH ON HALIDE SUPERALLOY WINDOWS

4. DESCRIPTIVE NOTES *(Type of report and inclusive dates)*
Scientific Final 20 April 1972 - 30 October 1973
Approved

5. AUTHOR(S) *(First name, middle initial, last name)*
Perry A. Miles
D. W. Readey
R. T. Newberg

6. REPORT DATE
November 1973

7a. TOTAL NO. OF PAGES
176

7b. NO. OF REFS
31

8a. CONTRACT OR GRANT NO.
F19628-72-C-0307

b. PROJECT, TASK, WORK UNIT NOS.
2014

c. DOD ELEMENT
61101D

d. DOD SUBELEMENT

9a. ORIGINATOR'S REPORT NUMBER(S)
S-1642

9b. OTHER REPORT NO(S) *(Any other numbers that may be assigned this report)*
AFCRL-TR-73-0758

10. DISTRIBUTION STATEMENT
Approved for public release; distribution unlimited.

11. SUPPLEMENTARY NOTES
This research was supported by the Defense Advanced Research Projects Agency.

12. SPONSORING MILITARY ACTIVITY
Air Force Cambridge Research Laboratories (LQ)
L. G. Hanscom Field
Bedford, Massachusetts 01730

13. ABSTRACT The fusion casting of alkali halides has been investigated as a means of preparing polycrystalline materials with optical properties approximating those of the corresponding single crystals. The successful production of highly transparent, low-loss blanks of pure KCl and strontium-doped KCl is described. Strengthening of KCl by solid-solution hardening of single crystals and by grain-size control and solid-solution effects in cast and hot-forged materials has been demonstrated to give yield strengths in excess of 9000 psi. Effects of precipitation on mechanical and optical properties are detailed, along with the effect of reactive gas treatments of optical blanks on their 10.6μm low-loss coefficients. Protective films of As_2S_3 have been deposited with a near intrinsic bulk loss of 1.5 cm^{-1} measured at 10.6μm.

DD FORM 1473 NOV 68

Unclassified
Security Classification

14. KEY WORDS	LINK A		LINK B		LINK C	
	ROLE	WT	ROLE	WT	ROLE	WT
Vacuum-deposited coating						
Alkali halides						
Polycrystalline materials						
Infrared domes						
Infrared windows						
Solid solutions						
Hot forging						
Infrared materials						
Optical coatings						
Protective coatings						
CO_2 laser materials						

ABSTRACT

The fusion casting of alkali halides has been investigated as a means of preparing polycrystalline materials with optical properties approximating those of the corresponding single crystals. The successful production of highly transparent, low-loss blanks of pure KCl by solid-solution hardening of single crystals and by grain-size control and solid-solution effects in cast and hot-forged materials has been demonstrated to give yield strengths in excess of 9000 psi. Effects of precipitation on mechanical and optical properties are detailed, along with the effect of reactive gas treatments of optical blanks on their 10.6μm low-loss coefficients. Protective films of As_2S_3 have been deposited with a near intrinsic bulk loss of 1.5 cm^{-1} measured at 10.6μm.

TECHNICAL PROGRAM SUMMARY

Single crystal alkali halides offer significant promise as high-power infrared laser window materials because of their intrinsically low bulk optical absorption coefficients and small changes of optical path with temperature. However, they are mechanically weak and moisture sensitive. The primary goal of this program has been to investigate strengthening techniques, fabrication processes, and surface protective films for polycrystalline forms of these materials.

The specific objectives are threefold: 1) to investigate casting of polycrystalline halides to produce large, high-quality optical windows, 2) to develop strengthening techniques via grain size control, solid-solution alloying, and precipitation hardening, and 3) to develop low absorption protective and antireflective layers for halide windows.

Emphasis has been placed on $SrCl_2$ alloy additions and the effects of concentration and heat treatment. With high $SrCl_2$ content and proper heat treatment, single crystal yield strengths in excess of 9000 psi have been obtained. Strength values between 4000 and 6000 psi are common. At intermediate annealing temperature, precipitation in the KCl-$SrCl_2$ system leads to a decrease in hardness and strength. In no case can any increase in hardness or strength be attributed to precipitation.

The effects of precipitation on mechanical and optical properties have been investigated. Analysis of the optical scattering at visible wavelengths in the precipitated alloys indicates that precipitation of a second phase in this system contributes very little to the apparent absorption coefficient measured at 10.6μm.

Eight-inch diameter castings were made in a specially designed furnace. By proper baking out of the system and using high purity starting material, as-cast ingots having 10.6μm absorption coefficients below $10^{-3}cm^{-1}$ have been obtained. This is an extremely significant result for three reasons. First, the importance of starting material purity is demonstrated. Second, the use of graphite crucibles and furnace parts does not lead to contamination. An ability to use graphite permits easy low cost, scale-up of the casting

process to larger sizes. Third, and most important, the low optical absorption proves that grain boundaries produced during casting do not contribute to 10.6μm absorption. The cast alloys retain a large amount of residual strain after cooling and this is the major remaining obstacle to their use as laser windows.

Hot forging of polycrystalline cast materials has been carried out successfully and illustrates the feasibility of hot forging ingots after casting to introduce grain size refinement. Although the presence of $SrCl_2$ in the KCl limits the grain size to no smaller than about 20μm, increases in yield strength by a factor of two above those for the as-cast starting ingots have been obtained in hot forged material.

Protective films of As_2S_3 have been deposited with internal loss at 10.6μm is near $1.5 cm^{-1}$. Bulk As_2S_3 has a loss coefficient of approximately $1.4\ cm^{-1}$ and this result must be considered as the state-of-the-art.

A dislocation etching procedure has been developed and used to study residual stresses and polishing damage.

Finally, reactive gas treatment after fabrication has been applied to both single crystal and polycrystalline materials with a resultant decrease in 10.6μm absorption.

PREFACE

The aim of this program has been to create a new class of polycrystalline halide materials with optical clarity approaching that of single crystals with vastly improved mechanical properties. While the development of these materials can make a significant contribution in the general field of wideband infrared optics, the primary consideration has been to provide new materials for use as high power 10.6μm laser systems.

The need for new high power materials has been evident since our observations in 1967 - 1968 of the distortion and fracture of the then available germanium, sodium chloride and potassium chloride windows used at laser power levels above 1 kW. Horrigan's original analysis of failure modes in laser optics and the introduction of figures of merit for window materials, supplemented by new measurements by laser calorimetry of low level absorption, has since led to a much clearer understanding of the relationships between laser window design and performance and the basic mechanical, thermal and optical properties of the window material. The form of any material figure of merit, and the consequent ranking of materials, is to some extent flexible because specific assumptions of the philosophy of mechanical, thermal and optical design and design tolerances must first be made. Sparks et al. have made progressive elaborations on this theme.

In particular, the degradation in optical performance due to thermally induced distortion has been recognized as the most significant problem in present-day materials. In this case, the phase front distortion is proportional to the factor $\beta\chi$, where β is the material bulk loss coefficient and χ measures the temperature dependence of the optical path length. At the same time, an increase in the yield or fracture strength of the material allows the use of thinner window panes and a corresponding reduction in optical path length. Thus, the primary requirements for high power materials are low β, low χ and high strength.

Broadly speaking, there are three groups of materials of immediate interest for high power optics in the infrared region between 3μm and 14μm.

They are alkali halides, alkaline earth fluorides, which are both ionic wideband-gap insulators, and the III-V and II-VI medium group semiconductors. In contrast to the semiconductors, the first two groups of materials are found to have very low γ factors, and in pure materials, comparatively low infrared absorption. In concert, these properties lead to an improvement of performance when used in high power 10.6μm laser systems. The power handling capacity of alkali halides is over an order of magnitude higher than for the II-VI materials.

These considerations led us to propose in mid-1971, a program on polycrystalline alkali halides designed to overcome these obvious drawbacks associated with the use of these materials in a practical laboratory and field environment, namely, their tendency to yield at very low stress levels, their sometimes susceptibility to abrasion and finally their relative high water solubility and low resistance to water damage.

These goals have been largely accomplished as a result of work summarized in this report and in parallel efforts in other laboratories. Various techniques for the extrusion or hot-forging of single crystal ingots have been developed, along with our own casting technique, for the fabrication of large-size polycrystalline ingots. This has been accomplished without any great effect on their optical transparency, although internal porosity or inclusions, in these materials may prohibit their use in laser systems in which optical field intensities approach the breakdown level. While some material strengthening has been accomplished by reductions in grain size, the most significant strengthening has been the result of solid-solution effects, notably by the use of aliovalent additions. As a result, yield strengths in excess of 4000 psi have been achieved in KCl superalloys, as compared to some 250 psi for the single crystal material of two years ago. A corresponding increase in hardness from 10 Knoop to above 20 Knoop has also been achieved. This increase in strength is significant and permits the design of thinner and more durable windows. By comparison to the more common optical glasses, however, the halides are still very soft materials which need protection from impact damage.

Improvements in thin film antireflective layers, including the double layer designs using amorphous arsenic trisulfide specified in our original proposal, have resulted in low absorption, water impervious coatings. These

provide a basic protection against the direct effects of water and humidity and against the minor abrasions from the normal handling and cleaning of optical components. Halide optics, however, are still susceptible to a combination of scratch damage that breaks the coating, followed by water attack. Their use in optics exposed to a rugged field environment is therefore highly questionable. Nevertheless, considerable advances in the state-of-the-art of halide optical materials have been made and halide superalloys should find increasing use in conventional broadband infrared, visible and ultraviolet optical equipment, as well as in internal and laboratory-type high power laser optics.

TABLE OF CONTENTS

TABLE OF CONTENTS (CONT'D)

TABLE OF CONTENTS (CONT'D)

LIST OF ILLUSTRATIONS

LIST OF ILLUSTRATIONS (CONT'D)

LIST OF ILLUSTRATIONS (CONT'D)

LIST OF ILLUSTRATIONS (CONT'D)

LIST OF ILLUSTRATIONS (CONT'D)

LIST OF ILLUSTRATIONS (CONT'D)

LIST OF TABLES

1. INTRODUCTION

The continued progress in the design and realization of laser sources and optical systems, particularly high power infrared lasers operating at 10.6μm, has created the need for improved window and lens materials suitable for use in large, high resolution optical systems. Specifically, these materials must be mechanically strong and scatter-free with absorption coefficients less than $10^{-3}cm^{-1}$. Furthermore, these properties must be achieved in optical blanks whose large size would make difficult their fabrication by conventional fabrication techniques. The basic arguments in favor of the alkali halides as the materials most suitable for high power optics at 10.6μm have now become widely recognized.[1-5] The alkali halides have the double advantage of exhibiting the lowest loss coefficient, β, and the lowest optical distortion of all the various materials under consideration.

The major disadvantages of the pure alkali halides have been their low mechanical strength, the absence of a suitable process for their fabrication into large high quality optical elements, and their sensitivity to water damage.

The goals of this program are threefold: 1) to investigate fusion casting of polycrystalline halides as a fabrication technique; 2) to investigate and compare the effects of grain size, alloy additions and precipitation on strength of polycrystalline halides; and, 3) to develop antireflection and protective coatings for halides. The overall objective is to develop a hardened, protected form of halide by a technique capable of scaling to large sizes, whose absorption and scattering coefficients approach those of pure single crystals.

Fusion casting is an attractive fabrication process because it offers the possibility of obtaining dense, scatter-free, polycrystalline halides and can easily be scaled to large sizes. Conversely, the alkali halides are difficult to cast because of their poor thermal conductivities, and large volume contractions on solidification. We have shown that porosity can be largely eliminated by slow directional vacuum casting. This technique leads to a large

grain size material that is susceptible to cracking, either due to thermal stresses during cooling or to stresses introduced during subsequent fabrication. Accordingly, hot forging of cast halides is also being investigated as a technique to refine the grain size.

Both monovalent and divalent alloy additions lead to increased strength of the alkali halides and both types of alloy additions in this program have been investigated with primary emphasis on divalent additions. Those alloy systems which offered the possibility of precipitation hardening are of major interest for study of its effects on optical properties.

In order to establish base-line strength and optical data for alloy and annealing effects, single crystals of the various compositions were grown. Pure crystals were also grown to investigate the effects of starting materials and purification techniques on the 10.6 μm absorption. Although crystal growth was not a major effort in this program, the data obtained from single crystals provided a standard of comparison for the polycrystalline materials in which grain boundary effects such as segregation or precipitation can be difficult to distinguish from bulk alloy effects.

In addition to low bulk loss, surface loss coefficients below 10^{-3} per surface are needed for components designed for use in high power lasers. Surface loss can be due to both scatter of the incident radiation followed by its absorption and conversion to heat internal to the component and in its immediate surroundings, or by direct absorption in the film itself. Both the form of the halide substrate and the chemical and physical nature of the coating materials are of importance. These problems have been examined only briefly in this program, primarily because the growing size of the ARPA and AFML program on halides made this aspect of our work redundant.

In fact, the common experience is that the apparent bulk absorption coefficients for the materials composing the films is significantly higher than the corresponding values measured on actual bulk samples. Both structural and compositional variations along with contamination by absorptive impurities may be the cause of excess loss. Unfortunately, little definitive data is obtainable from commercial coating houses who are reluctant to release even the most elemental information on specific coatings and who usually avoid the use of As_2S_3.

2. PROGRAM SCOPE

A. Strengthening Techniques

1. Grain size effects

Polycrystalline alkali halides should have higher yield strengths than single crystals of the same material, either because of dislocation pileup at grain boundaries or simply because of a limited number of active slip systems. Thus, the yield strength would be expected to increase as the grain size decreases. To reach a yield point of 6000 psi, the level considered desirable in laser window designs, a grain size on the order of five micrometers would be required in alkali halides. To reach 10,000 psi, a grain size of about two micrometers would be necessary, assuming an inverse-square-root dependence of yield strength on grain size.

Fracture in polycrystalline materials which undergo a small amount of plastic deformation as single crystals can be initiated also by crack nuclei produced by plastic flow. Analysis of this mechanism also leads to an inverse square root dependence of fracture strength on grain size. It is expected, therefore, that both the yield and fracture strengths of the alkali halides can be increased significantly by producing fine-grain polycrystalline materials. However, the practical difficulties associated with obtaining a sufficiently small and uniform grain size in a large piece to produce the necessary yield strength are quite severe. Therefore, other strengthening mechanisms have also been investigated in this program.

2. Solid solution strengthening

Another extremely important hardening technique, applicable to either single or polycrystalline materials, is solid-solution hardening. As impurities are added to both metals and nonmetals, the yield strength and hardness increase. This effect can be ascribed simply to the spherical distortion of the lattice caused by atoms or ions (or clusters of them) of slightly different size which impede the movement of dislocations that produce plastic deformation.

For concentrated solid solutions on the order several tens of percent, an order-of-magnitude increase in yield strength is expected. For the halides, in particular, yield strengths on the order of 2500 psi have been observed on single crystals of both NaCl-NaBr and KCl-KBr solid solutions. The yield strength of both KCl and NaCl in pure single crystal form is on the order of 250 psi.

In contrast to monovalent impurities in the alkali halides, divalent impurities produce very significant increases in yield stresses at very low concentrations. Large increases in hardness have been observed in Sr^{2+} doped KCl.[6] Several explanations of the strong hardening effect of divalent impurities have been proposed. Several possible mechanisms have been suggested, based on impurity-vacancy dipole pairs interacting with dislocation motion. When a divalent cation substitutes for a monovalent alkali ion in the alkali halides, in order to maintain charge neutrality, a vacancy is formed on an alkali ion site. There is a strong tendency for the divalent impurity and vacancy to form a dipole pair since they are oppositely charged species. These dipoles can impede dislocation motion by the tetragonal distortion produced along the dipole axis.[7] Another possible mechanism is that the divalent impurity-vacancy pairs produce an increased drag on jogs in moving dislocations, hence impeding dislocation motion. Finally, the reorientation of the dipole pairs in the stress field of the moving dislocations, a process which requires energy and impedes dislocation motion, has been offered as an explanation[8] for the hardening effects of divalent cation impurities in the alkali halides. All of these mechanisms are different on an atomic scale but they all produce the same results; namely, an increase in the observed yield stress.

3. Precipitation alloys

Yield strengths on the order of 15,000 psi have been obtained in KCl-NaCl precipitation hardened alloys.[9] Values as high as 25,000 psi have been measured with NaCl-AgCl alloys.[10] The maximum hardening is obtained when: 1) The crystal lattices of the two phases are coherent; 2) the second phase particles are small; and 3) the volume fraction of the second phase is large. In the case of both the KCl-NaCl and AgCl-NaCl alloys, the maximum hardness

is achieved around the 50 m/o composition. However, it is impossible to cool the 50 m/o KCl-NaCl alloys rapidly enough to maintain the solution state at room temperature. Precipitation occurs quickly and the precipitate particles rapidly grow to a size sufficient to produce an opaque material, making it impossible to control the particle size and degree of precipitation. However, the solution phase in the AgCl-NaCl system can be maintained down to room temperature and the precipitation easily controlled.

The difference in behavior between the two systems can be seen from the following discussion. If spinodal decomposition is not considered, precipitation in the solid state is a nucleation and growth-controlled process. Consider, for example, an alloy which has been solution-treated and quenched to room temperature. Precipitation is brought about during subsequent heat treatment by heating for a certain period of time below the equilibrium phase separation temperature, T_E. The lower the heat treatment temperature below T_E, the greater the thermodynamic driving force for nucleation of the second phase and the higher the nucleation rate. However, growth of the second phase particles, whether coherent or incoherent, is determined by solid-state diffusion in the matrix. The lower the temperature, the slower the diffusion. Therefore, at low temperature, the rate of precipitation is controlled by diffusion and is slow. At high temperatures, just below T_E, the diffusion rate is high but the nucleation rate is low due to a smaller driving force. Hence, at high temperatures, the rate of precipitation is also slow since the nucleation rate is now controlling. At some intermediate temperature, both diffusion and nucleation are relatively rapid and a maximum rate of precipitation occurs.

These effects produce the characteristic c-shaped time-temperature-transformation curve of a solid state nucleation and growth process. The location of this curve in the temperature-time plane is also strongly dependent on the composition of the alloy since T_E increases or decreases as the concentration of the solute varies. The higher T_E, the more difficult it is to obtain the alloy in the solid solution state at room temperature. As a result, KCl-NaCl alloys with $T_E \approx 500°C$ are virtually impossible to quench without precipitation while the NaCl-AgCl alloys which have an equilibrium phase separation temperature around 200°C, can easily be quenched to room temperature. Therefore, in order to investigate precipitation effects, alloys

should be studied which have a low or controlled phase separation temperature so that the alloy may be quenched to room temperature and subsequently precipitation annealed.

In general, the maximum strengthening effect is obtained in metal systems when the precipitate size is small, on the order of a few hundred angstroms, and coherent with the matrix lattice. Since the wavelength of interest is 10.6μm and optical scattering is proportional to the ratio of the particle size to the wavelength to the fourth power (Rayleigh scattering), one expects negligible effects at 10.6 μm if the precipitate size can be kept small. In fact, analysis of scatter data taken on our precipitated halide alloys bear out this prediction.

B. Alloys Investigated

For the primary components in our study we have concentrated on potassium halides rather than sodium compounds since they[2] have lower intrinsic bulk absorption at 10.6μm. Furthermore, in light of the preceding discussion, the KCl-KBr-KI ternary system offers several distinct advantages from a thermodynamic point of view for monovalent alloying. Although not all of the details of this ternary system have been worked out, the proposed phase diagram has been constructed from available phase equilibrium[11] data and is shown in Fig. II-1. From data on the three binary systems and on the liquidus of the ternary, a ternary miscibility gap certainly must exist and may even extend over to the KCl-KBr and KBr-KI binaries. Therefore, an alloy of composition X having a melting point near 670°C can be cooled to room temperature and maintained in the solid solution state if the equilibrium phase separation temperature, T_E, is sufficiently low. Subsequent heat treatment at a temperature, T_H, somewhat below T_E, will cause separation into two phases of compositions X' and X'' producing a precipitation hardened material. The existence of such a ternary miscibility gap has the advantage that the composition, X, may be chosen so that the equilibrium temperature T_E is sufficiently low to allow the solid to be maintained in the solution state as it cools from the melt.

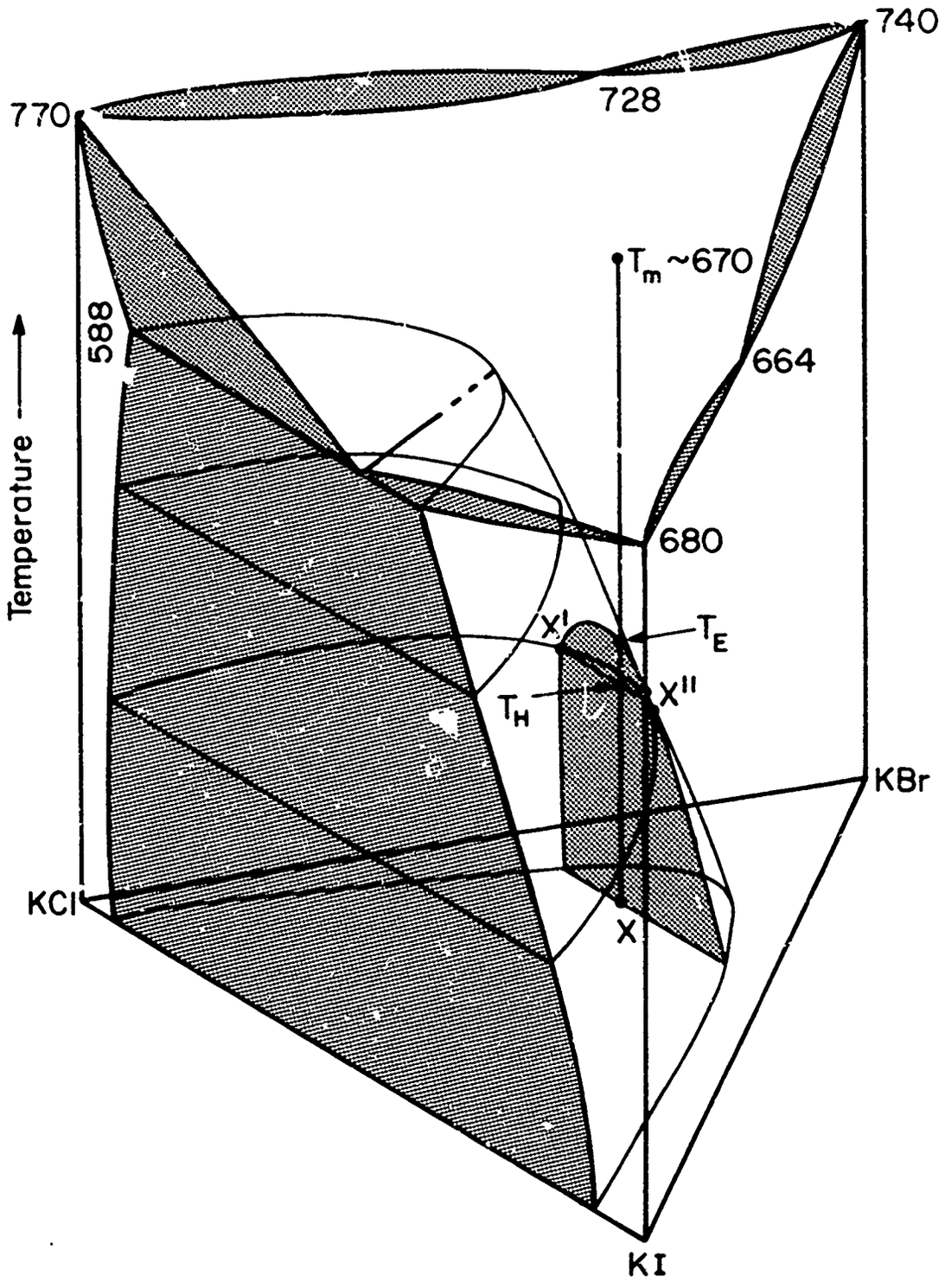

Fig. II-1 KCl-KBr-KI Ternary Phase Diagram Derived from Ref. 11.

As can be seen from Fig. II-1, the KCl-KI system also offers the possibility of investigating precipitation effects as there is limited solubility at each end member of the binary. Finally, since we are investigating casting as the primary fabrication process, the congruently melting compositions in the KCl-KBr and KI-KBr binaries provide the possibility of casting alloys without segregation. Furthermore, the minima in the liquidus curves of the two binaries may also extend into the ternary, preventing segregation when freezing a ternary precipitation hardening alloy. Whether or not this is possible depends, of course, on the details of the phase diagram.

As was pointed out, however, a major potential drawback of these KCl-KI-KBr alloys is the fact that large substitutions of anions result in a significant decrease in thermal conductivity, and this complicates the cooling of alloys and results in a material more sensitive to thermal shock. Poor thermal shock was indeed found to be a major limitation to the fabricability of the monovalent alloys and the major effort was actually expended on KCl-$SrCl_2$ alloys.

The large strengthening effects with small additions of such aliovalent impurities produce only a small decrease in thermal conductivity permitting much easier alloy fabrication and handling. Potassium chloride was chosen as the primary host material since it has been better characterized than the other potassium halides, is more readily available with high purity and has a sufficiently low intrinsic absorption at 10.6 μm. Strontium chloride was chosen as the divalent dopant for potassium chloride primarily since its ionic radius is close to K^+ [12] and Sr^{2+}-containing KCl has been reported to have the highest strength of divalent cation-containing KCl [13]. Also, since $SrCl_2$ has limited solubility, precipitation effects could also be studied in this alloy system.

C. Fabrication Processes

1. Casting

We are investigating the casting of polycrystalline halide alloys as the major processing technique in this program. The distinct advantages of casting are: conceptual simplicity; applicability to a wide variety of compositions; relatively rapid fabrication rate; ease of scale up; control of microstructure; uniformity of microstructure; and potential for more random or more favorable crystallographic orientation.

There are difficulties inherent in casting halides, particularly alloys, because of their poor thermal properties and large volume contractions on freezing. Table II-I lists some of the pertinent thermal and casting parameters of the alkali halides and, Fig. II-2 compares the volume contraction of KCl with that of pure aluminum during cooling from melts at about 1000°C to room temperature. KCl over this temperature range undergoes over twice the volume contraction of aluminum, including an almost 25 volume percent volume change during solidification. This behavior is typical of the alkali halides and clearly indicates that careful allowances should be made for melt contraction. In particular, the occurrence of unsolidified regions completely enclosed by solid must be suppressed to prevent the formation of voids. This strongly suggests that the alkali halides should be directionally solidified from the bottom and sides of the mold, leaving free liquid at the top to take up the volume contraction.

Another problem is the occurrence of plastic flow within the solid ingot due to the stresses developed because of thermal gradients. These effects are made more severe by the poor thermal and mechanical properties of the halides. The maximum cooling rate set by this process can be found from the following analysis. For a unit cube of material in contact with the mold wall, the maximum temperature difference between the mold-casting surface and a point one centimeter into the casting is given approximately by

$$\Delta T = \frac{\sigma_{YP}}{\alpha E} \quad , \qquad (2\text{-}1)$$

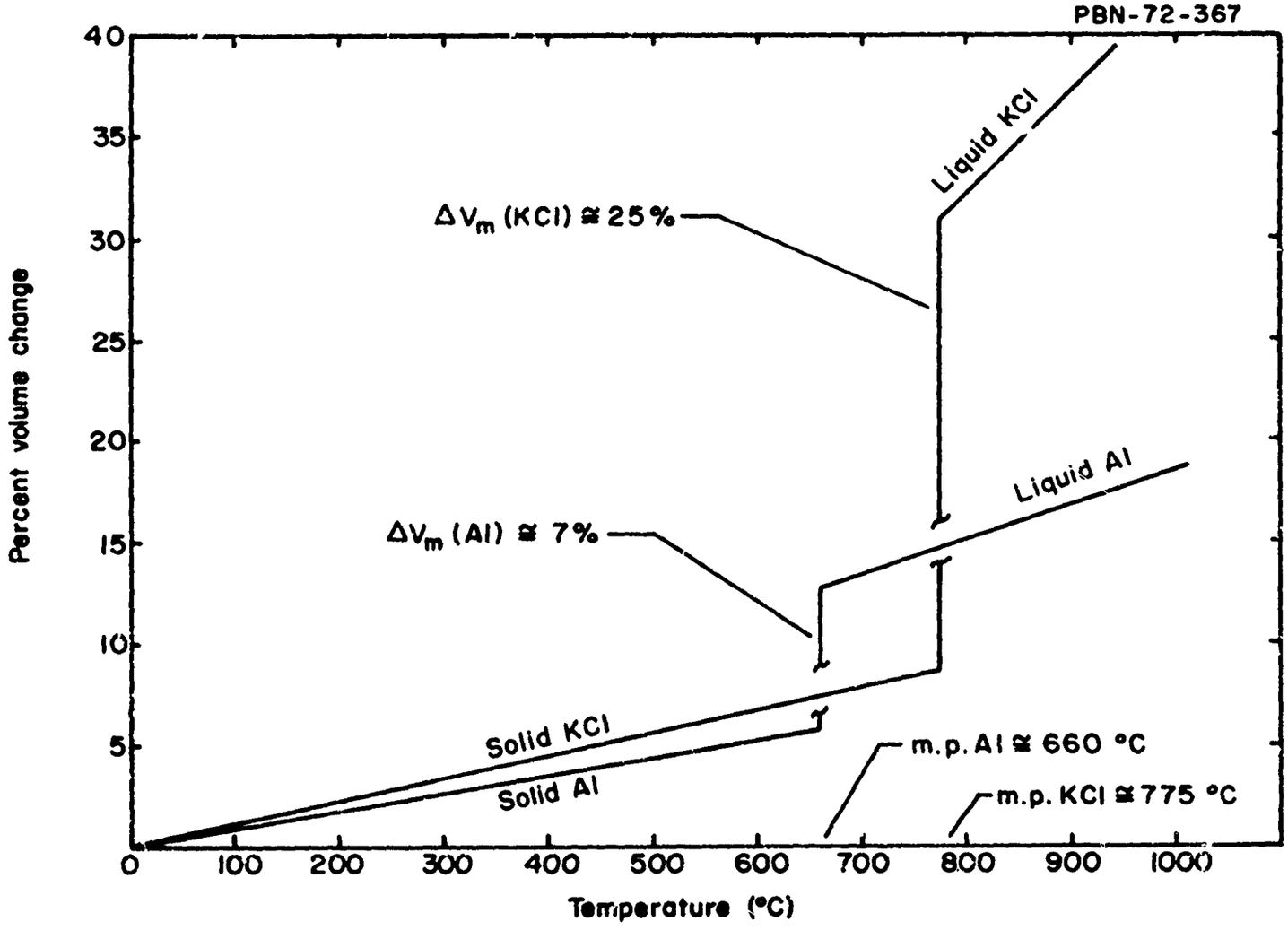

Fig. II-2 Comparison of Volume Contraction of KCl with That of Pure Aluminum During Solidification (Data from Several Sources).

TABLE II-I

Casting Parameters* of Potassium Halides Compared to Aluminum

Material	Thermal Expansion Coefficient ($^{o}C^{-1}$)	Thermal Conductivity (cgs)	Specific Heat (cal/gm)	Melting Point (^{o}C)	Percent ΔV RT - 900°C	Percent ΔV on Melting	Surface Tension (dyn/cm)	Viscosity (centipoise)
KCl	35.5×10^{-6}	0.0167	0.162	770	36.8	21.9	90 (900°C)	0.95 (900°C)
KBr	40×10^{-6}	0.0050	0.104	740	37.4	20.2	73 (900°C)	0.75 (900°C)
KI	40×10^{-6}	-	0.075	680	40.4	20.9	60 (900°C)	1.00 (900°C)
Al	23.9×10^{-6}	0.57	0.215	660	17	7	865 (800°C)	2.5 (800°C)

*Room temperature values unless specified.

Data from various sources

where α is the thermal expansion coefficient, E is Young's modulus and σ_{YP} is the yield point. The heat flux of this unit cube is $\dot{q} = k\Delta T$ where k is the thermal conductivity. The maximum rate of cooling without yield is given by

$$r \cong \frac{\dot{q}}{\rho C_P} = \frac{k\sigma_{YP}}{\alpha E \rho C_P} \quad , \tag{2-2}$$

where ρ is the density and C_P is the specific heat. Inserting the values of the various parameters appropriate for KCl[14] and assuming $\sigma_{YP} \cong 450$ psi, a cooling rate of only 4°C/min is obtained. Clearly this is a very simple model but it indicates the magnitude of the problem of cooling the alkali halides to prevent residual stresses. The only parameter which can be significantly affected in the above expression is σ_{YP}. Therefore, the greater the yield strength of the alloy, the greater the cooling rate at any given temperature which can be permitted without the introduction of residual stresses.

Clearly casting alkali halide alloys, which may include those of the precipitation type, will involve rather complex cooling cycles to prevent both unwanted phase separation and the introduction of residual stresses. For example, Fig. II-3 schematically depicts a possible casting time-temperature cycle designed to cool as rapidly as possible and yet prevent the buildup of severe residual stresses. A rapid cooling rate can be maintained until relatively low temperatures are reached at which point the cooling rate must be decreased to allow any residual stress development caused by thermal gradients to relax. This is particularly important with materials like the alkali halides which do not have five active slip systems at low temperatures. For these materials, according to the Von Mises criterion, the absence of five active slip systems does not allow homogeneous plastic deformation of individual grains. As a result, if any plastic deformation is produced by thermal gradients, stress concentrations at grain boundaries will result. Therefore, cooling through this region of restricted plasticity must be slow as possible to prevent any thermal gradients and attendant deformation. Hopefully, the temperature at which the slower cooling rate is initiated can be kept as low as possible to prevent impractical long cooling times.

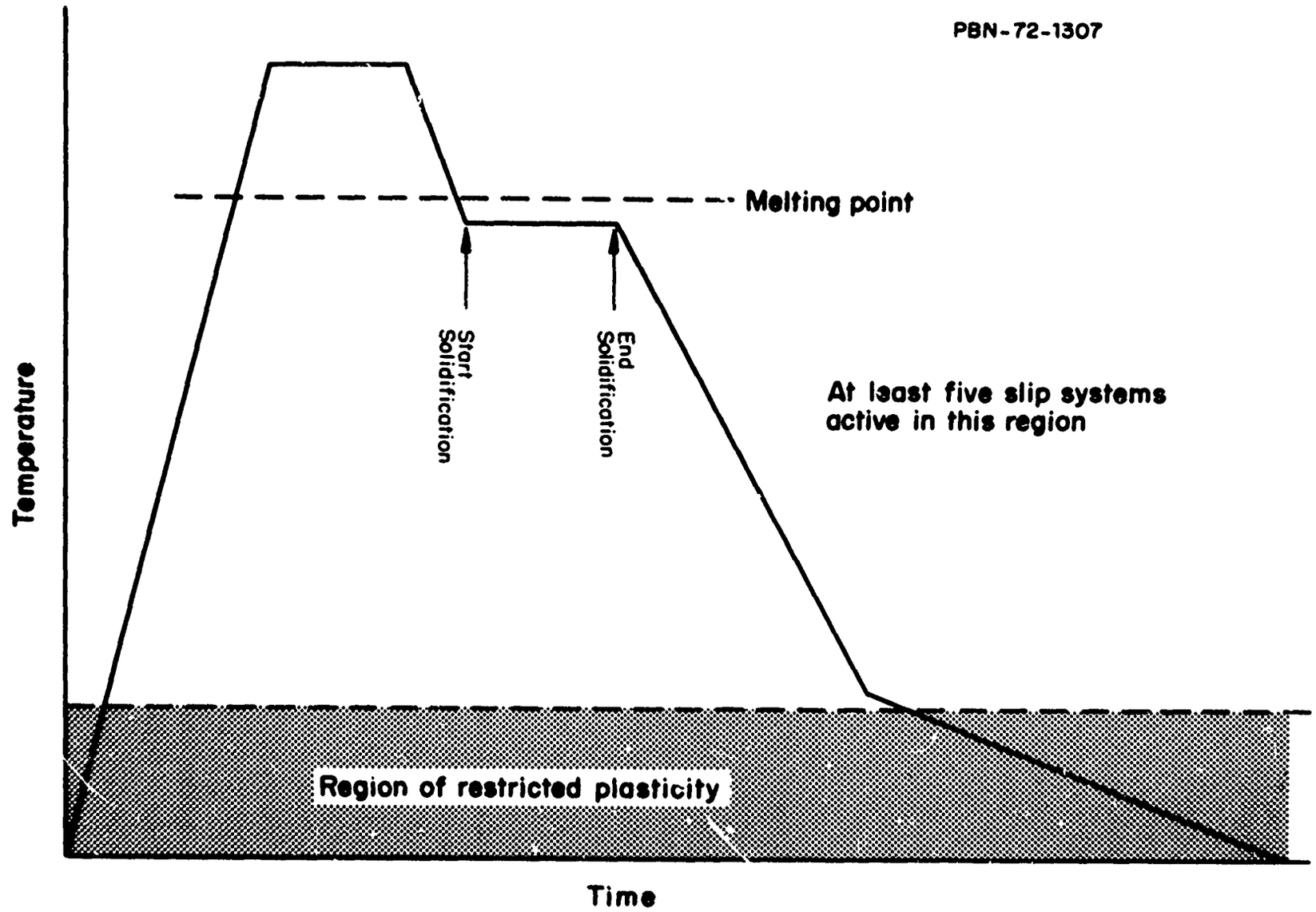

Fig. II-3 Schematic Time-Temperature Schedule Required for Casting Materials Having Regions of Restricted Slip.

There apparently is a significant solubility of gases in melts of alkali halides.[15-16] Although data are not available for all the common gases, dissolved hydrogen chloride (HCl) in particular may reach concentrations as large as 0.001 m/o. If all of this were to be released during solidification of a melt of KCl, the amount of gas at atmospheric pressure would have roughly half the volume of the solid KCl. If only a small fraction of this gas were entrapped as bubbles in the solid, a large number of scattering centers would be produced. This solubility of gases in alkali halide melts even further underlines the need for directional solidification under vacuum.

2. Hot forging

As was pointed out above, directional solidification of alloys is virtually mandatory. This leads to a large columnar grain structure, which although not deleterious from an optical standpoint, is not as mechanically desirable as is a fine-grained equi-axed structure. Therefore, post-casting hot-forging and recrystallization or strain-relief anneal may be an advantage in producing an optimal microstructure and maximum strength. Furthermore, a much finer grain size may be more readily achieved by hot-forging than by casting. By comparing the properties of a fine-grain alloy of a given composition with those of the as-cast material, hot-forging will tell us whether or not a finer grain size should be sought in the casting process. Therefore, we have investigated hot-forging as a means of evaluating the effects of grain size for a given alloy composition and as a possible technique for refining the grain size for a given alloy composition and as a possible technique for refining the grain size of the as-cast material.

We have also hot forged single crystals grown in our laboratory to gain familiarity with the technique, to establish optimum forging parameters for the various alloy compositions, and to provide small grain size material for property comparison with as-cast, cast and forged, and single crystal material. This has provided a means for separating grain size effects from alloying effects.

3. Starting materials and purification

Most of the measurements on optical properties of alkali halides in the

past have been performed on commercially available single crystal materials. The exact purification procedures if any, used, by the single crystal suppliers are not known, although analyses performed on commercially available single crystals indicate that they contain a higher concentration of cation impurities than reagent-grade powders.[17] Only a limited investigation into the effects of starting materials and purification was carried out in this program. The primary effort has been to grow single crystals and fabricate castings using different grades of starting materials. The optical properties of the single crystal or polycrystalline material were then compared with the chemical analysis of the raw material to determine whether any correlations could be made.

D. Protective and Antireflective Layers

The low refractive indices of the alkali halides and alkaline earth fluorides ($n \approx 1.5$), preclude the use of a single layer design for antireflective coatings. Materials with refractive indices greater than 1.5 can be used as single integral half wavelength layer protective coatings, but in this case, the minimum surface reflection achievable is the same as for an uncoated surface, approximately 4 percent per surface.

In theory,[18-21] two layer coatings can be designed to give zero reflectivity for a single wavelength of operation, and a fixed angle of incidence. These designs are appropriate for monochromatic laser optics, but must be improved upon substantially for use in broadband spectral systems. The two layer design, however, introduces considerable flexibility in the choice of film materials, and is likely to be the one chosen for low scatter, low loss optical components for use in high power laser systems.

At normal incidence, the appropriate layer thicknesses, t, are determined by the individual refractive indices according to the relationships:

$$t_{inner} = \frac{\phi_i \lambda}{2\pi \eta_i} \quad ,$$

$$t_{outer} = \frac{\phi_o \lambda}{2\pi \eta_o} \quad ,$$

$$\text{with } \tan^2 \phi_1 = \frac{\eta_i^2 (\eta - 1)(\eta - \eta_o^2)}{(\eta_o^2 \eta - \eta_i^2)(\eta_i^2 - \eta)} \quad ,$$

$$\tan \phi_o = - \frac{\eta_o (\eta_i^2 - \eta)}{\eta_i (\eta_o^2 - \eta)} \tan \phi_i$$

The refractive index choices can be summarized graphically (Fig. II-4), and it becomes clear that several combinations of standard coating materials can be used such as germanium, sulphides, fluorides and oxides. A first approximation to the appropriate layer thicknesses, the spectral sensitivity of the film and the anticipated absorption coefficient of these designs is now available in the computer-solutions tabulated by Loomis.[22] These calculations indicate that optical thickness control to better than 1 percent is required to maintain adequate phase uniformity and reflectance in 10.6μm designs, and that in general, films must be made with bulk loss coefficients below 3.5 cm^{-1} if total film loss is to be kept below 0.1 percent. In practice, the refractive index of a film depends on the deposition process and on the thermal anneal applied, so that any final film design must be evolved by experiment. Furthermore, the apparent bulk absorption coefficient of films can be one or two orders of magnitude higher than the corresponding bulk material. They are presumably dependent on deposition conditions, and again can only be properly assessed by experiment.

At the beginning of this program, the only published work available on coatings for halides as 10.6μm laser components[18] gave two important indications for the requirements for a stable, water resistant coating for the alkali halides. The first necessity is a pore-free layer, and for this, vitreous As_2S_3 proved more suitable than BaF_2 of MgF_2 films which are polycrystalline. The second observation was that under extreme humidity conditions, the protective coatings

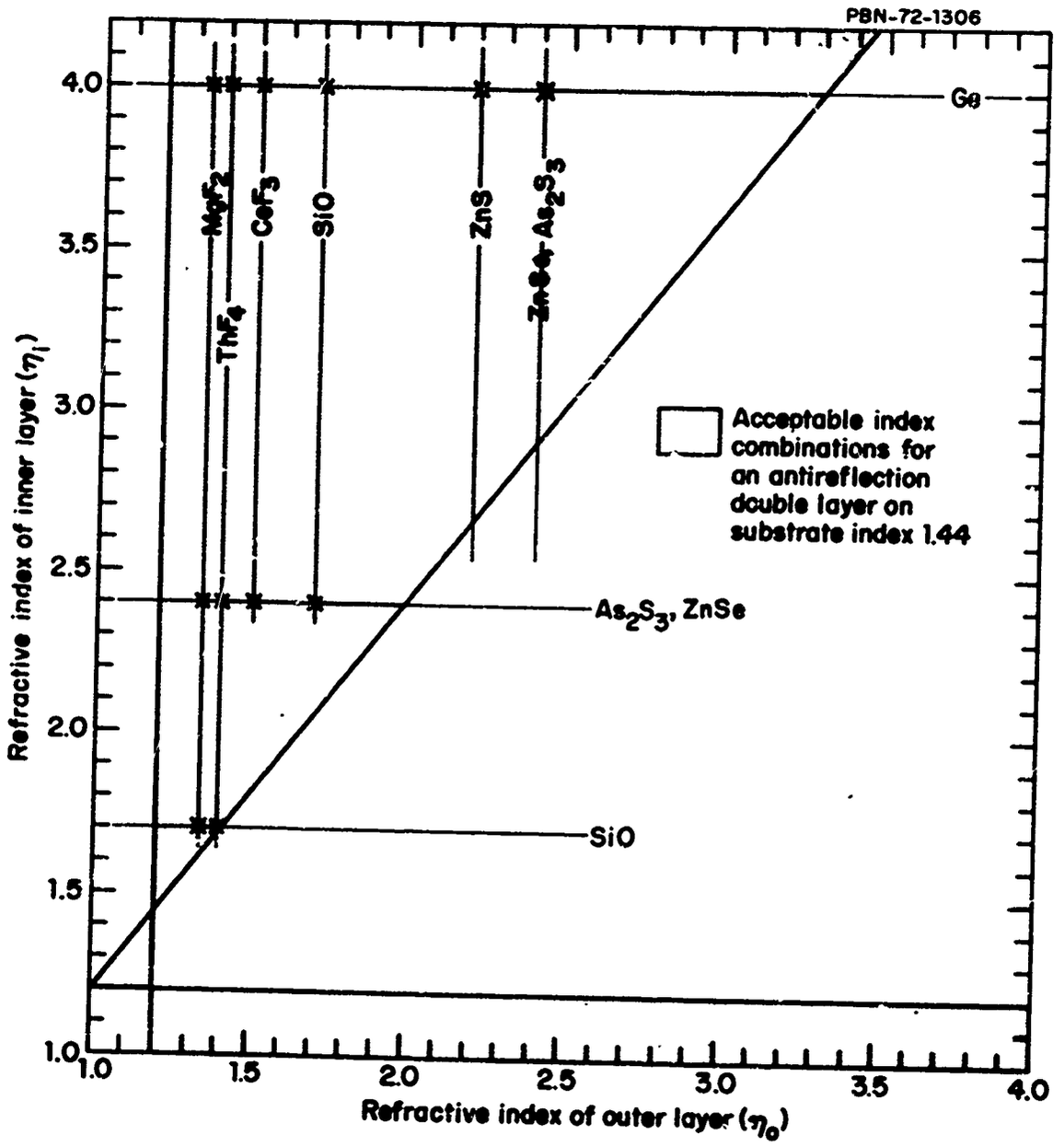

Fig. II-4 Map of Materials Combinations Appropriate for Double-Layer Antireflection Coatings.

finally failed at scratch lines in the underlying halide surface. In absolute terms, a 0.9μm film of As_2S_3 showed no attack after 1 1/2 hours at 100 percent humidity, while a 2.2μm film showed no deterioration after 4000 hours exposed to the atmosphere.

In line with these observations, current attempts to produce low loss, water-proof antireflection coatings for alkali halide and alkaline earth fluorides are based primarily on the use of As_2S_3 or Ge as an impervious, amorphous, high-index layer used in conjunction with a low index fluoride. The films using As_2S_3 are transparent in the long wavelength end of the visible spectrum. If germanium is used as the high index layer, a greater range of choice is allowed in the companion film, although the resultant layer is opaque at visible wavelengths.

Current figures for film loss coefficients[23] indicate that fluoride losses are still excessive. Our own films of As_2S_3, described later in this report, have shown bulk losses near 1.5 cm^{-1}, and are therefore at an acceptable level for a low-loss film design. If a germanium film could be made of corresponding quality, we would have the possibility of a coating that combines two amorphous films that should give a superior resistance to water attack.

The resistance of any of these thin film combinations to physical abrasion, and their adherence to the halide substrate can only be determined by experiment. Furthermore, the resistance of any such film to mechanical damage depends to a large extent on the mechanical properties of the substrate. Any flexibility or tendency to plastic deformation of the substrate greatly increases the forces borne by the film itself, and initiates film fracture. We can expect, therefore, that the hardened halide substrate-film combination will be much more resistant to abrasion and scratch damage than would a soft single crystal-film pair. By implication, it will be useless to characterize the mechanical properties of a film by measurement of films deposited on single crystal substrates - this had best be done on a hard substrate. In this context,

the film adhesion should depend both on the chemical and physical structure of the film and substrate materials and on the chemical and physical cleaning processes applied to the substrate before coating. This wide range of possibilities explains the need for the extended program on halide surfaces and coatings currently being funded by ARPA.

3. EXPERIMENTAL PROCEDURES AND APPARATUS

A. Single Crystal Growth

Single crystals of pure KCl and alloys were grown in our laboratory in a standard induction heated Czochralski apparatus with a platinum crucible in a flowing argon atmosphere. All crystals were seeded with the <100> direction parallel to the growth direction. Typical growth rates varied between 1 and 10 mm/hr. and the resulting crystals were approximately one inch in diameter and three inches long.

B. Casting of Halides

1. Small castings

a. Two-furnace castings

An initial series of experiments was performed with a two-furnace pouring technique in which the starting material was melted in an inert gas in one furnace and then poured into a crucible in the second furnace. The second furnace was then evacuated during solidification of the ingot to ensure removal of dissolved gases. This technique had the advantage of permitting us to investigate the effects of mold temperature on microstructures. However, it had the obvious disadvantage of exposing the molten halide to the atmosphere during transfer between furnaces.

b. Small vacuum casting furnace

To avoid the atmospheric contaminants in the two furnace technique a vacuum casting furnace designed to provide two-inch diameter castings was constructed and is shown schematically in Fig. III-1. The principle of operation of this furnace is as follows. The halide powder starting material is inserted in the inner quartz tube and heated slowly under vacuum. At a temperature just below the melting point, the vacuum valve is closed and the system is brought to atmospheric pressure with an inert gas such as argon. The temperature is then raised and the halide melted. Because of the high surface

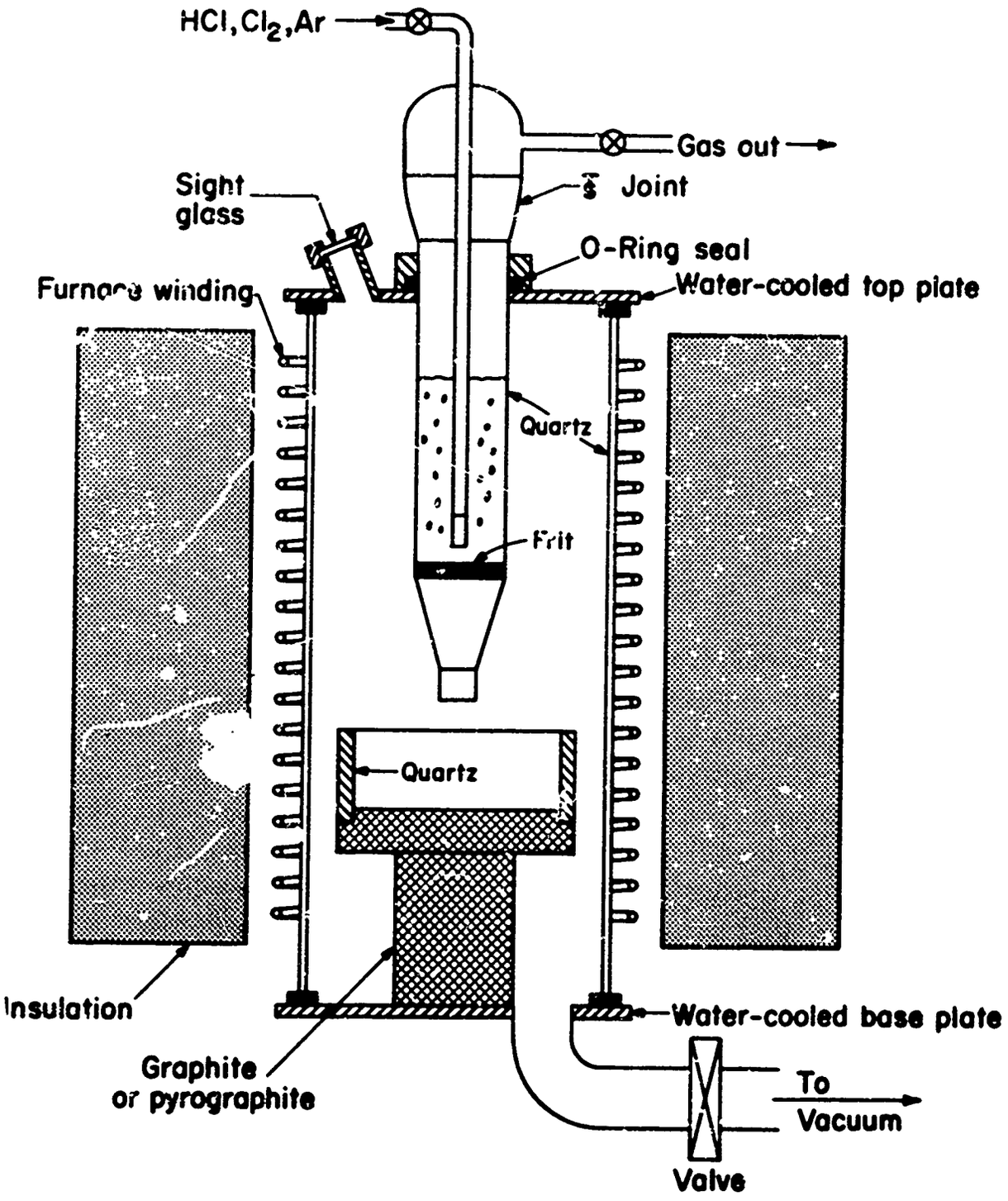

Fig. III-1 Halide Purification and Casting Apparatus.

tension, the molten halide remains on the quartz frit in the inner tube. HCl and Cl_2 could then be bubbled through the molten halide to remove OH^- and O_2. The bubbling of the gas also helps to insure mixing of the molten alloy. After purification is complete, the gas is shut off and the vacuum line reopened. The vacuum pulls the molten halide through the frit into the quartz-graphite mold which, in this drawing, is designed to promote directional solidification of the ingot. A vacuum is maintained during solidification to insure removal of dissolved gases.

The cooling of the molten ingot depends on the configuration of the mold, the position in the furnace, and the cooling rate of the furnace. In such a system, casting and purification can be carried out without exposing the alkali halide to the ambient atmosphere. The furnace is equipped with a controlled temperature drive-down and a vacuum system capable of evacuating the system to 10^{-6} torr. In addition, provision was made to cool the bottom of the crucible with a stream of helium to promote directional solidification of the ingots.

Several problems arose with this furnace design early in the program. First, with the small two-inch diameter castings and the high thermal conductivity graphite crucible, freezing proceeds just as rapidly from the sides of the mold as from the bottom. As a result, only a small volume of controlled, directionally solidified material results in the center of the ingot. Also, major difficulty was experienced in drawing the molten halide through the quartz frit.

Therefore, this furnace was modified for in situ casting using the following procedure. In general, the halide starting material is heated under vacuum to just below the melting temperature. Argon is then allowed into the system until it reaches atmospheric pressure. After the material has melted, a vacuum is drawn and the melt subsequently solidified by a combination of methods, i.e., dropping the crucible out of the hot zone, allowing a flow of nitrogen through the cold finger on which the crucible rests, and turning down furnace power. Most of the castings were performed in grafoil-lined graphite molds to facilitate removal of the ingot from the mold.

Unfortunately, the grafoil also enhances solidification simultaneously from the bottom, sides, and top of the ingot, causing some porosity and a shrinkage pipe, rendering a large fraction of the ingot unusable. However, if a good casting was obtained, a blank at least a one-half inch thick could usually be cut from the bottom of the ingot.

Neither of these furnace designs gave sufficient control over the casting temperature-time cycle requirement for fine grained castings discussed in previous sections. As this discussion indicated, cooling from the solidification temperature should be as rapid as possible to prevent grain growth. At low temperatures, however, the alkali halides do not have the five active slip systems required by the Von Mises criterion for general deformation of the grains. Therefore, the cooling rate must be decreased to prevent stress concentrations and possible cracking, particularly at grain boundaries.

2. Large castings

The deficiencies in the purification and casting furnace were realized during the first quarter of the program and a larger vacuum furnace was designed. This larger, eight inch diameter capability furnace (Fig. III-2) was delivered at the end of the first year of the program. It allowed us to obtain better control over both directional solidification and purity in much larger ingots. A schematic diagram of the two zone furnace is shown in Fig. III-3. The upper chamber is designated the melt zone and the lower chamber the casting zone. The two chambers are connected by means of a 1-inch diameter graphite funnel. The material to be cast is melted in the upper furnace chamber and then poured into the lower chamber by rotating the threaded plunger seal in the bottom of the crucible (Fig. III-4). This plunger is so designed to allow the molten halide to be poured into the mold by a simple rotation rather than by the actual removal of the plunger.

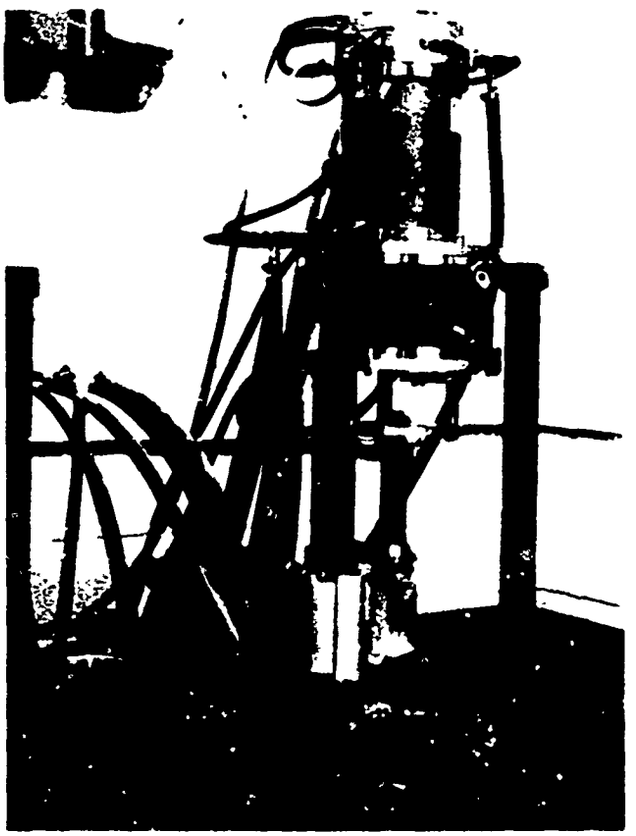

Fig. III-2 Two Zone Casting Furnace.

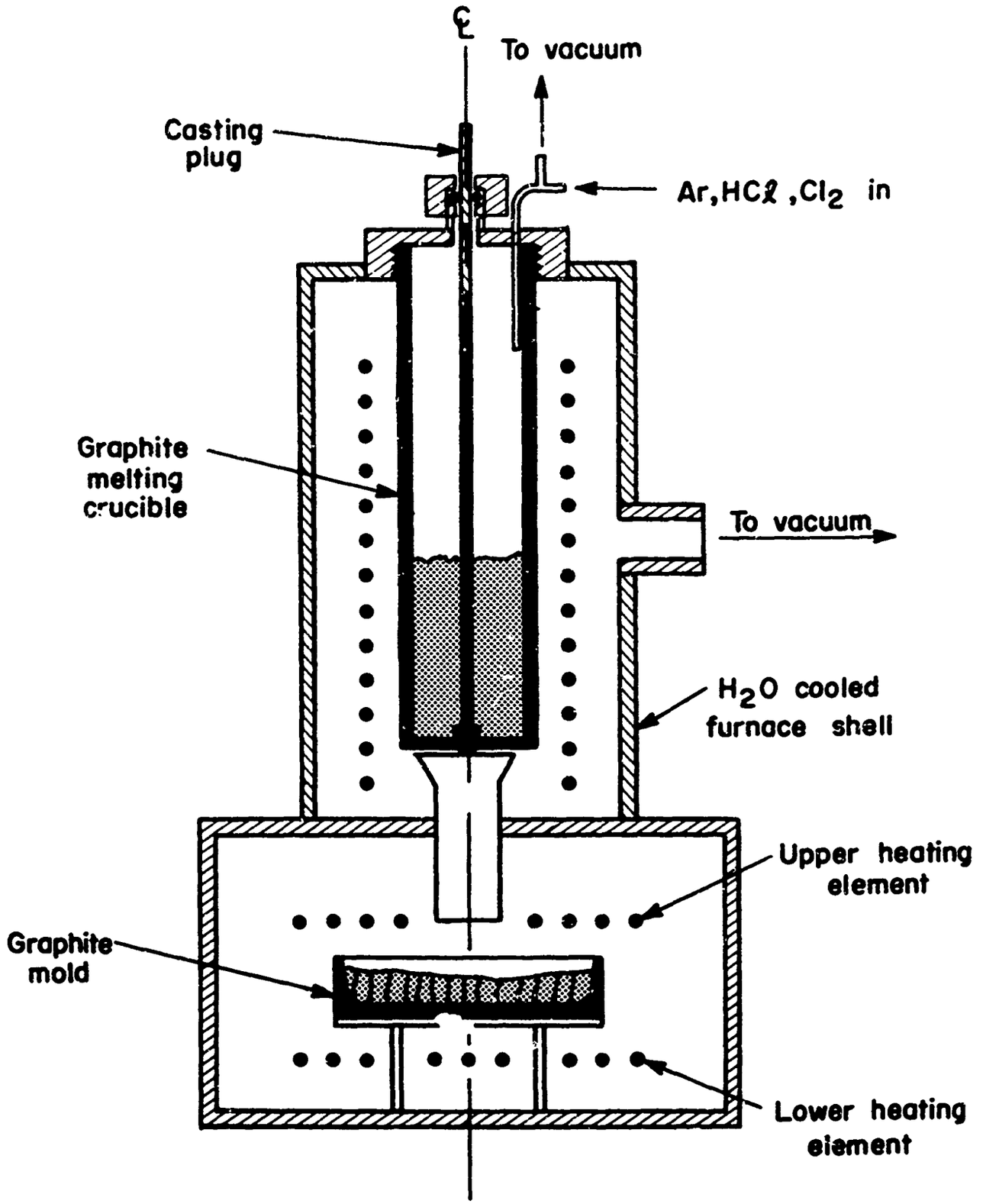

Fig. III-3 Schematic Diagram of Eight Inch Diameter Vacuum Halide Casting Furnace.

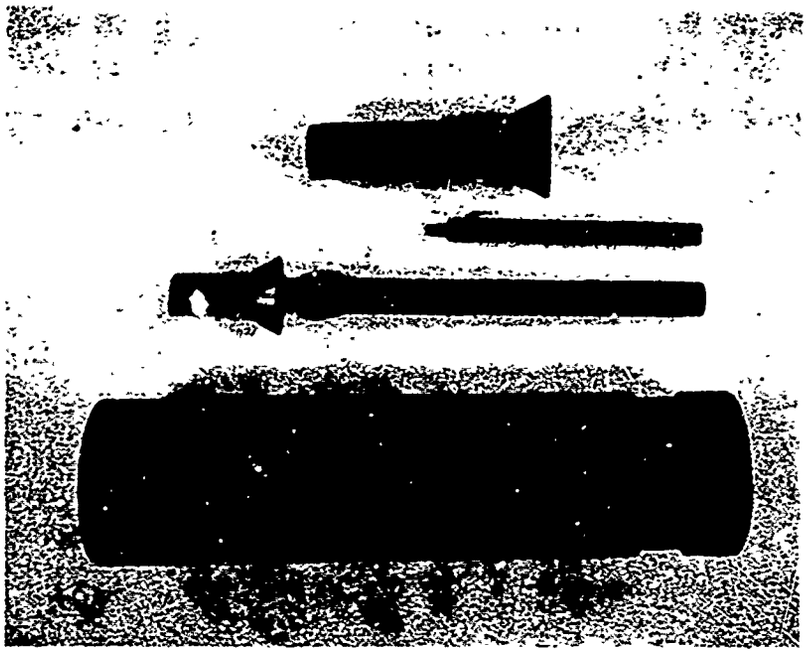

Fig. III-4 Melt Crucible with Threaded Plunger (Two Piece) and Funnel.

Prior to melting, the material is vacuum baked at 300°-400°C until gas evolution ends and a vacuum of about 10μm is realized. This gas evolution is probably water vapor adsorbed on the starting material and the amount evolved seems to depend strongly on the source of the material. The furnace is then back-filled to 1 atmosphere with purified argon and the charge melted. After melting is accomplished, the furnace is evacuated for vacuum degassing of the melt, and the upper melt is poured into the lower zone by turning the threaded plunger and allowing a controlled rate of flow into the lower zone. To avoid rapid vaporization of the melt at high vacuum, a vacuum of about 1 torr is maintained by careful adjustment of argon flow into the furnace.

Unidirectional-solidification is obtained by establishing a thermal gradient in the melt by means of adjusting the power to the bottom element of the casting zone, while maintaining the top element at the desired setting to keep the top of the melt molten until the last stages of solidification. The process of solidification is slow, taking generally 30-45 minutes. Solidification from the sides has remained a problem, but, as predicted, with the larger size it is not serious. With a maximum 1 inch edge effect a successful 6 inch casting can still be obtained by trimming away the edges.

After solidification, the top and bottom of the casting are temperature equalized by adjusting the power to the two elements. After equilibrium is reached, the casting is cooled to room temperature at the desired programmed rate using the Model 5500 Data-Trak programmer. Typical programs used are listed in Table III-1. Listed are the designated program number, the time for one complete program cycle, and the various programmed steps for each program at the various cycle times used.

C. Hot Forging

All hot forgings are unconstrained and have been made using a 30 ton capacity motor driven hydraulic press with a single top moving ram. Compaction of the sample is monitored by a linear displacement transducer. The

TABLE III-1

PROGRAMMED COOLING DATA

Cooling Program Number	Cycle Time (hr)	Program Steps
1	24	a) Cool at 75°C/hr
2	24	a) 1 hr anneal at 315°C b) Cool at 30°C/hr
3	24	a) Cool at 80°C/hr to 240°C b) Cool at 40°C/hr to 120°C c) 4 hr anneal at 120°C d) Cool at 20°C/hr
3	36	a) Cool at 53°C/hr to 240°C b) Cool at 27°C/hr to 120°C c) 6 hr anneal at 120°C d) Cool at 13°C/hr
3	72	a) Cool at 7°C/hr to 240°C b) Cool at °C/hr to 120°C c) 12 hr anneal at 120°C d) Cool at 7°C/hr
3	80	a) Cool at 24°C/hr to 240°C b) Cool at 12°C/hr to 120°C c) 13 1/3 hr anneal at 120°C d) Cool at 6°C/hr
4	24	a) Cool at 15°C/hr
4	72	a) Cool at 5°C/hr

samples to be pressed are placed within a Kanthal element furnace, and rested upon a graphite pedestal. The upper plunger is also made of graphite. It was found that the use of pyrolytic graphite foil ("grafoil") became necessary to prevent cracking of the crystals as they were pressed. This foil is placed on both sides of the sample which is then sandwiched between two pyrographite discs. The compression surfaces of the starting crystals as well as the pryolytic graphite foil are also coated with an air drying graphite emulsion (Dylon AE). This appears to further reduce cracking caused by friction at the die face.

Starting samples are either cleaved or sawed to cross-sectional areas of about one square inch. In preparing the samples for hot forging it became evident that it was necessary for the edges of the sample to be free from cracks to avoid crack propagation during forging. All edges were rounded with 600 grit paper and then water-polished. The sample to be forged is prepared and placed in the furnace as described. Without applying pressure, the temperature is raised to the desired temperature. After soaking at the given temperature for one to three hours, pressure is applied so that an initial strain rate of $1 \times 10^{-2} min^{-1}$ is obtained. After the desired compaction is reached, as determined by the linear displacement transducer output, the furnace is shut down and the pressure removed. Samples are allowed either to furnace cool or are removed from the furnace and allowed to air cool.

D. Property Measurements

1. Microstructure

For observation of microstructure on both hot forged and cast samples, the following polishing and etching technique was used. The samples are first rough polished on 600 grit silicon carbide paper with pure isopropyl alcohol as a coolant. Then a second polish is done with a slurry of 0.3 micrometer alumina in isopropyl alcohol on a polishing cloth. Final mechanical polishing is performed dry on a polishing cloth. A thirty second chemical polish-etch in 3:1 $HCl:H_2O$ [24] is used to develop the microstructure.

2. Hardness and stress-strain behavior

Hardness was determined with a Vickers DPH indenter and a 10g load mounted on a Vickers M-55 metallograph. No attempt was made to orient the indenter with specific crystallographic directions in single crystal samples.

Mechanical property test bars were cut on a nichrome string saw and polished using the polishing procedure described earlier. Yield and fracture strengths were obtained in a three-point bending geometry. All measurements were made on an Instron machine with a variable sample span and a deflection rate of .02 cm/min. All samples were chemically polished immediately prior to testing to eliminate any surface damage which might affect ductility. The sample dimensions were taken after the test to prevent damage.

3. Optical properties

Infrared transmission spectra were obtained on a Perkin Elmer type 457 double beam instrument. A Carey model 14 dual beam recording spectrophotometer was used to measure ultraviolet and visible spectra.

10.6μm absorption coefficients were measured on one of two laser calorimeters in our laboratory which can accurately measure values of β down to $10^{-4}cm^{-1}$.[25] In order to separate surface and bulk effects, the effective absorption coefficient was measured as a function of sample thickness for a given piece of material. The bulk absorption coefficient could then be obtained from the slope of the resulting linear plot.

4. RESULTS

A. General

In the following sections the results of this program are presented. They are arranged in logical order rather than chronologically. That is, the effects of alloying on single-crystal properties (i.e. hardness, strength and optical properties) are presented first to provide baseline data on alloy effects alone. The early single-crystal work indicated that the monovalent alloys were quite difficult to fabricate and handle because of their low thermal conductivities. Therefore, by far the greatest effort was expended on KCl $SrCl_2$ alloys.

Fabrication by casting is then discussed followed by the results of our hot-forging experiments since hot forging was performed on both single-crystal and cast material.

Finally, results of etching studies, reactive gas processing and protective films are presented. Each of these studies are less vitally related to the main emphasis of strengthening and fabrication and each stands alone as a separate study.

B. Single Crystals

1. Single crystal growth

Approximately 75 single crystals were grown during the course of this program. They had the following compositions:

Composition	Number
KCl	17
KCl -$SrCl_2$	49
KCl-KBr	6
KBr-KI	2
KBr-KCl	1

Typical crystals are shown in Fig. IV-1. Reagent grade starting materials were used in most cases. However, in certain crystals higher purity starting materials were used to investigate the effect on optical properties.

A large number of $SrCl_2$-doped crystals were grown to: 1) determine the effects of $SrCl_2$ concentration and heat treatment on mechanical and optical properties and 2) provide single crystal material for hot forging. Nominal $SrCl_2$ concentrations were: 200, 500, 1500, 5000 ppm and 1 and 2 mole percent $SrCl_2$ in KCl.

2. X-ray fluorescence analysis for strontium

In order to provide a basis for comparison of properties of cast, hot forged, and single-crystal $SrCl_2$-doped samples, an accurate knowledge of the actual strontium content in the material is necessary due to the segregation coefficient of strontium chloride in KCl. As a result, X-ray fluorescence analysis was chosen as the most convenient technique available in our laboratory to perform the analysis.

A set of KCl standards with known $SrCl_2$ additions was prepared by mixing KCl and $SrCl_2$ powder, or, for low concentrations, adding a strontium chloride solution of known concentration to KCl powder. The powders were pressed into disks and the SrK_α peak intensity monitored as a function of $SrCl_2$ content. Figure IV-2 shows the results. With the fluorescence technique, $SrCl_2$ concentrations down to about 50 ppm can be detected.

Figures IV-3 through IV-7 give the Sr content found in crystals grown from melts containing 500 ppm, 1500 ppm, 5000 ppm, 1 percent and 2 percent $SrCl_2$ nominal molar concentrations. In all five crystals, about one half of the original melt was used during crystal growth. As expected, the curves clearly indicate that the concentration increases as the melt is depleted. However, two points are worth noting. First, the apparent segregation coefficient increases as the nominal concentration decreases. As a result, the percentage difference in Sr concentration from the start (right hand side of the figures) to the end of the crystal is smaller, the higher the nominal concentration. From

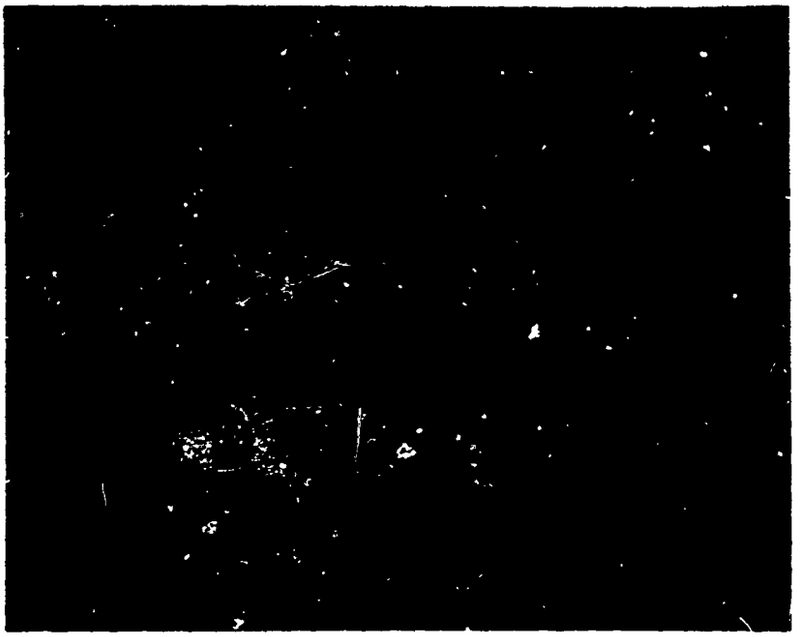

Fig. IV-1 Typical Czochralski Single Crystals.
Top: 1500 ppm-$SrCl_2$; bottom two, 1 percent $SrCl_2$.

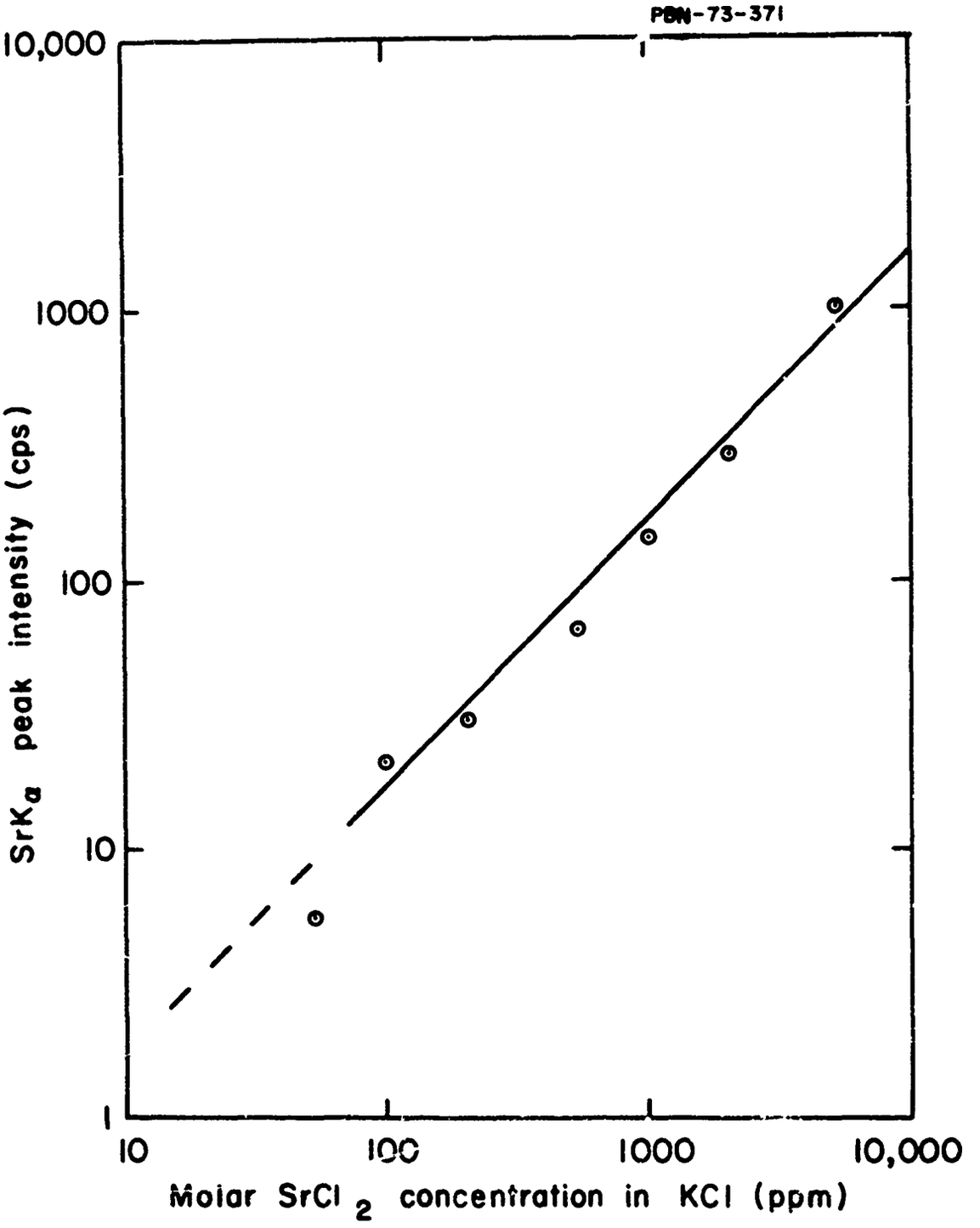

Fig. IV-2 X-Ray Fluorescent Intensity vs Molar Concentration of $SrCl_2$ in KCl.

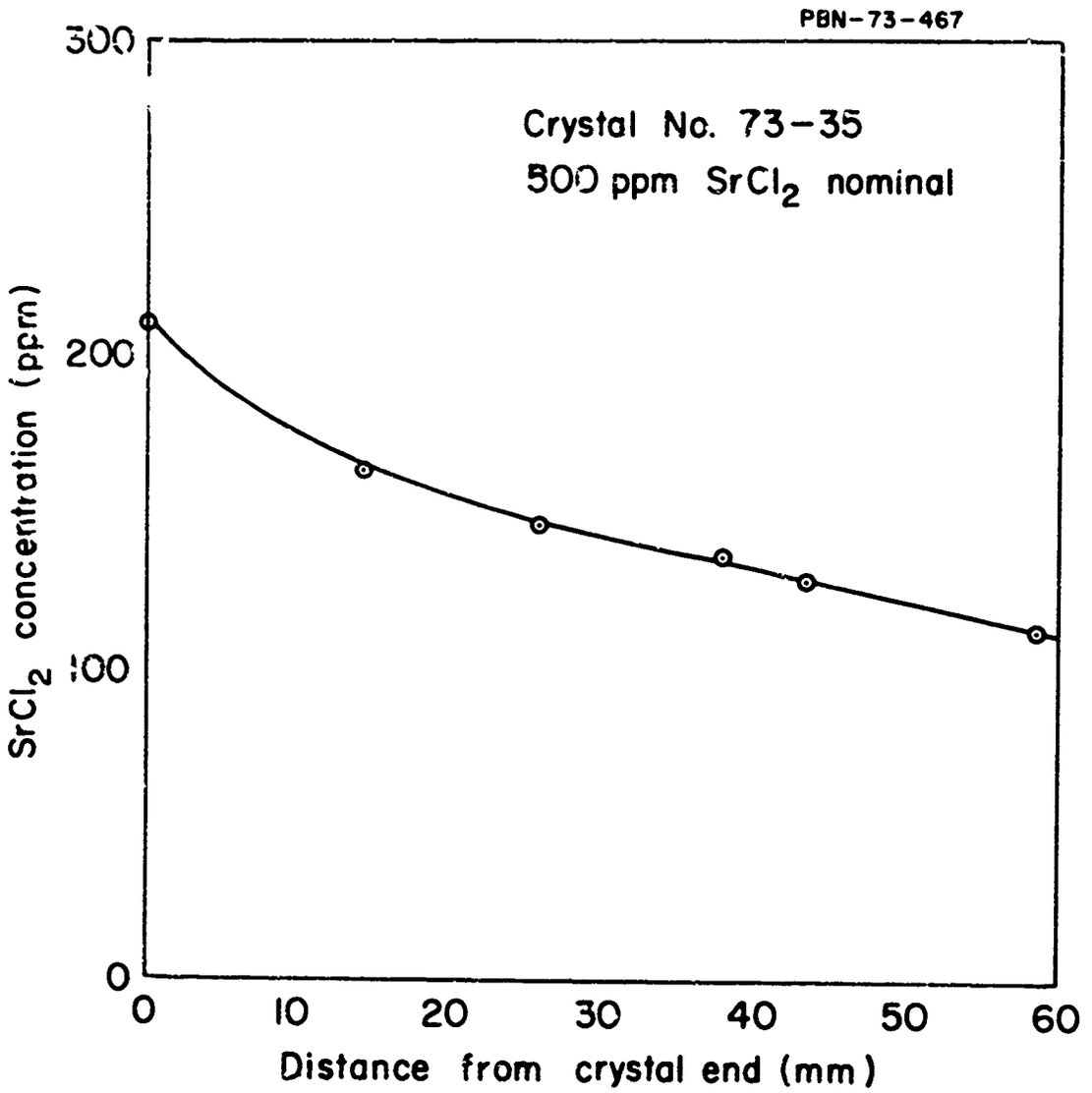

Fig. IV-3 $SrCl_2$ Concentration as Analyzed in Crystal 73-35.

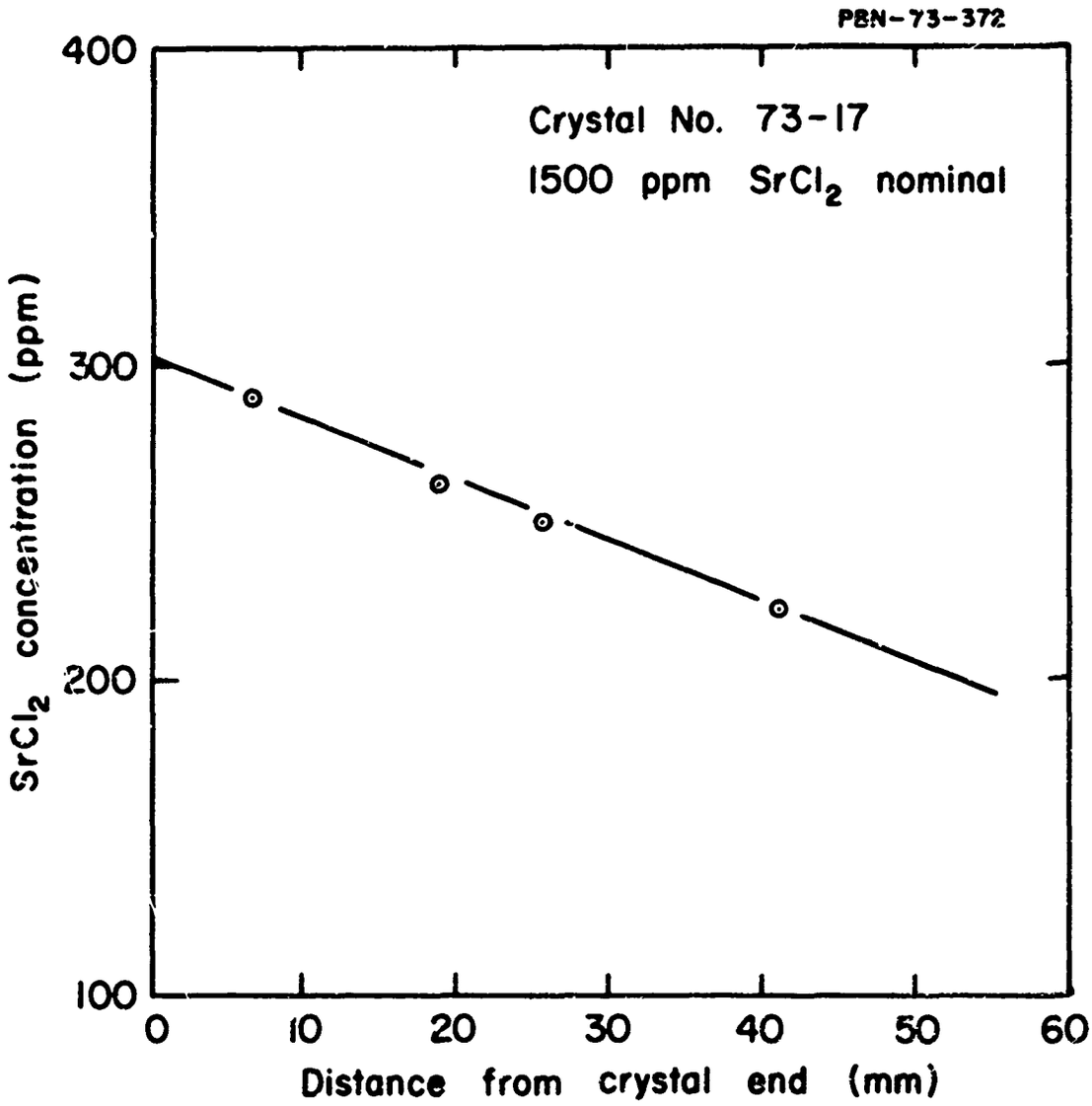

Fig. IV-4 $SrCl_2$ Concentration as Analyzed in Crystal 73-17.

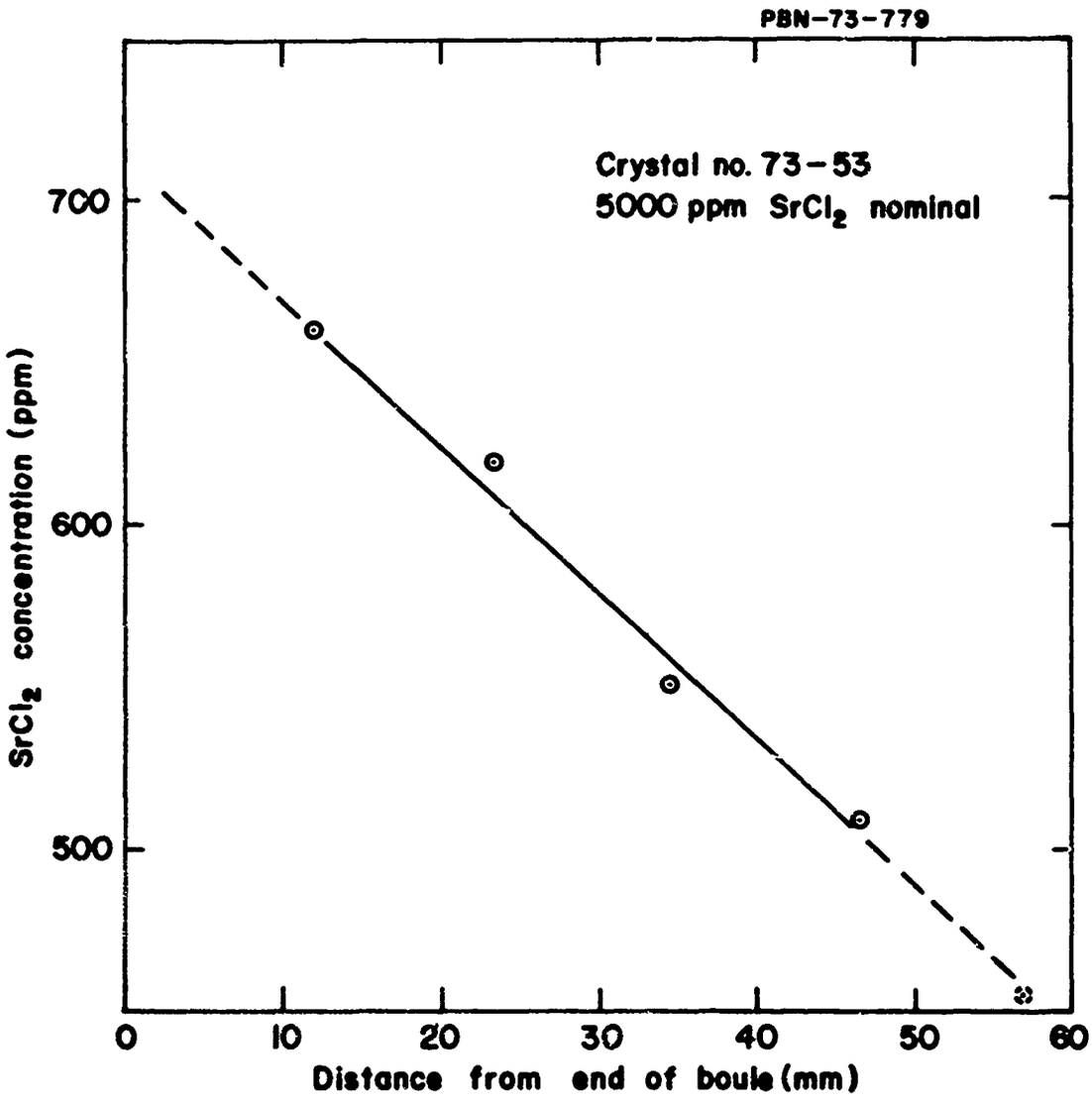

Fig. IV-5 $SrCl_2$ Concentration as Analyzed in Crystal 73-53.

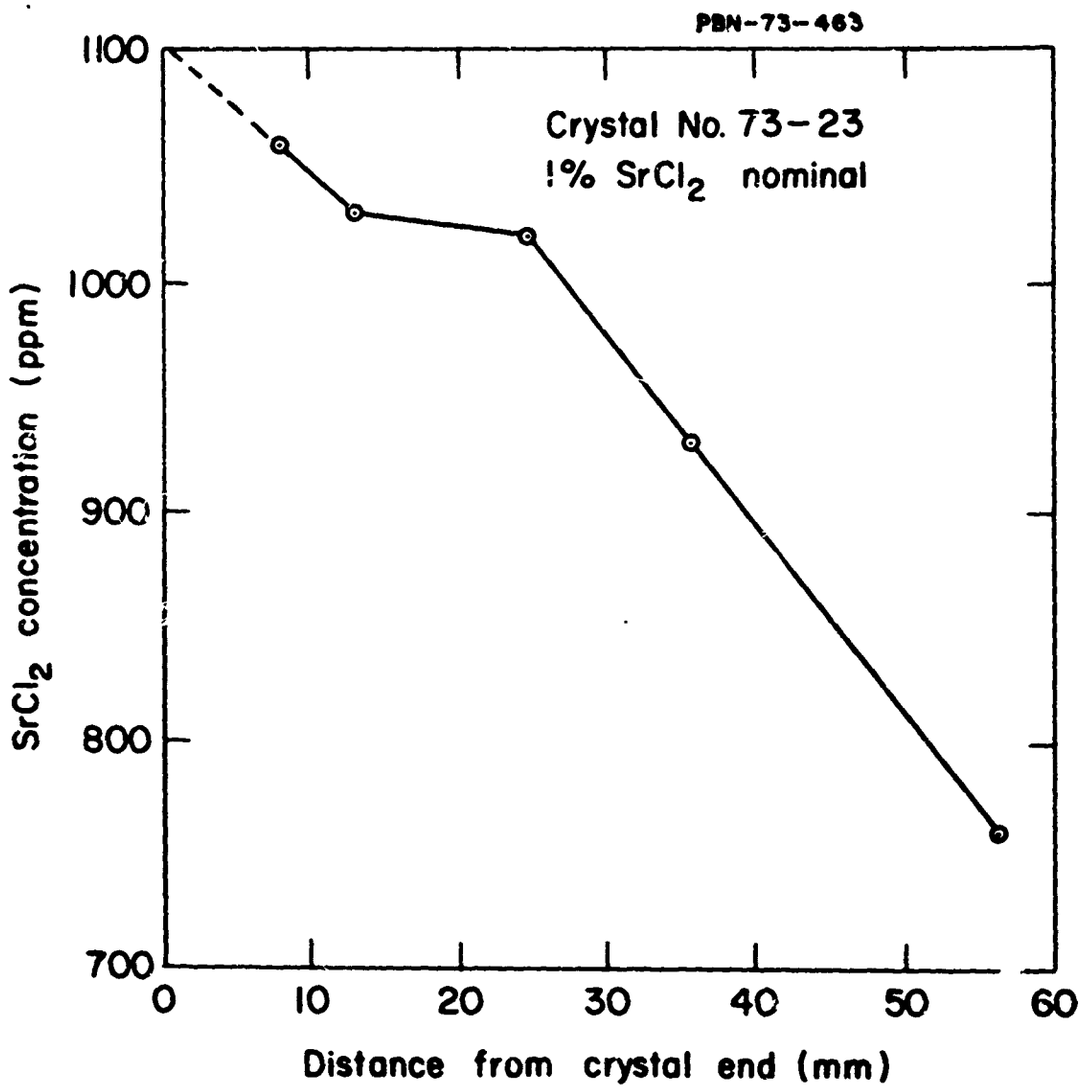

Fig. IV-6 $SrCl_2$ Concentration as Analyzed in Crystal 73-23.

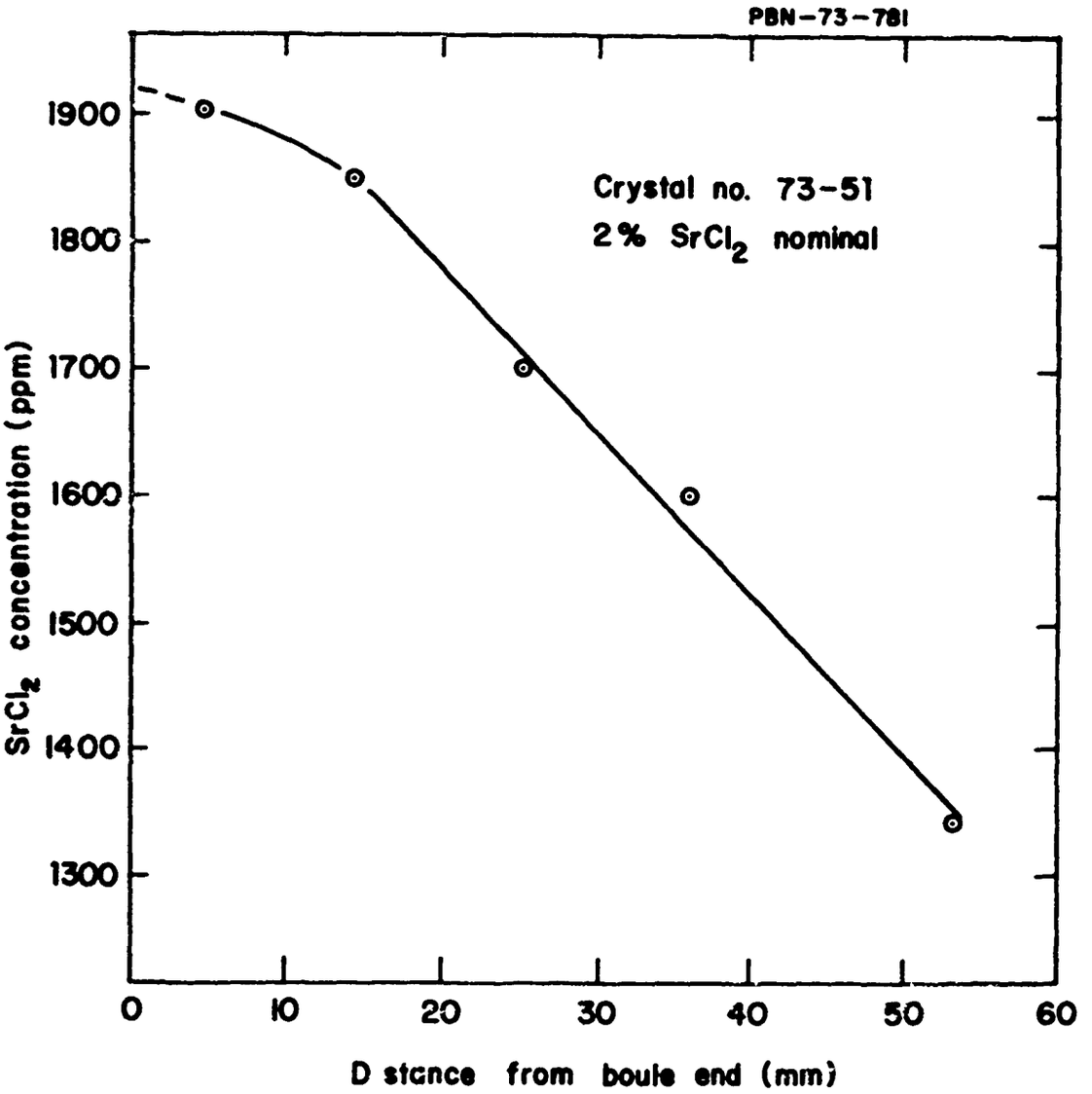

Fig. IV-7 $SrCl_2$ Concentration as Analyzed in Crystal 73-51.

a knowledge of the weights of the crystals grown, we obtained the plot of segregation coefficient versus melt composition (Fig. IV-8). The data clearly indicate a segregation coefficient that decreases with increasing melt concentration.

3. Hardness and mechanical properties

a. Hardness

Table IV-1 lists the hardness of all the various alloys studied. The tabulated hardnesses are for samples solution-treated at 650°C or 700°C. The KCl-KI crystals were heat treated for one hour at various temperatures between 200°C and 700°C with virtually no change in hardness indicating no precipitation effects. The KCl-$SrCl_2$ alloys exhibited precipitation as seen in Fig. IV-9.

The effect of heat treatment and attendant precipitation on the hardness of KCl-$SrCl_2$ alloys was investigated in detail. Figure IV-9 suggests that precipitation kineties might be affected by strain as the precipitated regions in this sample are the most highly strained during quenching from the solution anneal temperature. However, kinetic effects were not studied during this program.

The two main effects studied were: 1) the effect of $SrCl_2$ content in solution on hardness; and 2) the effect of heat treatment temperature on precipitation and hardness. The samples were solution-treated at 650°C or 700°C for 15 minutes and then air quenched. Precipitation anneals were carried out at temperatures of 200, 250, 375, 425 and 500°C for one hour. A minimum of four hardness readings were taken on each sample.

Figure IV-10 is a plot of $H-H_0$ versus actual $SrCl_2$ content as determined by X-ray fluorescence on the solution treated samples. H_0 is the hardness of pure KCl and determined to be $H_0 = 10.5\ kg/mm^2$. These data were also plotted on log-log paper and $H-H_0$ versus the square root of the $SrCl_2$ concentration. In no case was a linear curve obtained. This disagrees with previous results in which $H-H_0$ vs $C^{1/2}$ was found to be linear. However,

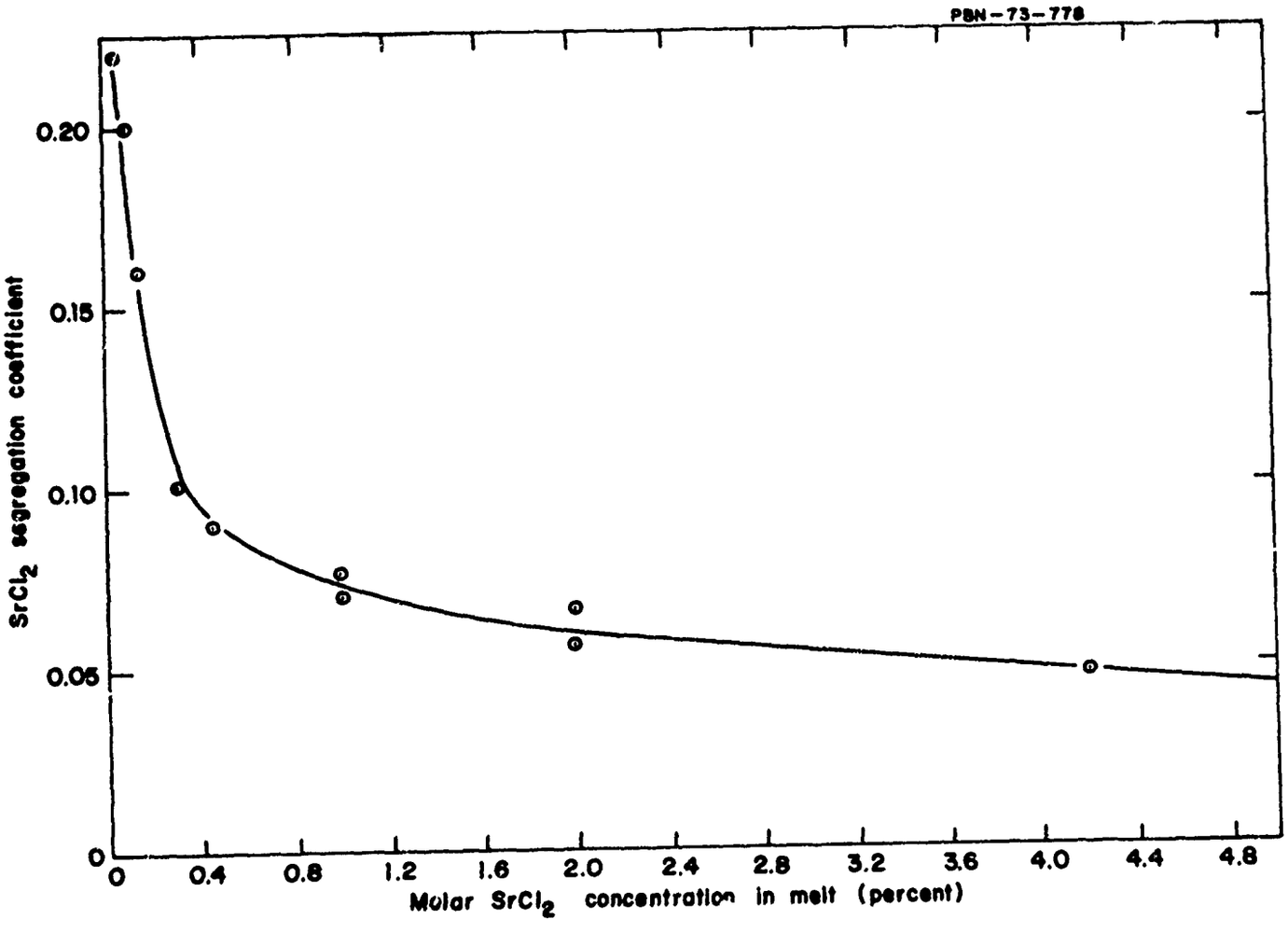

Fig. IV-8 $SrCl_2$ Segregation Coefficient in KCl as a Function of Melt Composition.

TABLE IV-1

VICKERS HARDNESS OF KCl ALLOYS

Composition	Hardness (kg/mm^2)
KCl	10.5
95 m/o KCl-5 m/o KI	15.2
92.5 m/o KCl-7.5 m/o KI	23.8
90 m/o KCl-10 m/o KI	22.8
62 m/o KCl-38 m/o KB2	27.8
KCl-500 ppm $SrCl_2$	12.7
KCl-1500 ppm $SrCl_2$	16.3
KCl - 5000 ppm $SrCl_2$	20.4
KCl - 1 percent $SrCl_2$	22.8
KCl - 2 percent $SrCl_2$	24.1

Note: 1. All compositions are nominal melt compositions
2. All samples were solution treated at 650°C

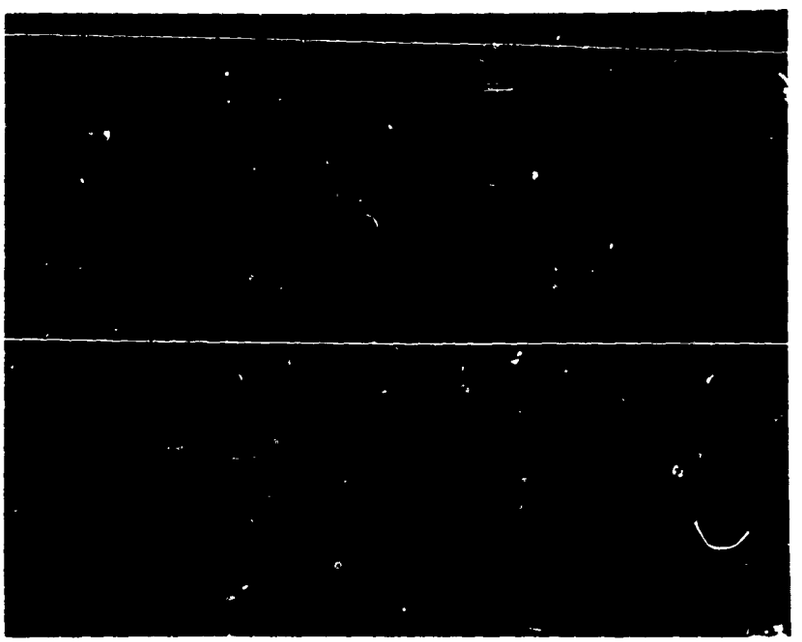

Fig. IV-9 Precipitation Pattern in Single Crystal No. 73-12C. (5000 ppm $SrCl_2$ nominal) Annealed 1 hr. at 375°C.

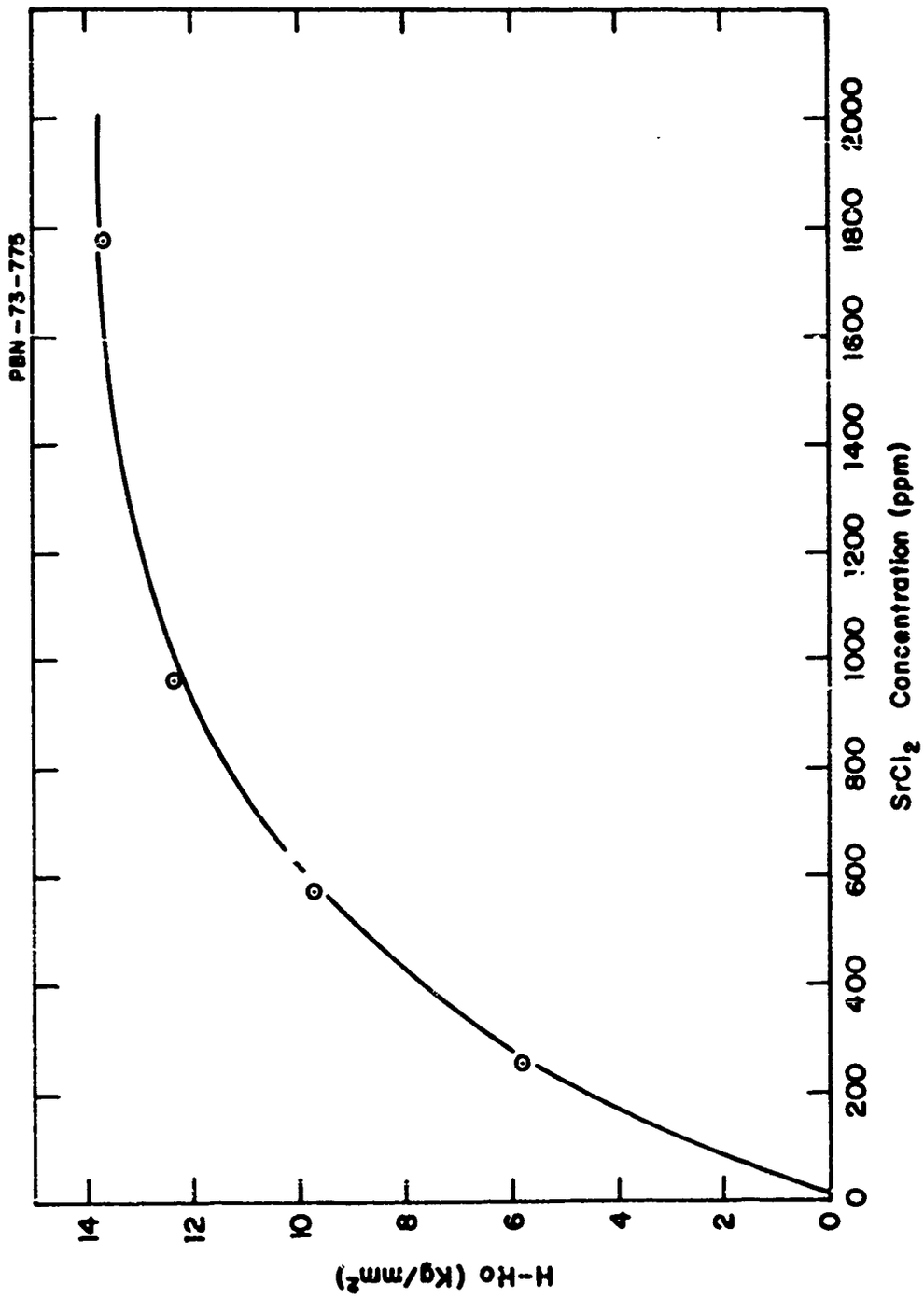

Fig. IV-10 Hardness of Solution-Treated KCl Crystals as a Function of the Analyzed $SrCl_2$ Content (H_0 = 10.5 kg/mm^2).

as will be shown below, the 2 percent nominal $SrCl_2$ crystal has a significant increase in hardness when annealed at 500°C after a prior anneal at 650°C. If the 500°C hardness were used to plot Fig. IV-10, then a reasonable linear dependence on $C^{1/2}$ is obtained. As is briefly discussed below, this increased hardness at 500°C may indicate a greater solid solubility at 500°C that at 650°C. That is, the 650°C anneal for the 2 percent nominal $SrCl_2$ crystal may not have all of the $SrCl_2$ in solid solution. In order to explain this enhanced solubility, rather complex solvus and solidus curves in the KCl-$SrCl_2$ system must be postulated. If a greater solubility at 500°C is accepted, then a square root dependence of hardness on $SrCl_2$ concentration is followed reasonably well. In any event, the hardness of KCl single crystals can be increased by about a factor of 2.5 by the addition of $SrCl_2$.

Figure IV-11 presents the effect of heat treatment temperature and $SrCl_2$ content on hardness. The nominal 500 ppm $SrCl_2$ data were not plotted due to the fact that these hardness values were sufficiently low (11-12 kg/mm^2) that the experimental error (± one half of a hardness number) produced very scattered data from which no conclusions could be reached. However, it is clear from Fig. IV-11 that all the remaining compositions clearly show a significant decrease in hardness at temperatures near 350 to 400°C. These decreases in hardness are associated with the precipitation of a second phase (presumably K_2SrCl_4) as evidenced by the turbidity developed particularly in the 1 percent and 2 percent nominal $SrCl_2$ samples. With the exception of a few data points, particularly the 2 percent $SrCl_2$ sample annealed at 500°C, a decrease in hardness apparently accompanies precipitation in this system.

The minima in the hardness versus annealing temperature curves can be explained by one or both of two different mechanisms both active in each of the high and low temperature regions. First, since precipitation is a nucleation and growth process, the precipitate nucleation rate is low at high temperatures and the particle growth rate is high. As a result, for a one hour anneal, only a small amount of $SrCl_2$ comes out of solution by precipitation. As an alternative explanation, the solubility of $SrCl_2$ increases with temperature and may not be exceeded at these $SrCl_2$ concentrations.

At low temperatures, the nucleation rate is high and the growth rate is low since it is controlled by solid-state diffusion. If follows that, although the $SrCl_2$ content exceeds the solubility limit, the amount precipitated during the

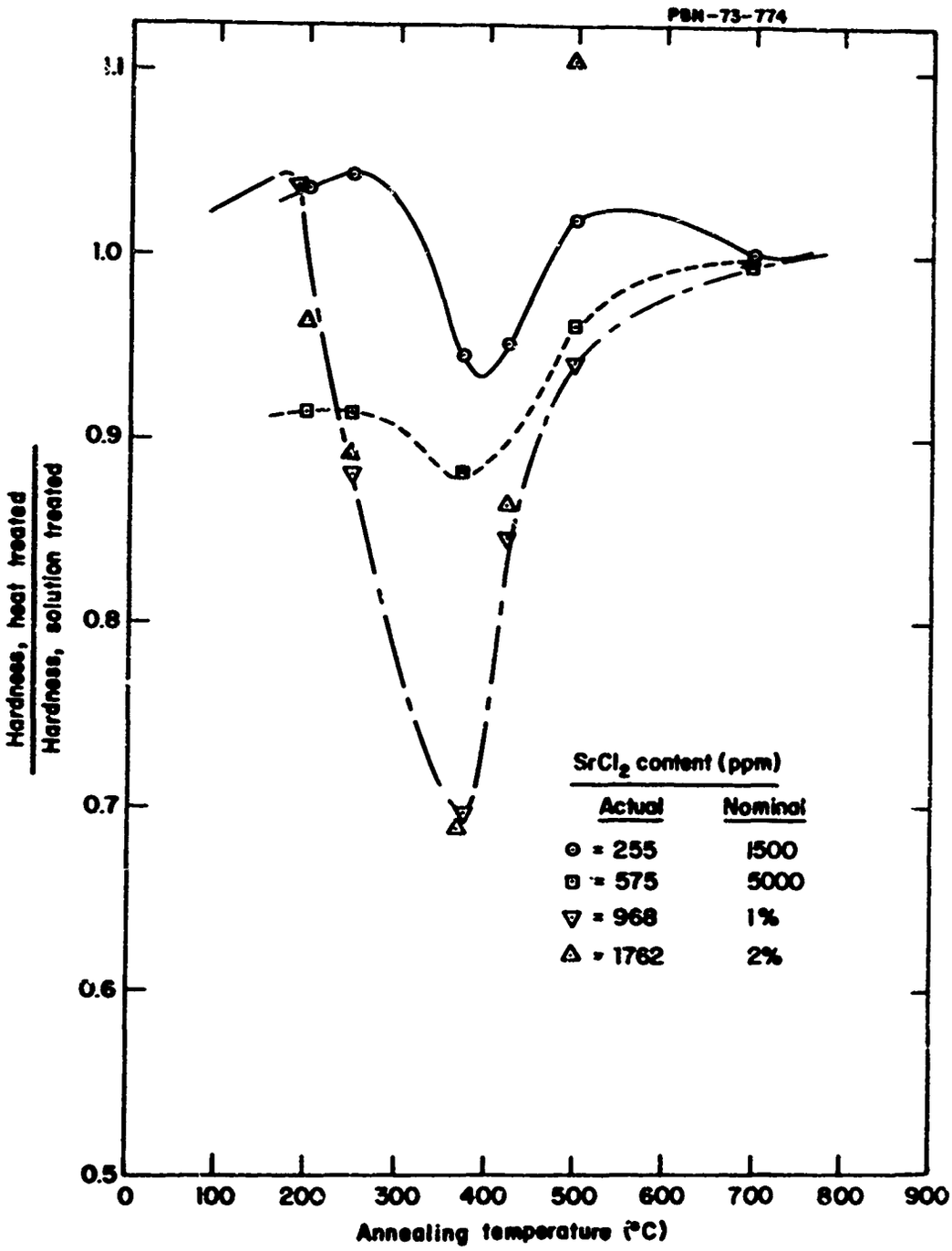

Fig. IV-11 The Effect of Heat Treatment (one hour) on $SrCl_2$-Doped Crystals as a Function of Annealing Temperature and $SrCl_2$ Content.

one hour anneal is insufficient to produce a significant decrease in hardness. Alternatively, since the nucleation rate is high, the precipitate particle size may be quite small and their concentration high. This small precipitate particle size may then maintain the high hardness. In this relative sense the material would be age- or precipitation-hardened. As will be seen later, the optical scattering data suggest that the precipitate particle size may be small at the lower temperatures lending weight to this second interpretation for the hardening mechanism.

At intermediate temperatures, both the nucleation and growth rates are high and a large amount of precipitation takes place rapidly. Certainly the existence of the precipitate particles should increase the hardness of the two phase material over that of the pure single crystal. However, from the data available, it cannot be determined whether the residual hardness is due to the $SrCl_2$ remaining in solid solution or due to the presence of precipitates.

b. Yield strength

1) General

Yield strengths, proportional limits and fracture strengths as a function of heat treatment and $SrCl_2$ content were determined on $KCl:SrCl_2$ single crystals. Samples were prepared by string sawing and polishing and then chemical polishing in $HCl:H_2O$ solution as described earlier. A typical stress-strain curve of a Sr-doped single crystal obtained in three point bending is shown in Fig. IV-12. Single-crystal samples typically had a sample span of 0.5 to 0.75 inches under stress. All of the yield stress data reported here will refer to σ_I; that is, the stress at the intersection of the two relatively straight portions of the curve, the elastic and easy glide regions. This is mainly for the sake of convenience since this value is less subject to error than is the measurement of the 0.2 percent offset yield or the proportional limit. The proportional limit is particularly difficult to determine with any degree of accuracy since the actual elastic portion of the curve may not be exactly straight due to sample misalignment, nonparallel sample faces, or plastic deformation at the load point. Therefore, the "yield point" values reported here will be somewhat higher than those on comparable materials reported by investigators using the proportional limit as the yield point.

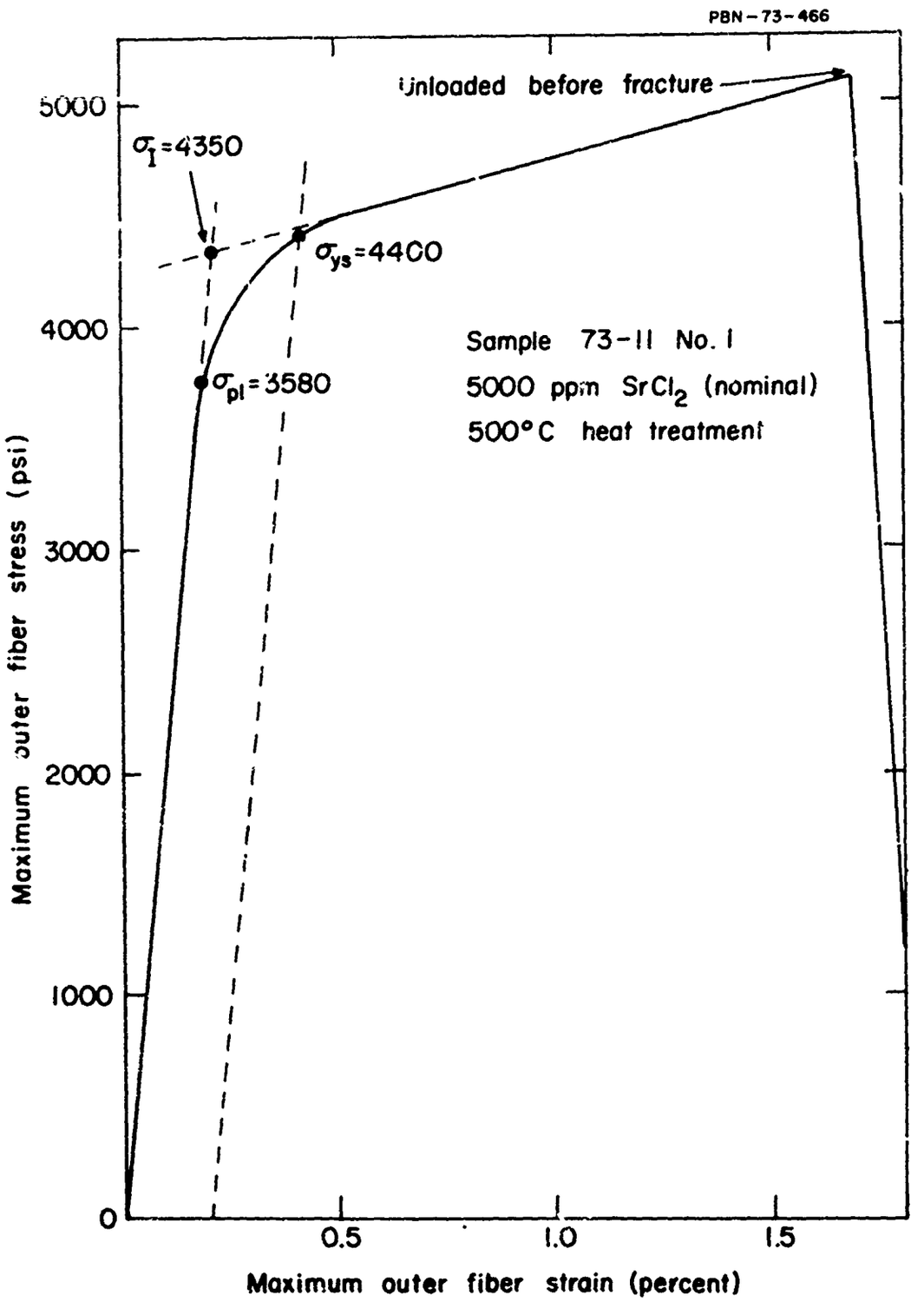

Fig. IV-12 Typical Stress Strain Curve.

The relation between proportional limit and yield strength is seen in Fig. IV-13. The porportional limit is linear with yield strength and can be expressed as

$$\sigma_{pl} = 0.72\ \sigma_I.$$

Therefore, for comparison of these results and those of others who report proportional limits, their values should be about 70 percent of the values we determine on a similar material.

Another point worthy of note is that a much more limited plastic strain was obtained if the samples were not chemically polished or if their dimensions were measured with a micrometer prior to testing. Thus, the surface damage introduced during mechanical polishing and handling greatly reduces ductility. This is clearly indicated in Table IV-2 by data taken on single crystals of pure KCl.

TABLE IV-2

EFFECT OF SURFACE FINISH ON DUCTILITY OF KCl

	Yield strength (psi)	Fracture strength (psi)	Deflection to Fracture (in.)
As-cleaved	~100	545	1.3×10^{-3}
	~100	648	4.2×10^{-3}
Mechanically Polished	619	767	2.5×10^{-3}
	390	835	6.2×10^{-3}
Chemically Polished	490	1152	36.3×10^{-3}
	594	782	13.0×10^{-3}

2) Yield strength versus $SrCl_2$ content

Figure IV-14 presents the yield strength as a function of $SrCl_2$ content (as analyzed) for solution treated and quenched samples. The yield strength is linear up to about 1000 ppm $SrCl_2$ and then abruptly levels off. Whether or not this reflects a change in the distribution of $SrCl_2$

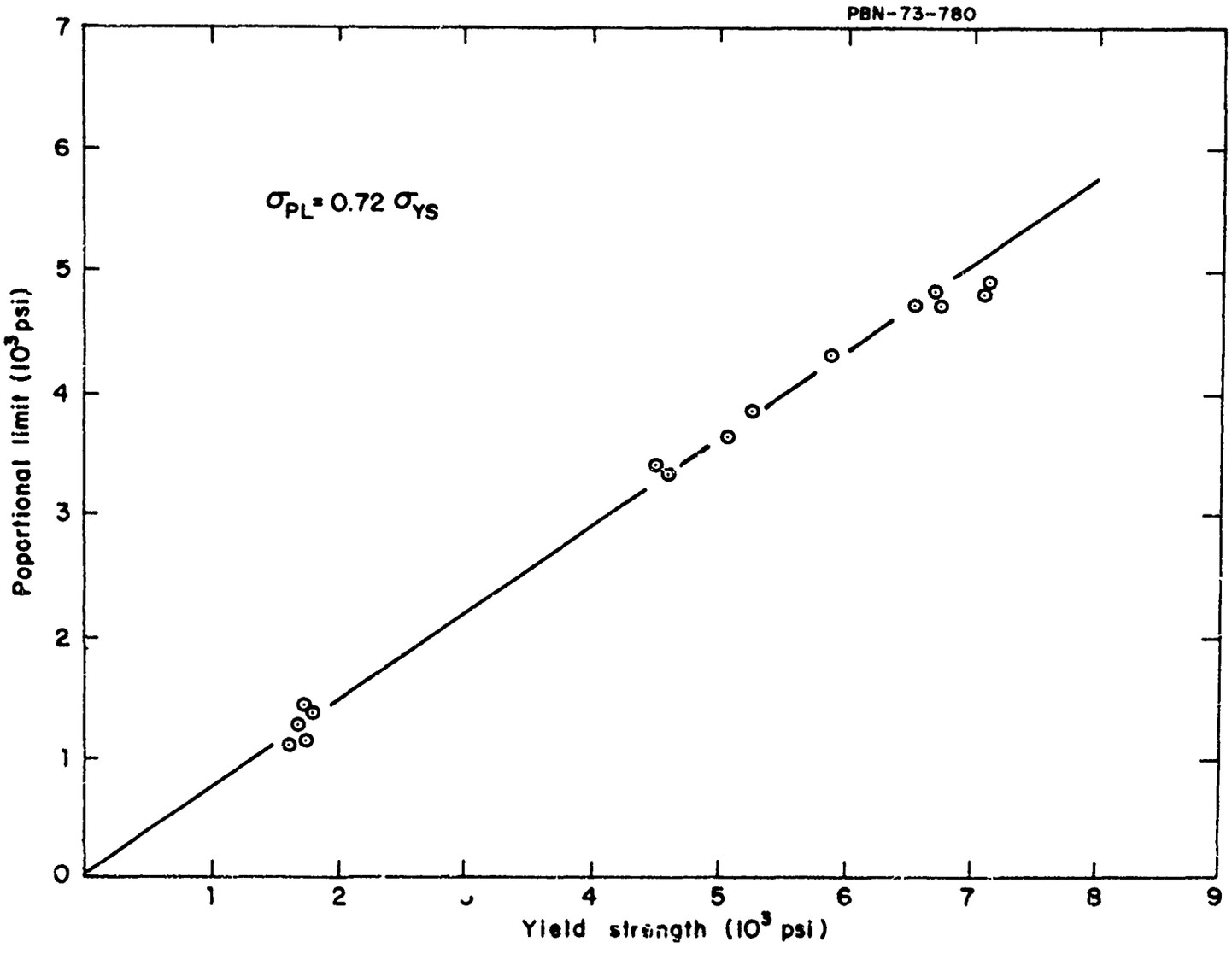

Fig. IV-13 Proportional Limit vs Yield Strength for $SrCl_2$-Doped Single Crystal KCl.

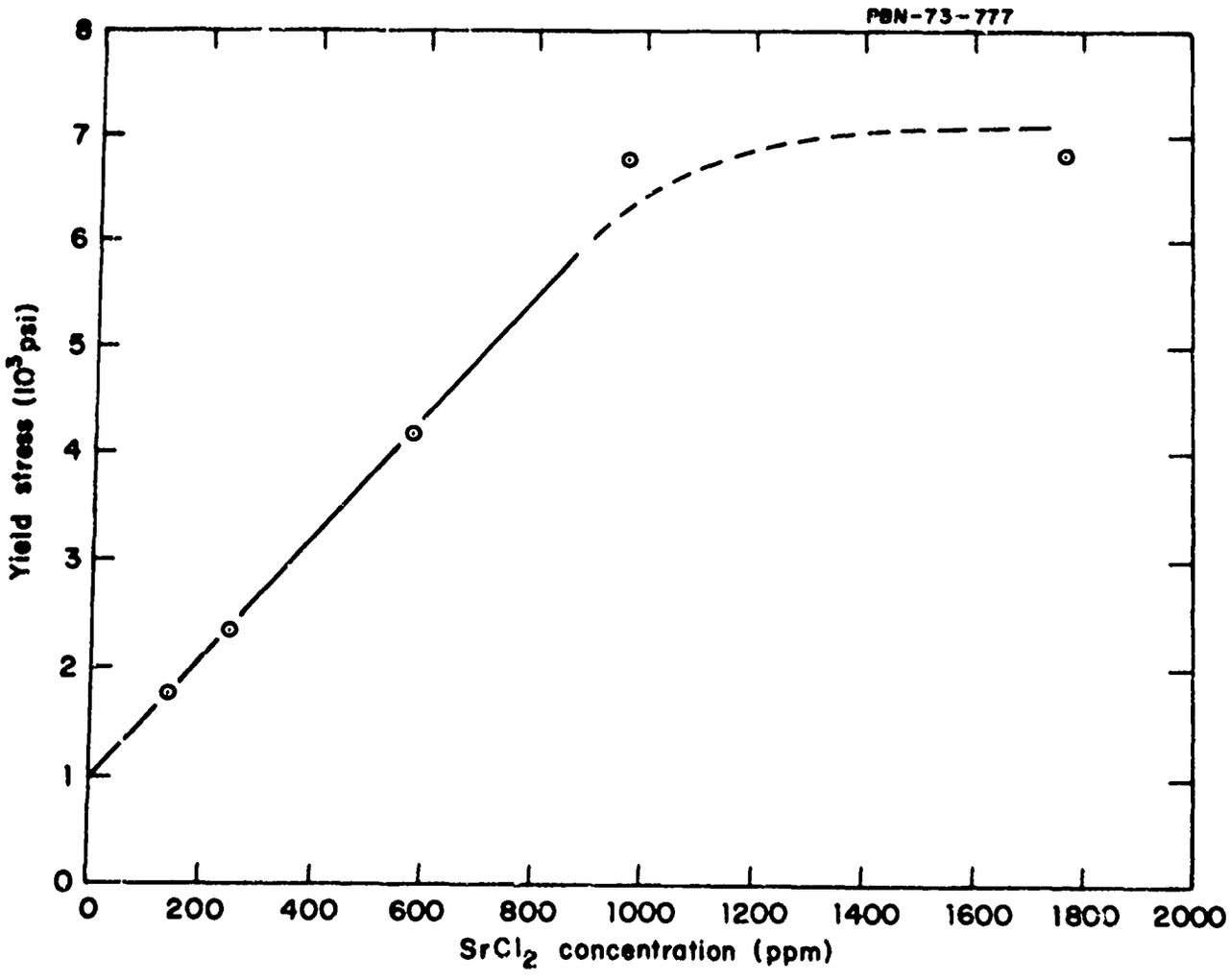

Fig. IV-14 Yield Strength as a Function of Actual $SrCl_2$ Concentration in Solution-Treated and Air Quenched KCl Crystals.

(i.e. isolated impurity-vacancy pairs to clusters) at the annealing temperature or that the quenching rate was insufficient to keep the $SrCl_2$ in solution is not known. It should be noted that yield strengths in excess of 5000 psi are possible at $SrCl_2$ concentrations greater than 700 ppm, and that yield strengths near 7000 psi are possible at the higher concentrations.

3) Correlation between yield strength and hardness

Figure IV-15 plots yield strengths of $SrCl_2$-doped KCl crystals from Table II with varying $SrCl_2$ content and heat treatment versus the hardness of the same samples. Although there is a fair amount of scatter a reasonably linear relationship between yield strength and hardness is obtained,

$$\sigma_I \text{ (psi)} = 530 (H-H_0) + 500 . \quad (1)$$

This relation is the solid line in the figure. The intercept is quite close to the yield strength of pure KCl. A similar linear relation has been reported previously[26] but the slope of the present line is somewhat higher. The large amount of scatter is not surprising because many of the samples have been precipitation annealed. There is also an excellent correlation between the hardness and yield strength of the nominal 2 percent $SrCl_2$ sample which had the 9000 psi yield. This is particularly noteworthy because the yield strength and hardness data were obtained from samples from different crystals. More will be said about this later.

4) Effect of heat treatment and $SrCl_2$ content on yield strength

Because of the demonstrated correlation between hardness and yield strength it is not surprising that yield strength data as a function of annealing temperature in Fig. IV-16 reflect the same features as the

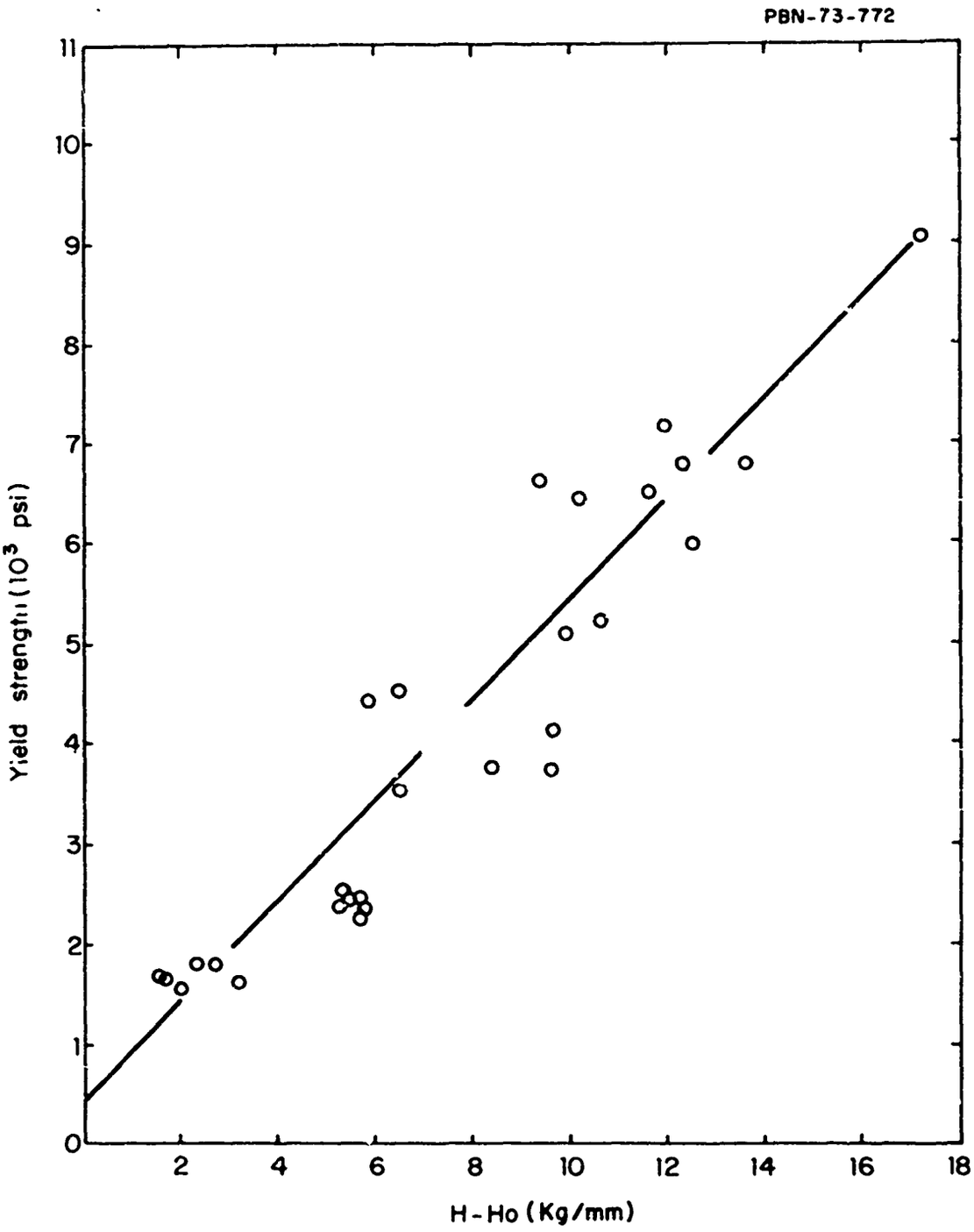

Fig. IV-15 Yield Strength vs Hardness of Heat Treated $SrCl_2$-Doped Crystals.

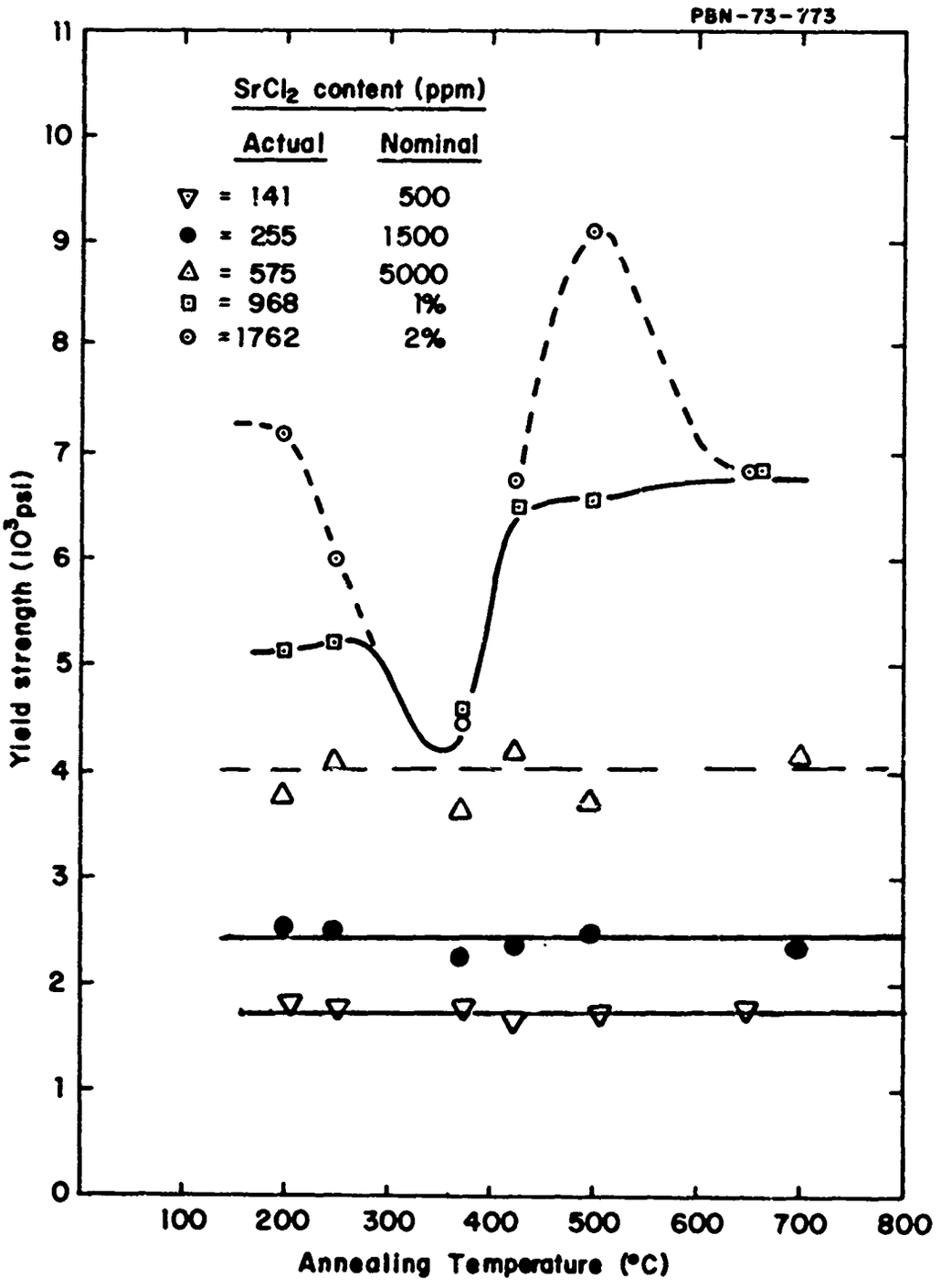

Fig. IV-16 Effect of Heat Treatment and $SrCl_2$ Content on Yield Strength.

hardness data presented earlier. There are several features of this plot worth noting. First, the yield strengths of the samples with low $SrCl_2$ content (less than 5000 ppm nominal) are relatively insensitive to heat treatment. This behavior is probably due to the fact that the $SrCl_2$ solubility is not exceeded until temperatures below 375°C are reached. At lower temperatures precipitation kinetics are too slow, and the yield strength remains high and reaches values near 4000/psi at a nominal concentration of 5000 ppm.

Second, the yield strengths of the 1 and 2 percent $SrCl_2$ samples in the 250 to 425°C range are virtually identical as were their hardnesses. This probably occurs because the $SrCl_2$ dissolved at the solution annealing temperature exceeds the solubility limit at these intermediate temperatures. The data suggest that precipitation up to the solubility limit has occurred at least at 375°C and 425°C for both concentrations, and that the $SrCl_2$ remaining in solid solution determines the residual strength. On that basis, from the data in Figs. IV-14 and IV-15 the solubility of $SrCl_2$ in KCl would be about 660 ppm at 375°C and about 960 ppm at 425°C. At low temperatures slow kinetics would again limit precipitation. This is not a completely satisfactory explanation, however, because the hardness does show a decrease for the lower concentrations.

Another extremely interesting feature of Fig. IV-16 is the apparent increase in yield strength for the 2 percent $SrCl_2$ sample annealed at 500°C. It was noted previously that this increase in yield strength at 500°C over that of solution annealed at 650°C parallels completely a similar increase in hardness at 500°C over the 650°C hardness. Since the hardness and yield strength data were obtained on different samples from different crystals it is unlikely that it is due an anomolously high $SrCl_2$ content in the particular samples nor to an insufficiently rapid quench of the 650°C samples. What is more likely is that the solubility of $SrCl_2$ is greater at 500°C than at 650°C. This is not at all unlikely since the phase diagram indicates a eutectic at 580°C.[11] Thus, the solubility might be expected to decrease both above and below this temperature. This would necessitate a rather complicated solidus curve in order to increase the solubility to over 1700 ppm

at the crystal growth temperature. Nevertheless, the behavior appears to be real and if the explanation is correct, even higher strengths might be obtained by annealing at temperatures between 500 and 530°C.

One final point is that the ductility of the $SrCl_2$ doped samples is greatly increased upon heat treatment. The 2 percent $SrCl_2$ samples annealed at 650°C and 500°C showed no ductile behavior at all while the intermediate samples gave plastic regions of several percent. This was even true of samples annealed as low as 200°C. One sample at 200°C plastically deformed almost eight percent before fracture and yet had a yield point of 7503 psi. Clearly, the low temperature anneal has some effect on ductility without any serious degradation in yield strength. That this is due to impurity clustering or coherent precipitation is a plausible but highly speculative possibility.

4. Effects of starting materials on optical properties

In order to investigate the effects of starting material on 10.6 μm absorption and to determine the cleanliness of our crystal-growing procedures, several pure KCl crystals were grown. The starting material and crystals were analyzed by emission spectroscopy (Performed by Jarrell-Ash, Newton, Mass.), by their IR spectra and by their 10.6 μm absorption determined calorimetrically. Table IV-3 lists the results of the emission spectroscopic analysis. Clearly, the Merck material showed the lowest impurity content, particularly for sodium and calcium, the most common impurities in the other materials. Also, it should be noted that the impurity content in the grown crystals is virtually identical to that in the starting materials. Figures IV-17 through IV-19 give plots of 10.6 μm absorption for the Baker, MacKay and Merck crystals. The results are inconclusive in that no clear correlation exists between the 10.6 μm absorption and the total impurity content or any specific impurity. Deutsch[27] has suggested recently that oxygen impurities in a chlorate complex may be producing an absorption band near 10 μm which determines the 10.6μm absorption. Clearly, the Merck starting material produces the best results. The measured 10.6 μm absorption coefficient would correspond to less than 1 percent total absorption in the 4.2 cm long crystal and would not be detected on the IR transmission spectrum of Fig. IV-20.

TABLE IV-3

ANALYSIS OF PURE KCl CRYSTALS AND STARTING POWDER

	Baker 3N Reagent		A. D. MacKay 6N Reagent		Merck "Suprapure" 6N		
Detected* Impurities	Powder	Crystal	Powder	Crystal	Powder	Crystal Top	Crystal Bottom
Na	10-100**	10-100	10-100	1-100	ND	ND	ND
Mg	ND***	< 1	< 1	ND	< 1	< 1	< 1
Al	< 1	< 1	< 1	< 1	1-10	< 1	< 1
Si	ND	< 1	< 1	ND	ND	< 1	< 1
Ca	1-10	1-10	1-100	1-100	< 1	< 1	< 1
Fe	ND	ND	ND	ND	ND	< 1	ND
Total Detected	11-111	11-113	11-203	2-201	3-13	5	4

* 44 other elements not detected
** ppm
*** ND ≡ not detected

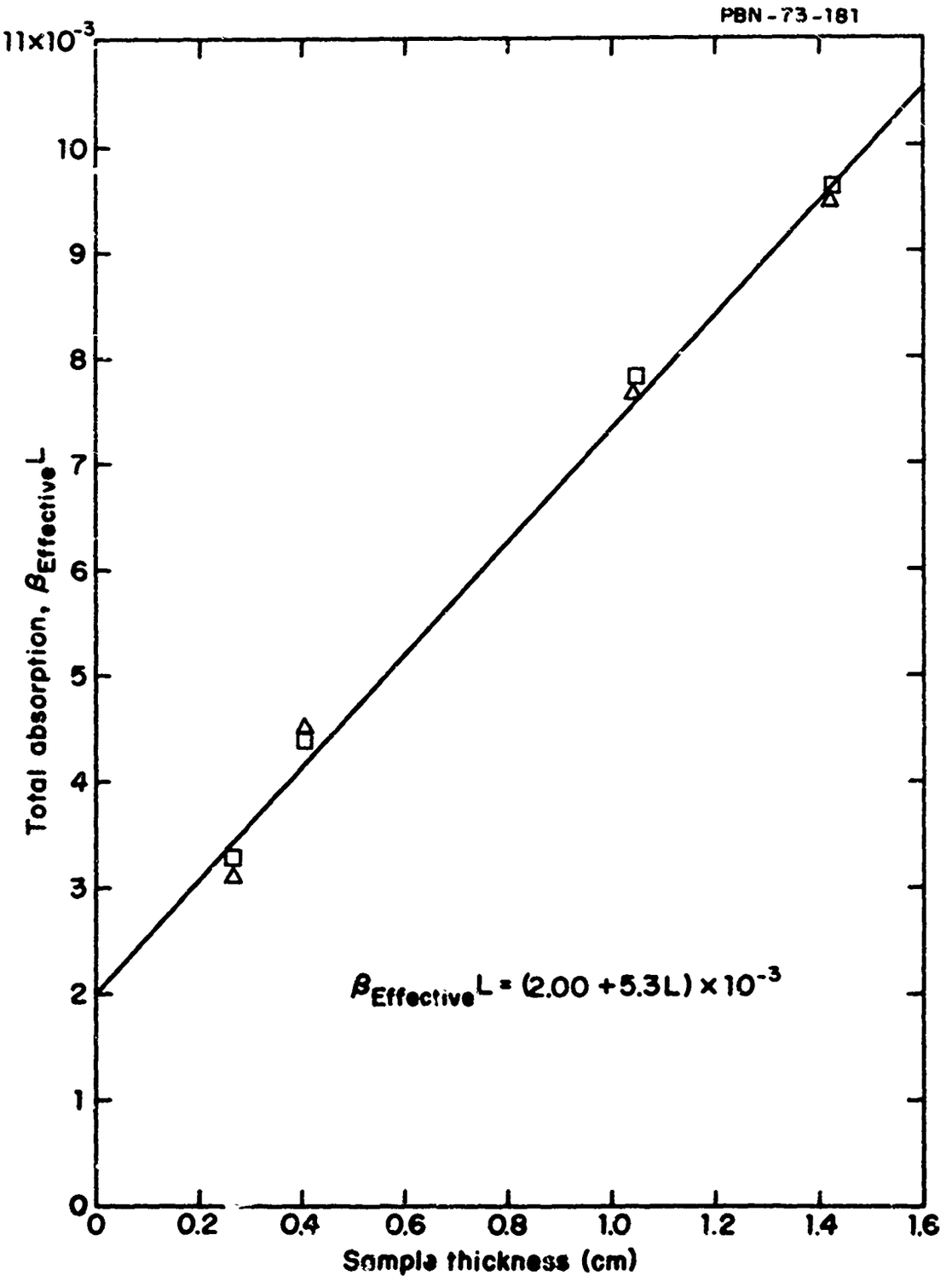

Fig. IV-17 10.6 μm Optical Absorption vs Length for Single Crystal 72-61. Baker reagent starting material.

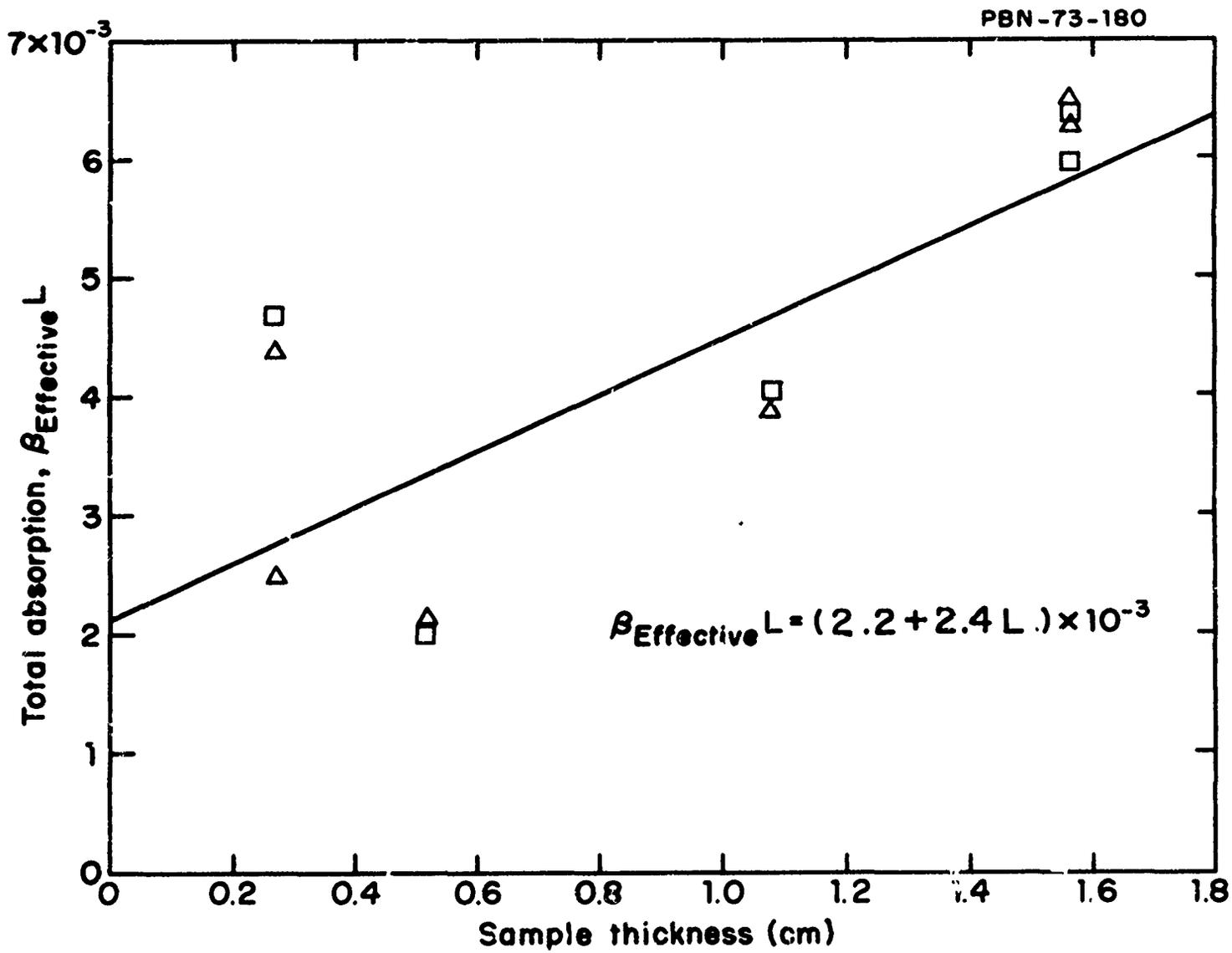

Fig. IV-18 10.6 μm Optical Absorption vs Length for Crystal 72-52. MacKay starting material.

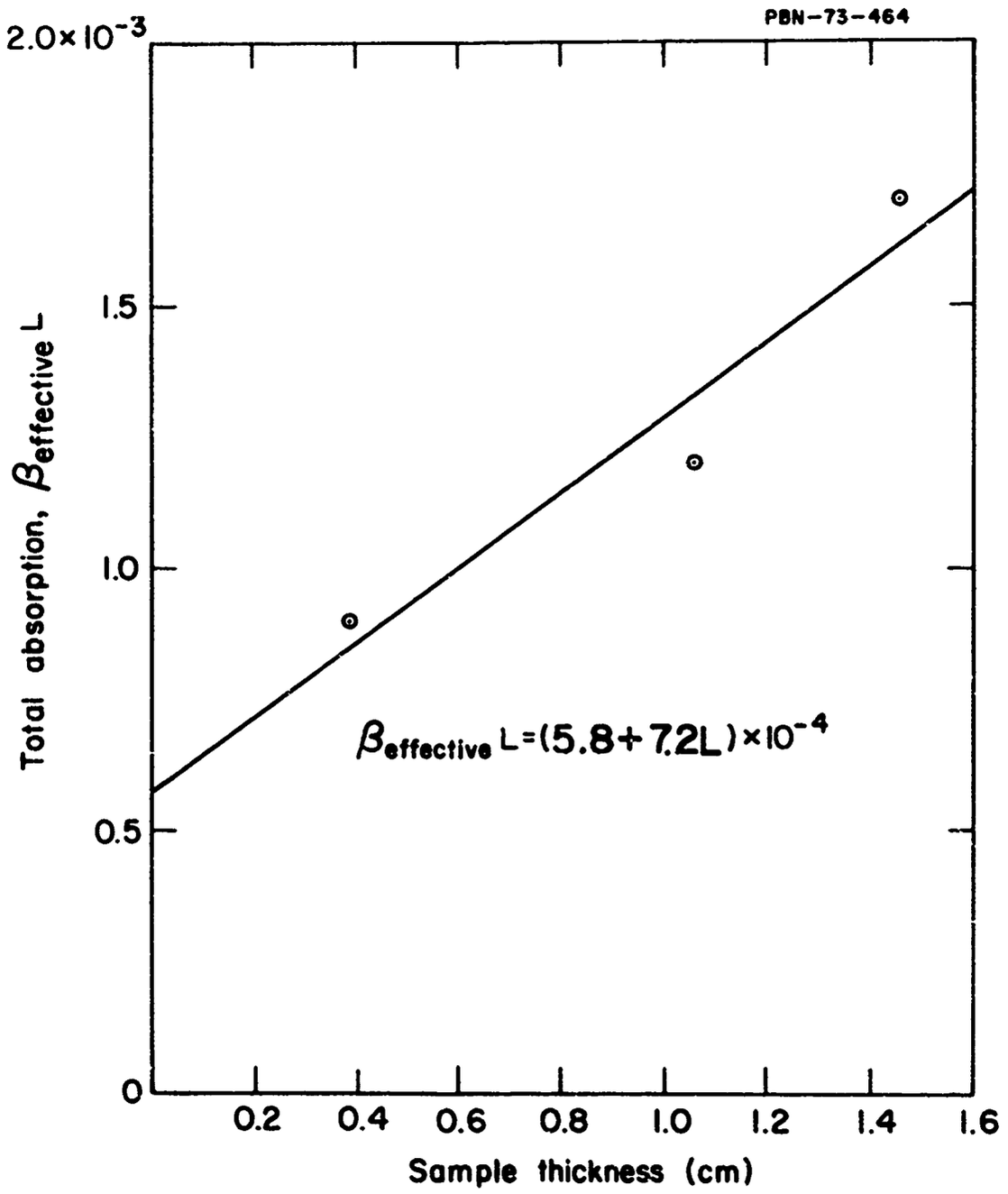

Fig. IV-19 10.6 μm Optical Absorption vs Sample Length for Crystal 73-29. Merck starting material.

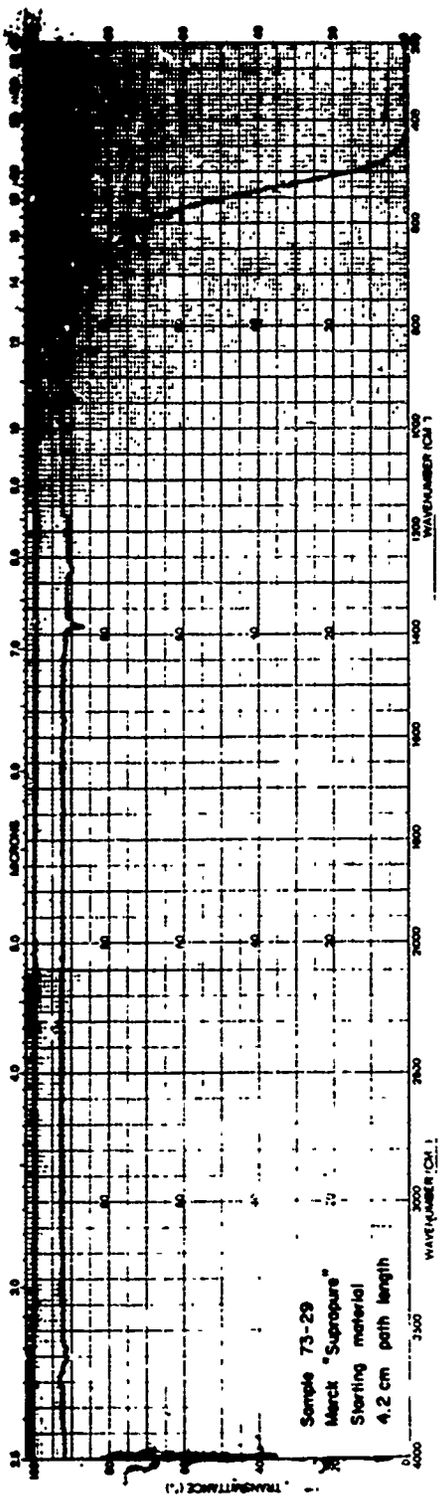

Fig. IV-20 Infrared Transmission Spectrum of Crystal 73-29, Merck starting material.

There are two final points worth noting. The surfaces of the samples for the 10.6 μm absorption measurements were polished both mechanically and chemically. It was found that cleaved surfaces gave nonreproducible results presumably due to scattering. Also, the necessity of determining the bulk absorption coefficient from a total absroption vs sample thickness curve is evident since for low absorption materials the surfaces produce a significant fraction of the total absorption. This is particularly true for thin samples, and will be even more important in crystals whose bulk absorption approaches the intrinsic level of 10^{-4} cm^{-1}.

5. Optical effects in $SrCl_2$ alloys

a. Effects of annealing temperature and $SrCl_2$ content

Accompanying the decrease in hardness and yield strength of the $SrCl_2$ -doped crystals in annealing is the development of turbidity or decrease in optical transmission in the visible region. This is particularly evident in the heavily-doped crystals annealed at temperatures in the 250°C to 425°C range. Figure IV-21 shows the transmission curves for the 2 percent nominal $SrCl_2$ crystal. Visibly, the 375°C sample is almost opaque and looks like milk glass. The 250°C sample has a faint haze present while the 500°C and 200°C samples appear clear. The relative effect of $SrCl_2$ content on turbidity is shown in Fig. IV-22. The 500 ppm nominal $SrCl_2$ crystal shows no change in optical transmission with annealing temperature and remains essentially transparent throughout the spectral range investigated. The turbidity is caused, of course, by light scattering from precipitate particles having a different index of refraction (index of $SrCl_2$ = 1.650) from that of KCl (index = 1.50).

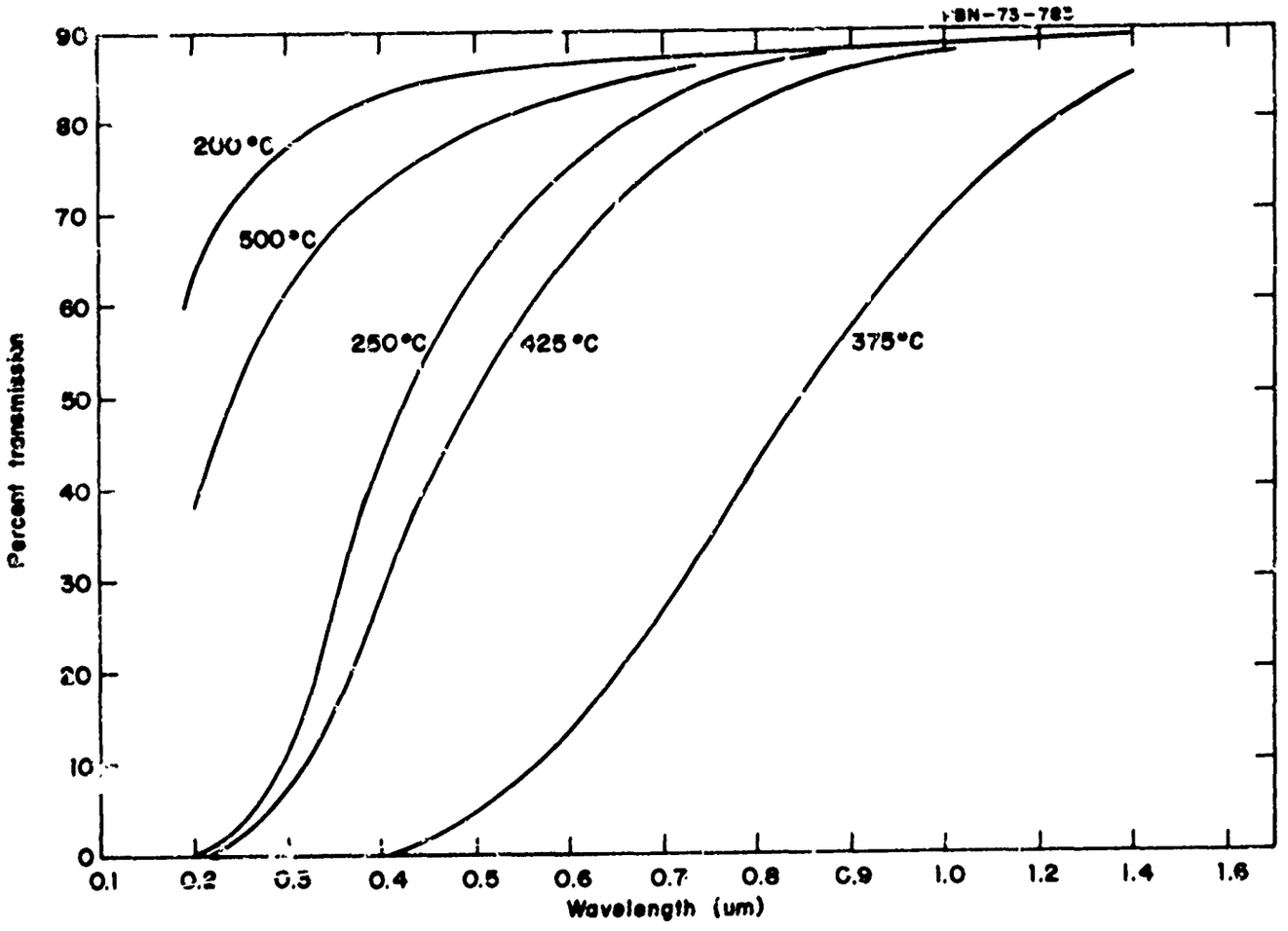

Fig. IV-21 Transmission Spectra of 2 Percent Nominal $SrCl_2$-Doped KCl As a Function of Annealing Temperature.

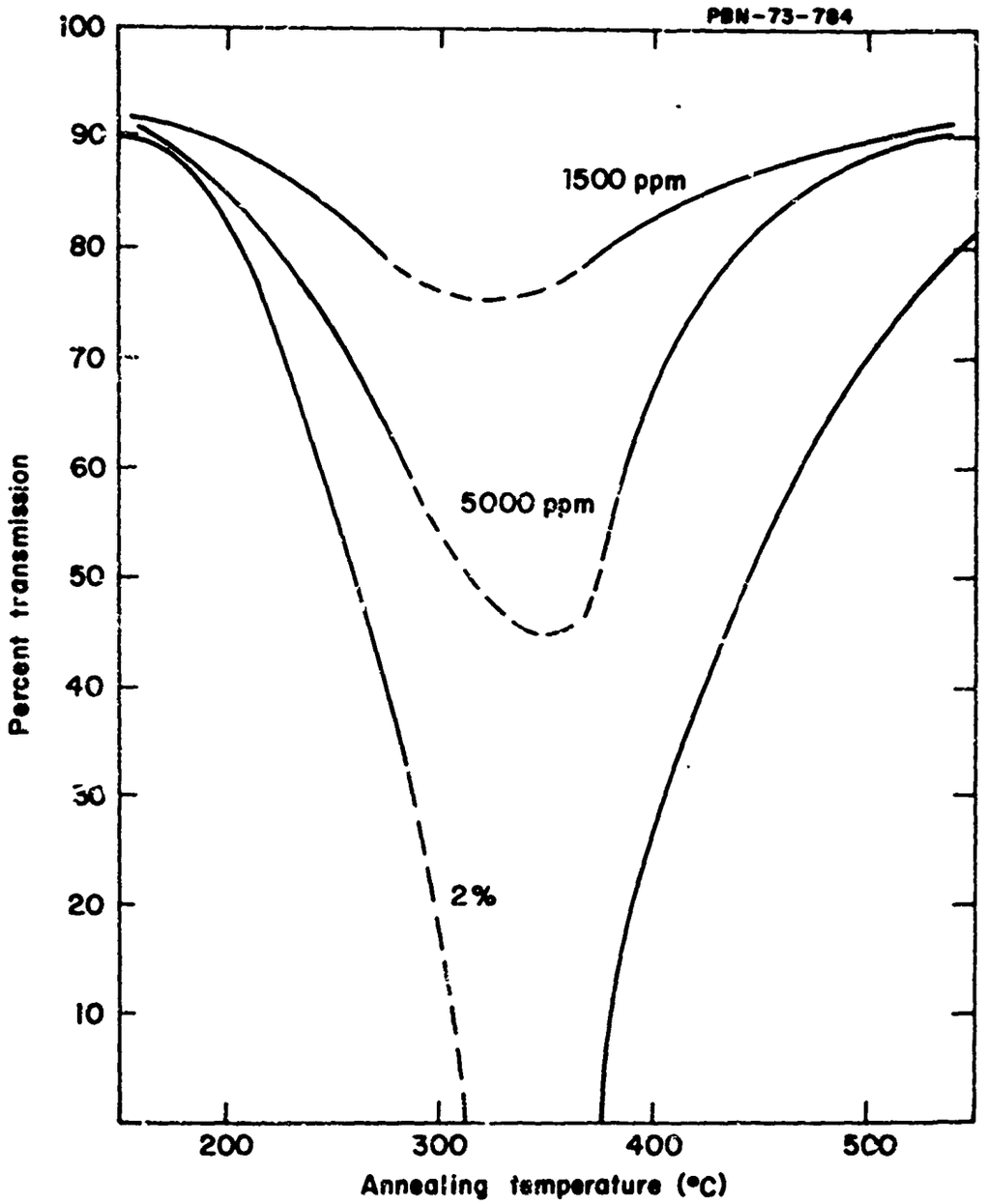

Fig. IV-22 Optical Transmission for Three $SrCl_2$-Doped Crystals at λ = 4500A as a Function of Annealing Temperature.

If the precipitate particle size is small compared to the wavelength, then Rayleigh scattering occurs and the transmitted intensity is given by:

$$I = I_0 e^{-\tau x} \qquad (4\text{-}1)$$

where

I_0 = initial intensity
x = sample thickness
τ = turbidity or scattering coefficient, which is given by

$$\tau = 24\pi^3 C \left(\frac{m^2-1}{m^2+2}\right) \frac{\rho_1}{\rho_2} \frac{V}{\lambda^4} \qquad (4\text{-}2)$$

where

C = weight fraction of scattering particles
ρ_1 = density of matrix
ρ_2 = density of particles
V = volume of particle
λ = wavelength
m = relative refractive index = $\frac{n_2}{n_1}$
n_2 = index of refraction of particles
n_1 = index of refraction of matrix.

To determine if Rayleigh scattering is the source of the turbidity in the heat treated $SrCl_2$-doped samples, the logarithm of τ was plotted vs wavelength for the 2 percent, 1 percent and 0.5 percent nominal $SrCl_2$-doped crystals as a function of heat treatment. The results are given in Figs. IV-23 through IV-25. As can be seen from the figures, the plots are indeed linear but the slopes, g, are nearer three than four. This deviation from the ideal slope of g = 4.0 can be explained by the fact that the particle size is too large for the Rayleigh formula to hold.[28] In this case, the turbidity coefficient still can be expressed as a simple power of the wavelength:

$$\tau = K\lambda^{-g} \qquad (4\text{-}3)$$

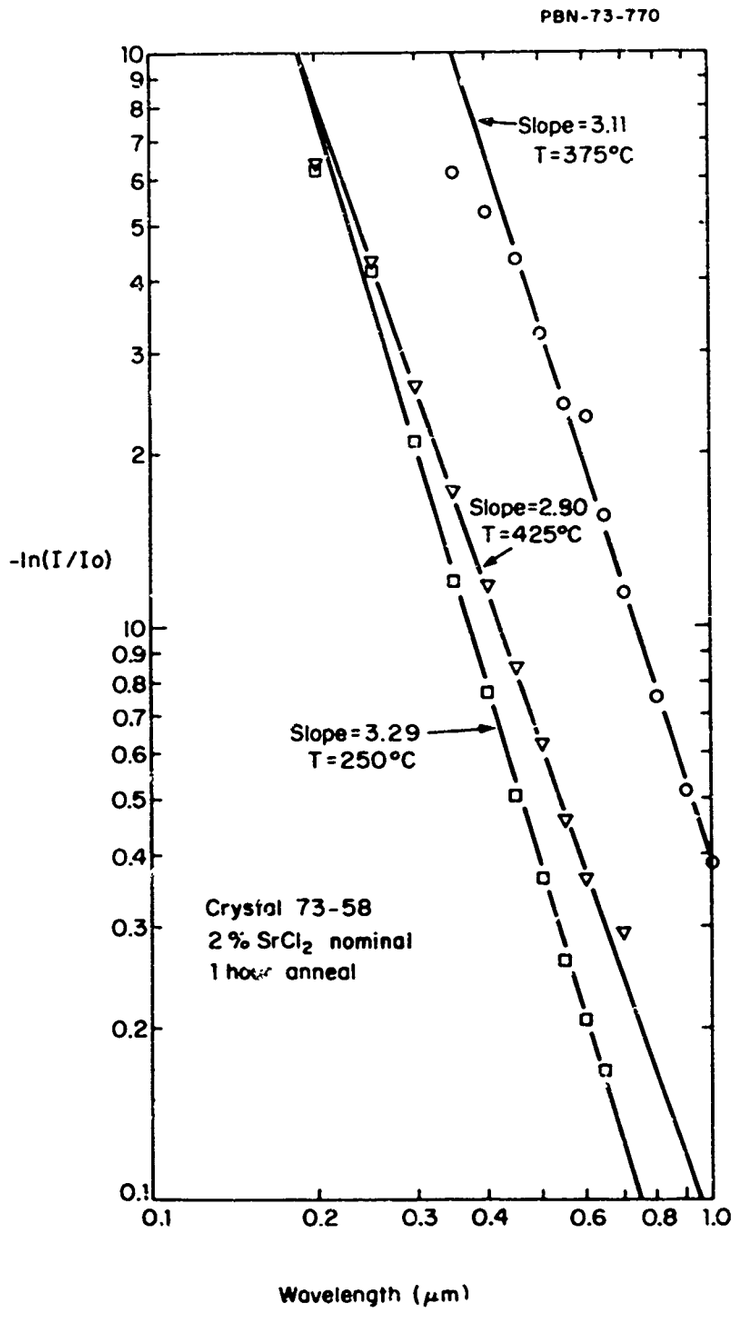

Fig. IV-23 The Logarithm of the Turbidity Coefficient, τ, vs Wavelength for the Nominal 2 Percent $SrCl_2$ Crystal as a Function of Annealing Temperature.

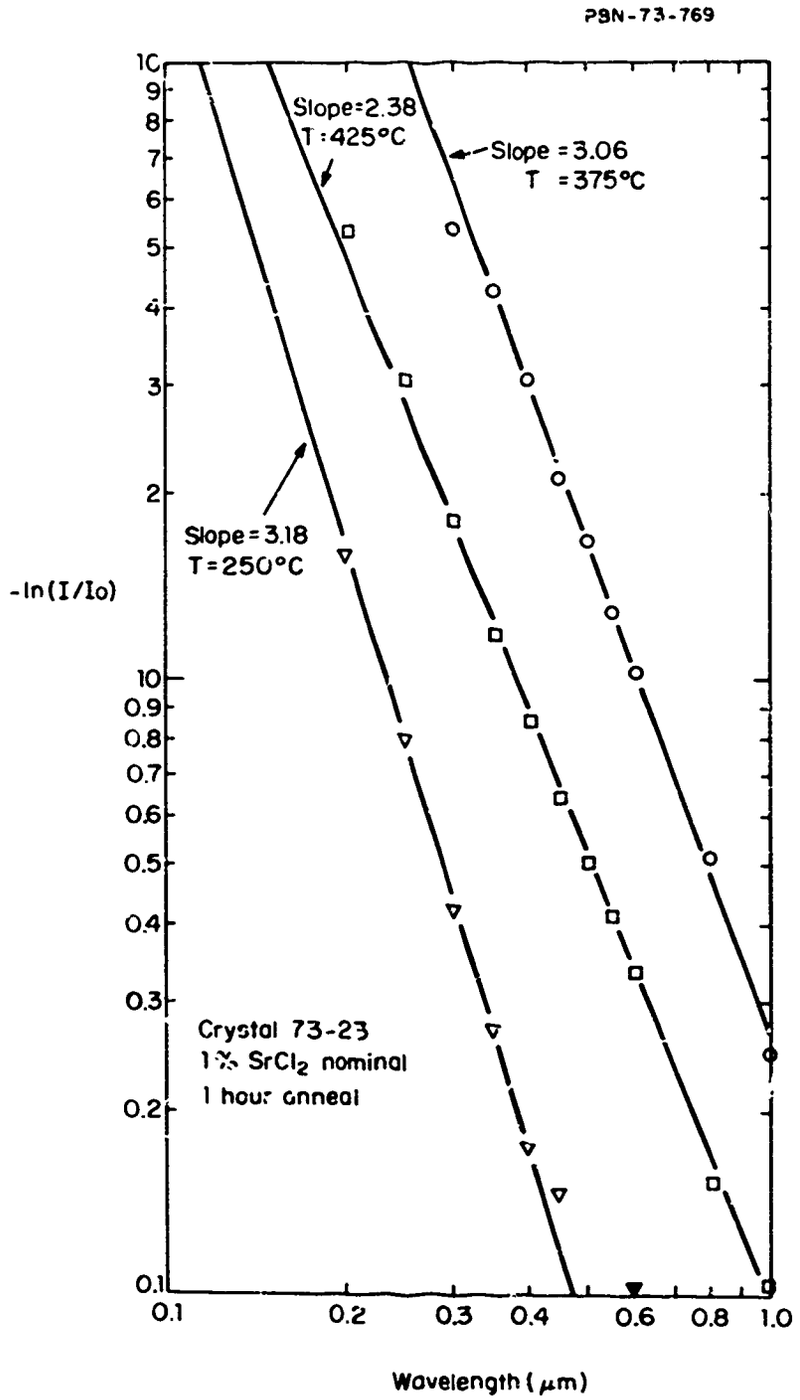

Fig. IV-24 The Logarithm of the Turbidity Coefficient, τ, vs Wavelength for the Nominal 1 Percent $SrCl_2$ Crystal as a Function of Annealing Temperature.

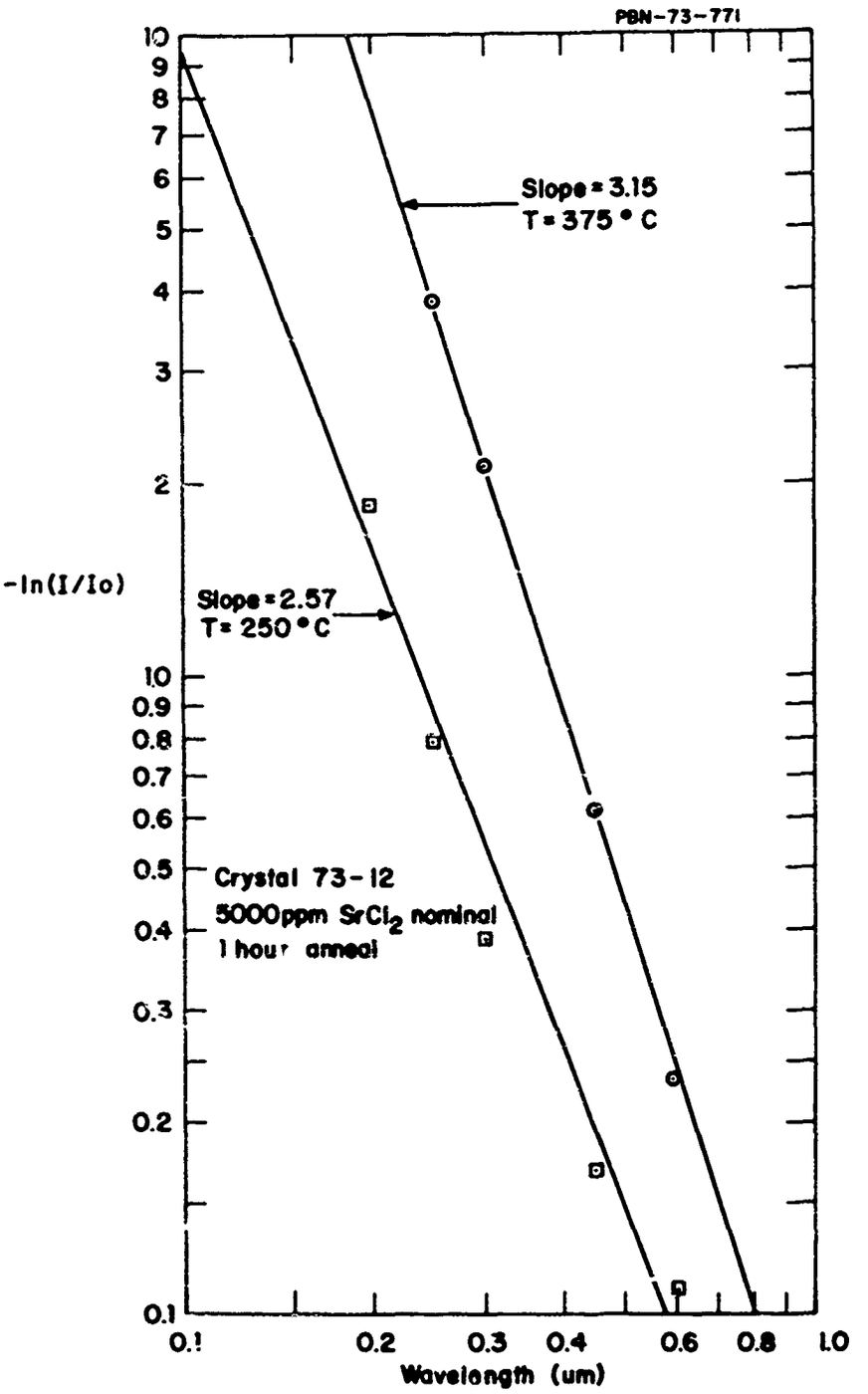

Fig. IV-25 The Logarithm of the Turbidity Coefficient, τ, vs Wavelength for the Nominal 5000 ppm $SrCl_2$ Crystal as a Function of Annealing Temperature.

and the deviation of the value of g from 4.0 can give information about the size of the scattering particles. Specifically,[29]

$$\alpha^2 = \frac{(g - 4)(m^2 + 2)}{2.4(m^2 - 2)} \qquad (4\text{-}4)$$

where

$$\alpha = \frac{2\pi n_2 a}{\lambda}$$

a = particle radius

Equation 4-4 was applied to the slopes of Figs. IV-23 and IV-24 and the precipitate particle sizes relative to that of the 250°C anneal were determined. These data are plotted in Fig. IV-26. The results are not at all unreasonable in that the higher precipitation temperature gives rise to the larger particle sizes. With the relative particle sizes determined from Eq. (4-4), the relative concentration of scattering particles can be determined from Eq. (4-2) and the measured values of the turbidity coefficients. These results are given in Fig. IV-27. The surprising result here is that the optical data imply that more complete precipitation has occurred at 250°C than at higher temperatures. This would be expected thermodynamically but, as was stated earlier, solid state diffusion would be expected to be too slow to produce much precipitation at such a low temperature. These data suggest that the high hardness and yield strength observed at lower annealing temperatures may be due to the hardening effects of small precipitate particles rather than the lack of exsolution of $SrCl_2$ due to slow kinetics. This is not a completely convincing explanation and the optical scattering data must be analyzed more fully in order to determine the validity of this conclusion.

From the α values determined in Eq. (4-4), the size of the scattering particles is estimated to be about 1000-2000 Å. One important goal of this program was to determine what effects optical scattering by precipitate particles would have at 10.6 μm. Extrapolation of the

PBN-73-767

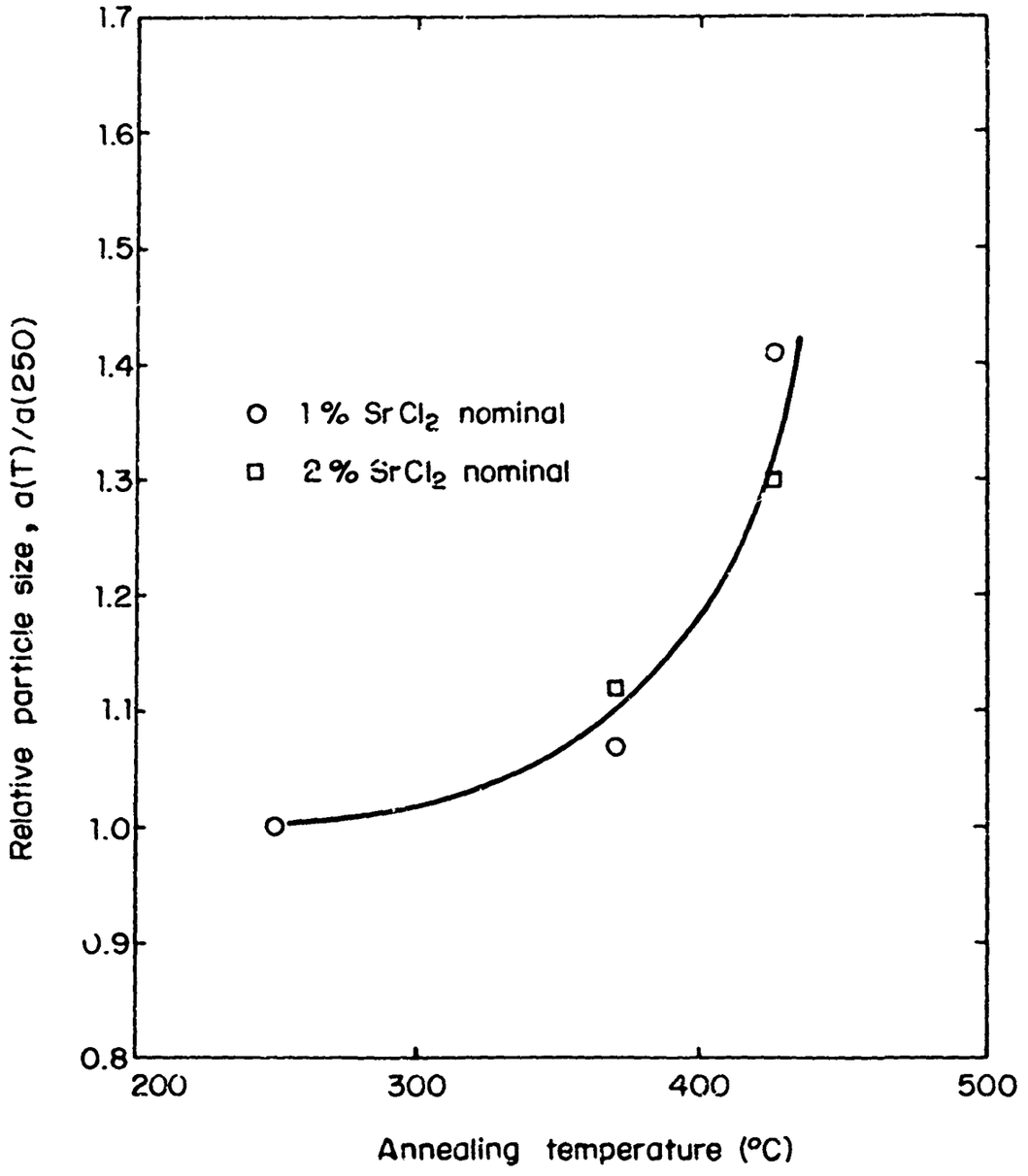

Fig. IV-26 Relative Precipitate Particle Size vs Annealing Temperature for 2 Percent and 1 Percent Nominal $SrCl_2$ Crystals Derived from the Wavelength Power Dependence of the Turbidity Coefficient.

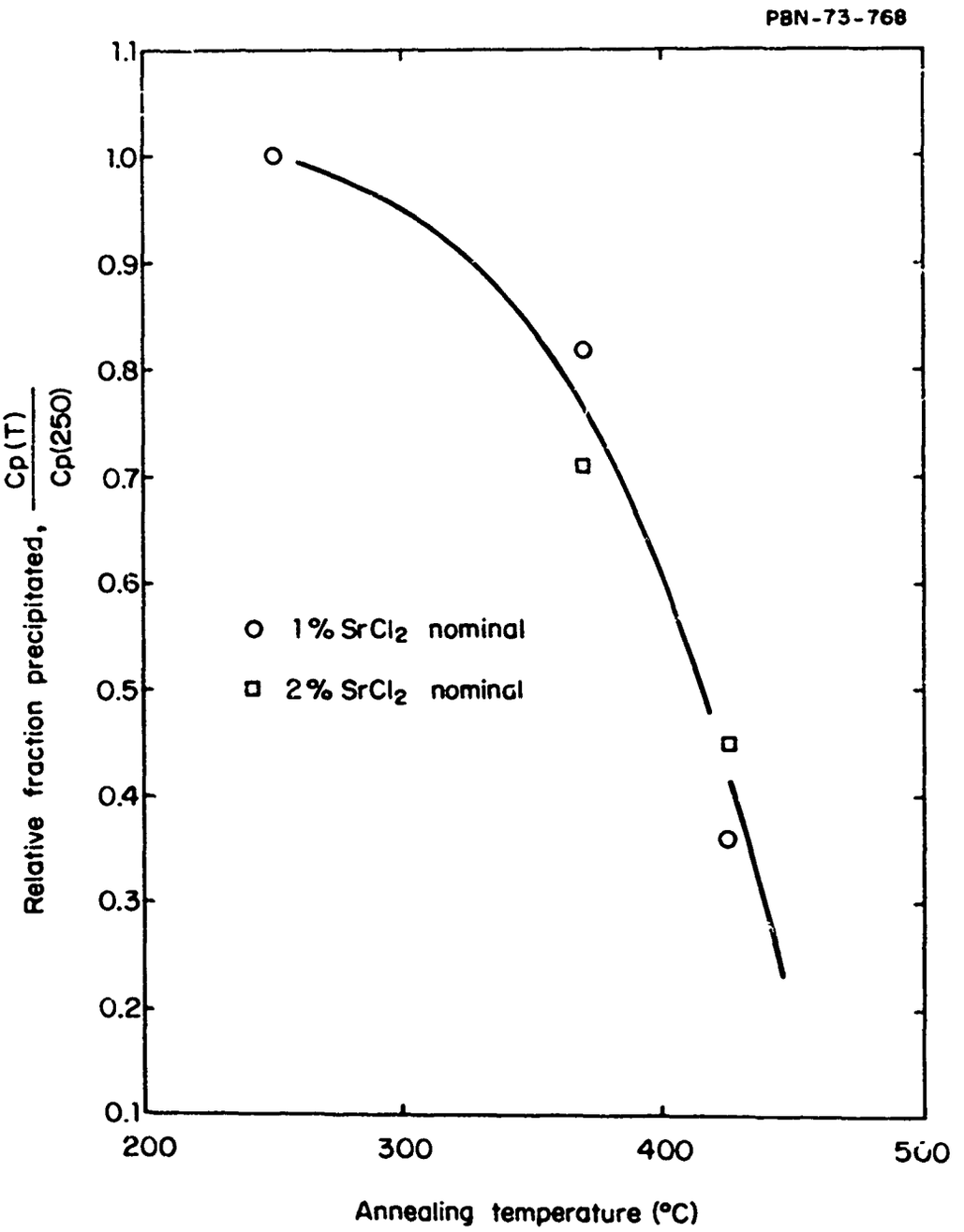

Fig. IV-27 **Relative Degree of Precipitation in the 2 Percent and 1 Percent Nominal $SrCl_2$ Crystals as a Function of Temperature as Determined Optically.**

curves of Figs. IV-23 to IV-25 to 10.6 μm gives the results of Table IV-4. The data indicate that, in most cases, the effect of precipitate scattering on the apparent absorption coefficient at 10.6 μm is small. It can be concluded, therefore, that in general visible scattering produced by precipitation in the $SrCl_2$-KCl system will contribute negligible scattering at 10.6 μm. Of course, this assumes that the precipitate particle size distribution is quite narrow, but this is generally found to be the case in other precipitated systems.

b. Effect of $SrCl_2$ on optical properties at 10.6 μm

In order to investigate more fully the effect of $SrCl_2$ on 10.6 μm absorption, two "suprapure" KCl crystals were grown, one doped nominally with 200 ppm $SrCl_2$ and the other 1 percent $SrCl_2$. The actual concentration of $SrCl_2$ in the doped crystals was not determined, but from data of $SrCl_2$ segregation coefficient KCl as a function of melt composition, concentrations of about 50 ppm and 700 $SrCl_2$ are predicted.

The 10.6 μm absorption for the 200 ppm nominal $SrCl_2$ crystal was determined to be 6.1×10^{-4} cm^{-1} as can be seen in Fig. IV-28. This strongly suggests that $SrCl_2$ additions in solid solution had little effect on optical properties. To show this more conclusively and to evaluate the effects of precipitation, the 10.6 μm absorption was measured in both solution-treated and precipitated conditions in the 1 percent nominal crystal. The data are shown in Fig. IV-29. The solution treated $\beta = 3.7 \times 10^{-4} cm^{-1}$ is as low as any we have measured to date and the increase in absorption after precipitation agrees reasonably well with the calculated increase of $1.2 \times 10^{-4} cm^{-1}$ from the visible scattering vs wavelength data described above. These absorption data indicate that neither $SrCl_2$ in solution nor the precipitate particles present a problem at 10.6 μm. This is not to say, however, that scattering can be ignored, and indeed, both impurity particles and residual porosity can be expected to provide a limiting background level of scatter.

TABLE IV-4

PRECIPITATE SCATTERING AT 10.6 μm

Nominal $SrCl_2$(%)	Annealing Temperature (°C)	Wavelength Exponent, g	Apparent Absorption Coefficient at 10.6 μm(cm^{-1})
2	425	2.80	2.33×10^{-4}
	375	3.11	6.14×10^{-4}
	250	3.29	3.26×10^{-5}
1	425	2.38	7.25×10^{-4}
	375	3.06	3.11×10^{-4}
	250	3.18	2.23×10^{-5}
0.5	375	3.15	5.5×10^{-5}
	250	2.57	1.3×10^{-4}

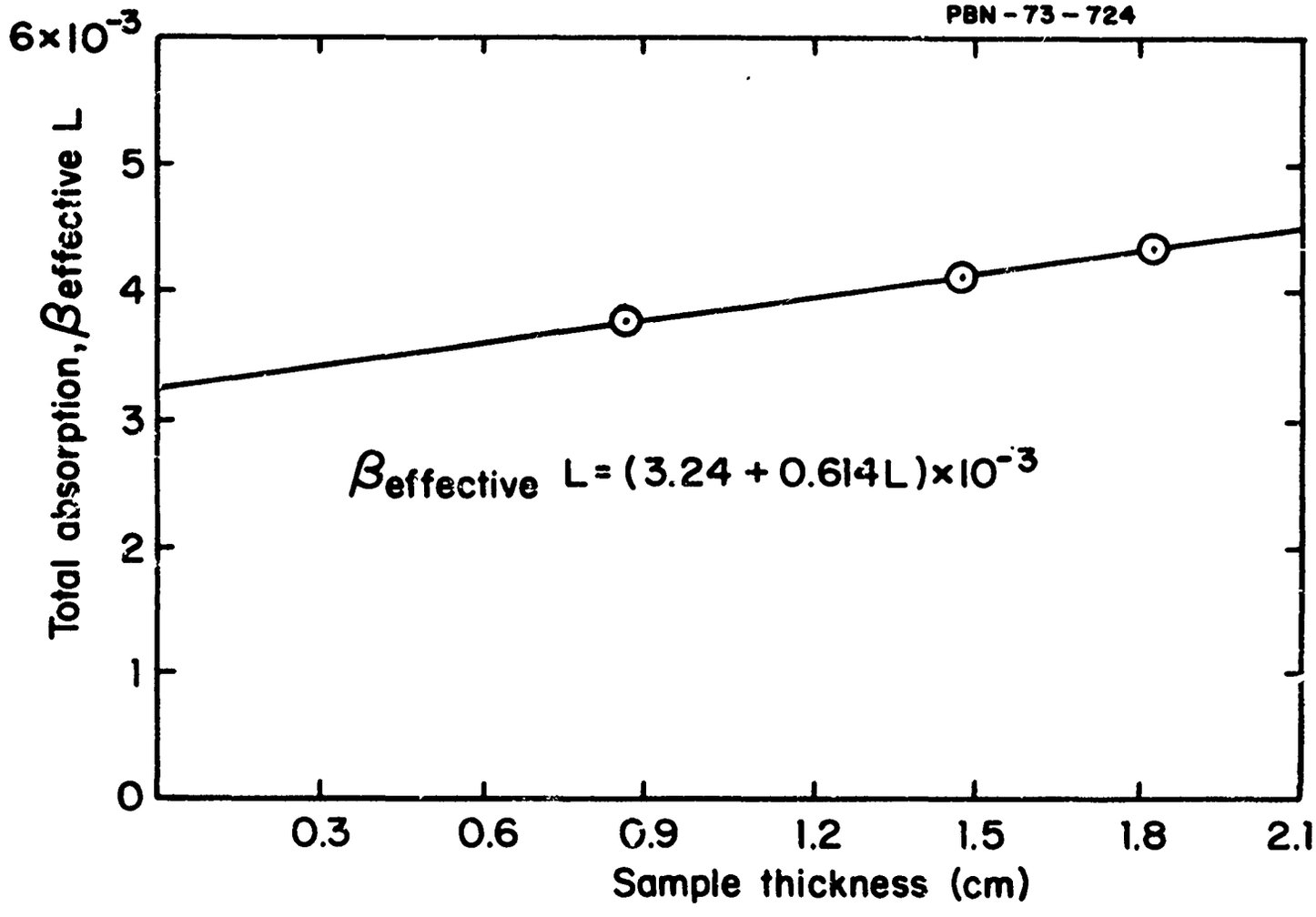

Fig. IV-28 10.6 μm Optical Absorption vs Sample Length for Crystal 73-62. Merck starting material; 200 ppm (nominal) $SrCl_2$.

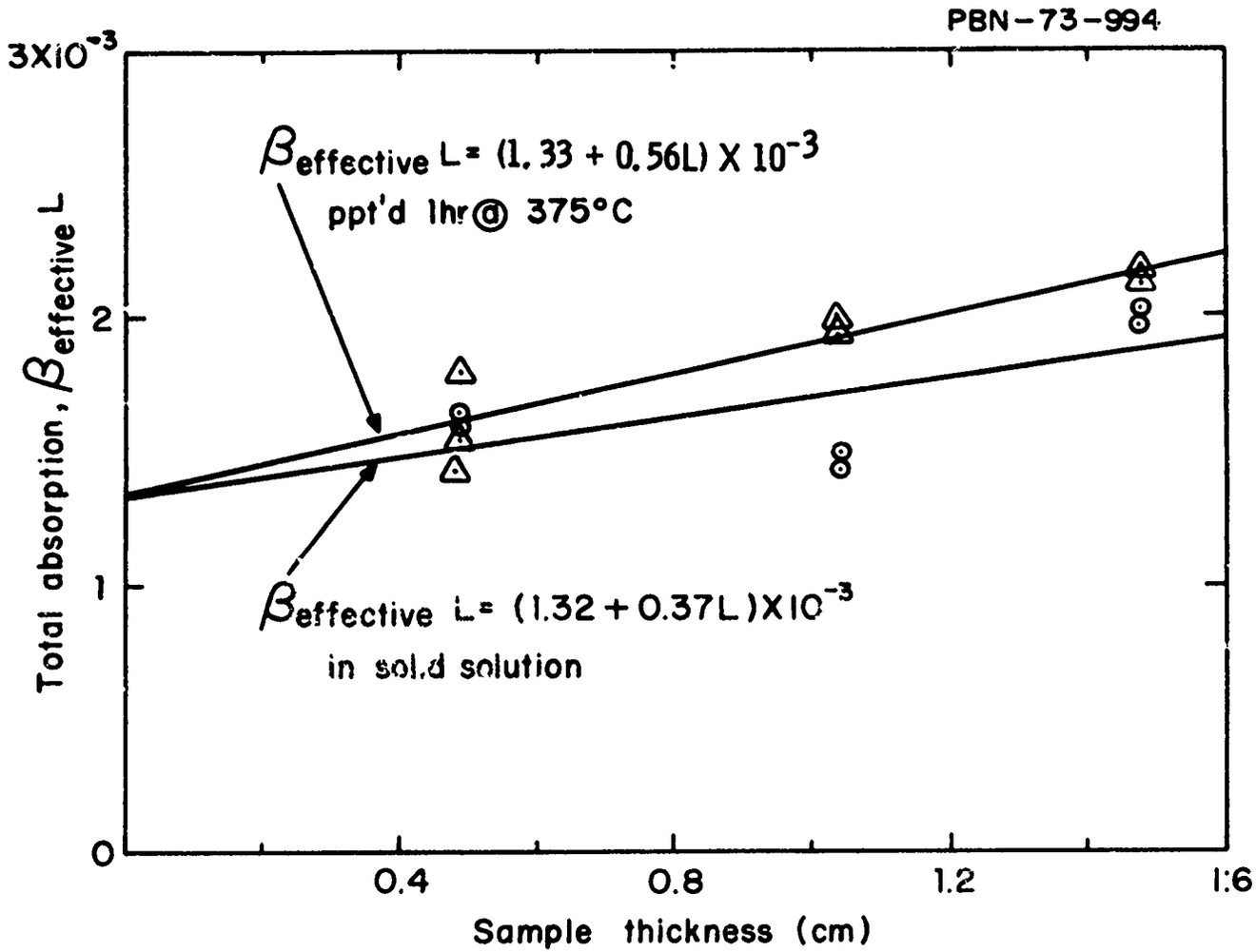

Fig. IV-29 Comparison of the 10.6 μm Absorption Coefficient of a Nominal 1 % $SrCl_2$ Alloy in the Solution-Treated and Precipitated Condition.

C. Casting

1. Small castings

a. In-situ castings

In general, the results of the in situ small diameter castings were poor. An attempt was made to investigate the effects of freezing rate on microstructure with inconclusive results. The main conclusions reached with this technique were that graphite crucibles with a grafoil liner could be used successfully and that vacuum casting and directional solidification could lead to pore and crack-free castings of undoped KCl as shown in Fig. IV-30. However, freezing conditions could not be controlled sufficiently and a rather large grain size resulted in all cases (Fig. IV-31).

b. Poured castings

These small castings were used to investigate the effects of $SrCl_2$ content and mold temperature on the microstructure and crystallographic orientation of the castings. Figure IV-32 shows the effects of $SrCl_2$ concentration and casting temperature on the poured ots. Clearly, $SrCl_2$ additions have a profound effect on reducing grain size while the mold temperature has little effect. With these castings, a reasonably equiaxed grain structure was obtained, particularly in those with higher $SrCl_2$ content (Fig. IV-33). Figure IV-34 shows, however, that with higher $SrCl_2$ content, pronounced grain boundary segregation occurs. Whether this segregation occurred during solidification or after freezing was not determined.

2. Large castings

a. General

The construction and installation of the large casting furnace was completed in April 1973. All casting during the last six months of the program was carried out in this furnace. Figure IV-35 shows a typical casting still in the mold with its grafoil liner.

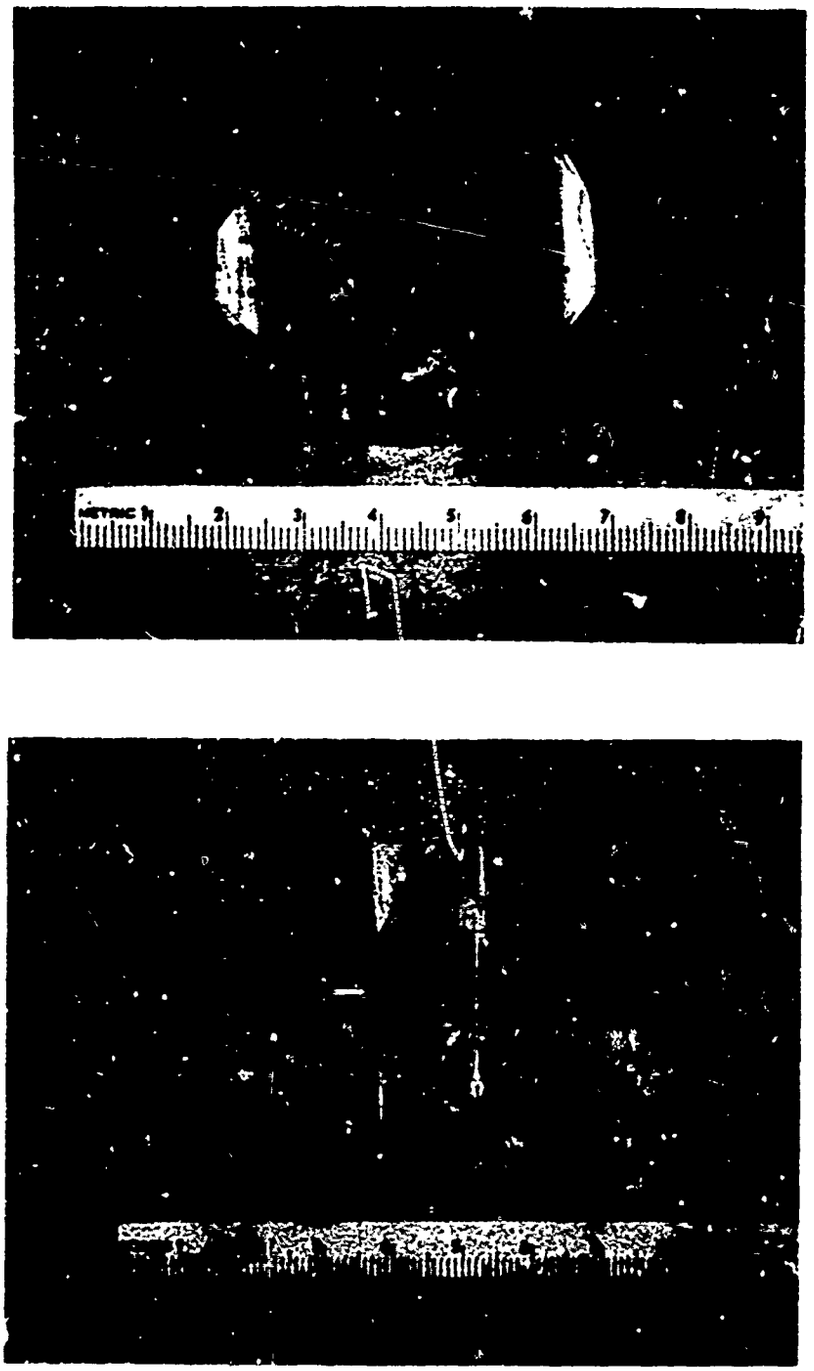

Fig. IV-30 Pore- and Crack-Free Polycrystalline KCl Sample. At the top is a view of the top surface; at the bottom, an edge of the sample.

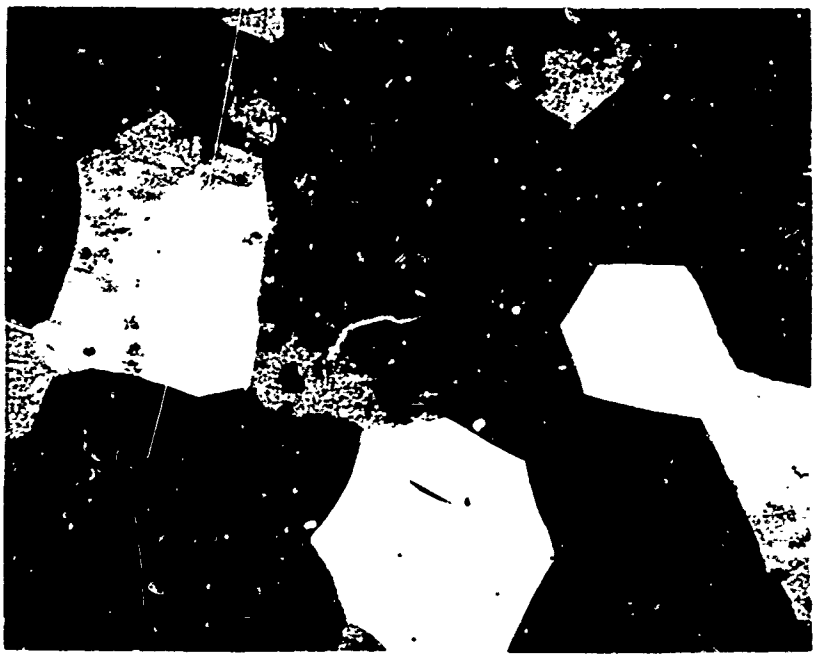

Fig. IV-31 Microstructure of Cast Pure KCl. (12X)

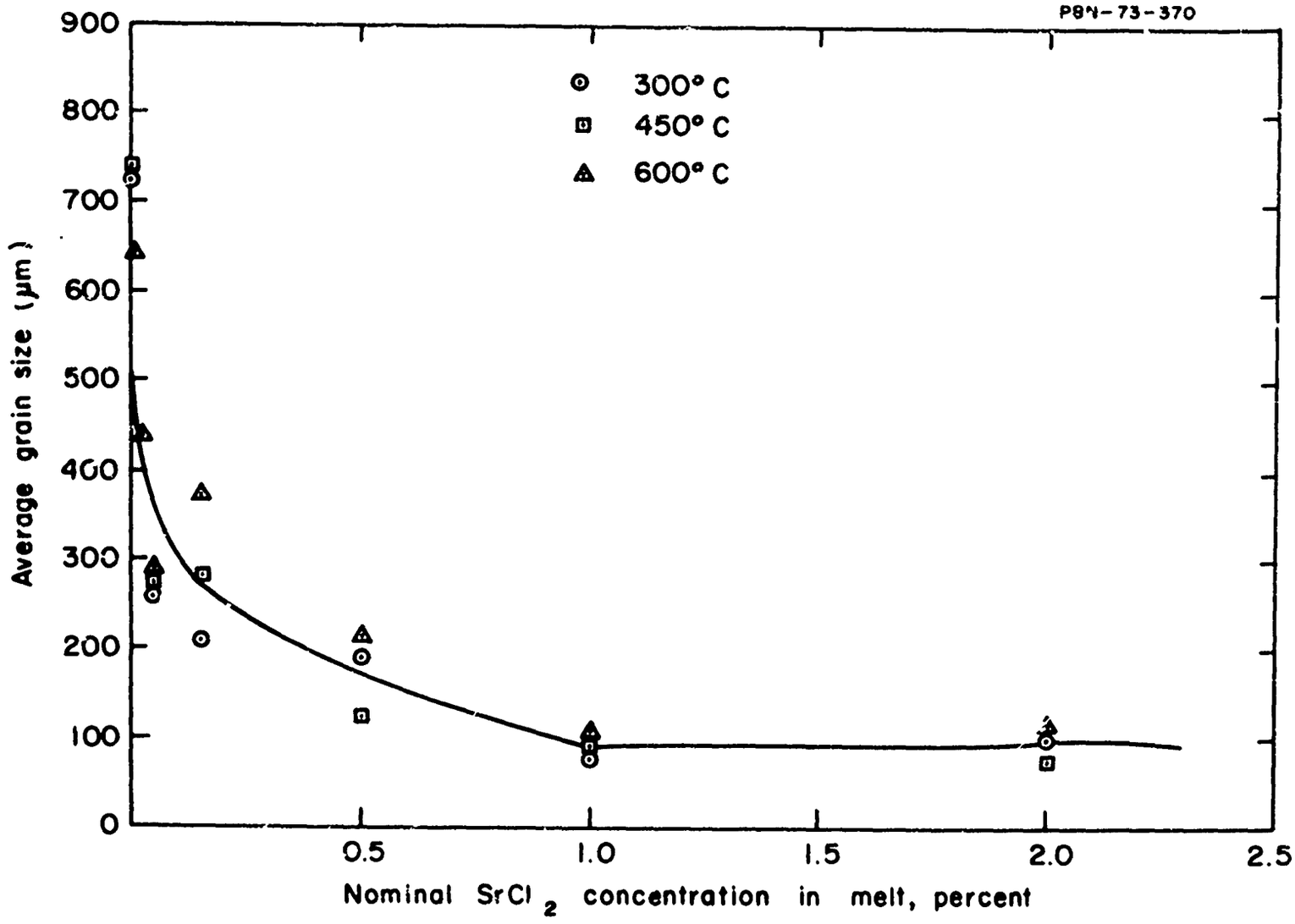

Fig. IV-32 The Effect of $SrCl_2$ Content and Casting Temperature on the Grain Size of Poured Alloy Castings.

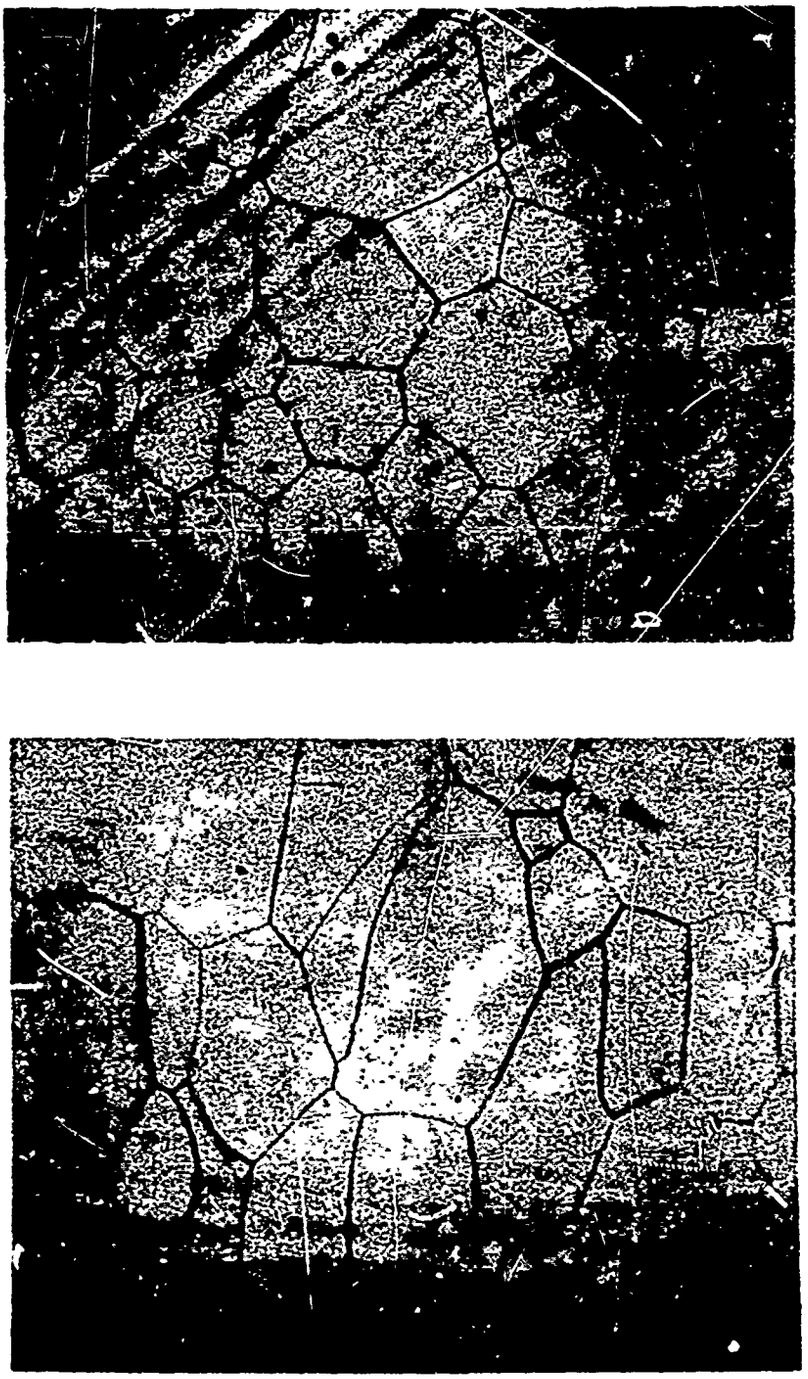

Fig. IV-33 Microstructure of Cast 1500 ppm Nominal $SrCl_2$ Alloy Cast at 600°C. Top: Transverse to freezing direction. Bottom: Parallel to freezing direction. 50X.

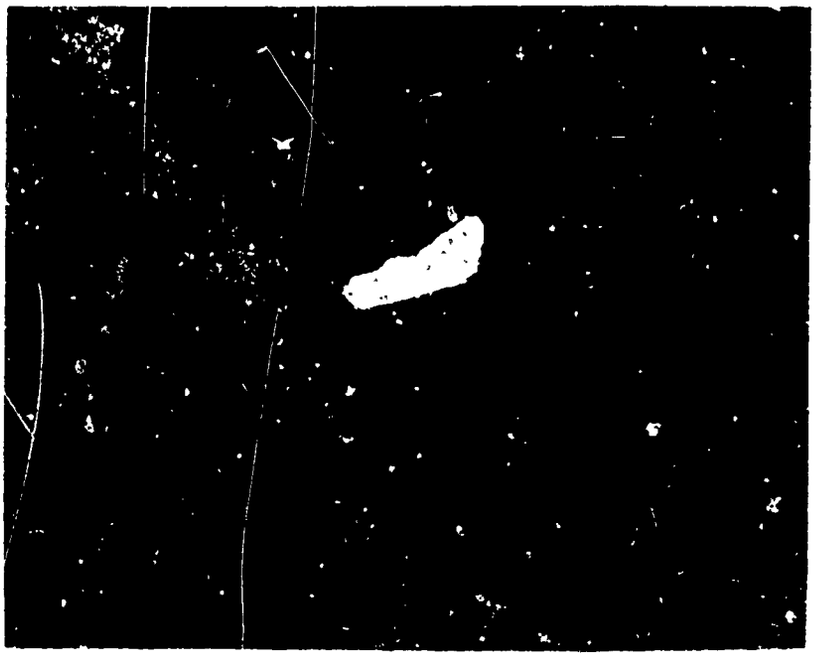

Fig. IV-34 Microstructure of Cast Nominal 1 Percent $SrCl_2$ Alloy. 250X.

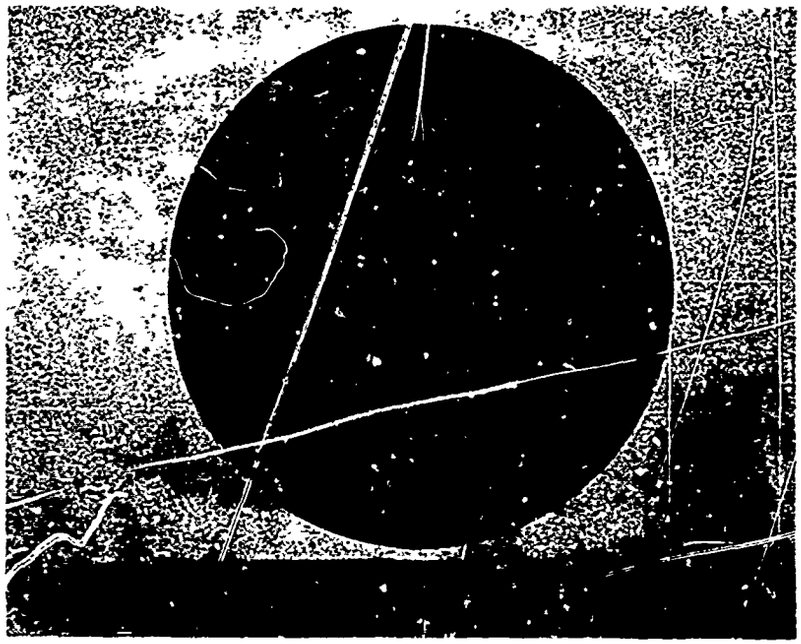

Fig. IV-35 Casting NPC-21 As Cast in Graphite Crucible with Grafoil Liner.

With the exception of two castings, all were doped with $SrCl_2$ at nominal levels of 200, 300, or 500 ppm using one of the cooling programs described earlier. Although many runs resulted in successful castings, cracking during subsequent cleaning or handling was still a problem. Because precipitation occurred during the cooling cycle, the 200 ppm dop. level was finally selected to produce optically transparent, precipitate-free material. Due to unidirectional solidification and the segregation of $SrCl_2$, even the 200 ppm castings contained precipitates, but these were concentrated in the center zone of the top portion of the castings leaving the main body of the casting transparent. In production, the precipitated area could be cut or polished away.

Figures IV-36 to IV-38 show typical castings doped at the nominal levels of 200, 300 and 500 ppm $SrCl_2$, respectively. The samples are shown as-cast and viewed from the bottom. As can be seen, precipitation in the 500 ppm-doped material occurs throughout the casting except for minor edge effects. The 300 ppm-doped casting shows less precipitates and a cross section, parallel to the direction of solidification, would reveal completely transparent material in the bottom 1/4 in. of the casting with the top 1/2 in. being opaque. The 200 ppm doped casting has even less precipitate and, as indicated above, is visibly transparent in the bottom 1/2 in. of the casting. Figure IV-39 shows a polished 1/2 in. thick section of a 200 ppm-doped casting.

b. $SrCl_2$ segregation

Due to the unidirectional solidification, a concentration gradient from bottom to top was expected, as shown empirically by the precipitation patterns of castings. Figure IV-40 plots the measured concentration gradient of $SrCl_2$ through the vertical cross section of a 200 ppm $SrCl_2$-doped casting. Concentrations were determined by the X-ray fluorescence method previously discussed. As measured, the concentration ranges from about 60 ppm $SrCl_2$ at the bottom to about 800 ppm $SrCl_2$ near the top of the casting. In addition, the concentration remains low up to about 10 mm from the base at which point precipitates were noticed. A detailed gradient analysis for a heavily precipitated 500 ppm-doped casting was not performed, but for NPC-2 the measured concentration ranged from about 200 ppm at the bottom and about 600 ppm in the center, to about 1000 ppm near the top. However, as indicated above, the presence of precipitates or of $SrCl_2$ itself appears to have little effect on

Fig. IV-36 Casting NPC-17 (200 ppm nominal $SrCl_2$) as Cast. Bottom view.

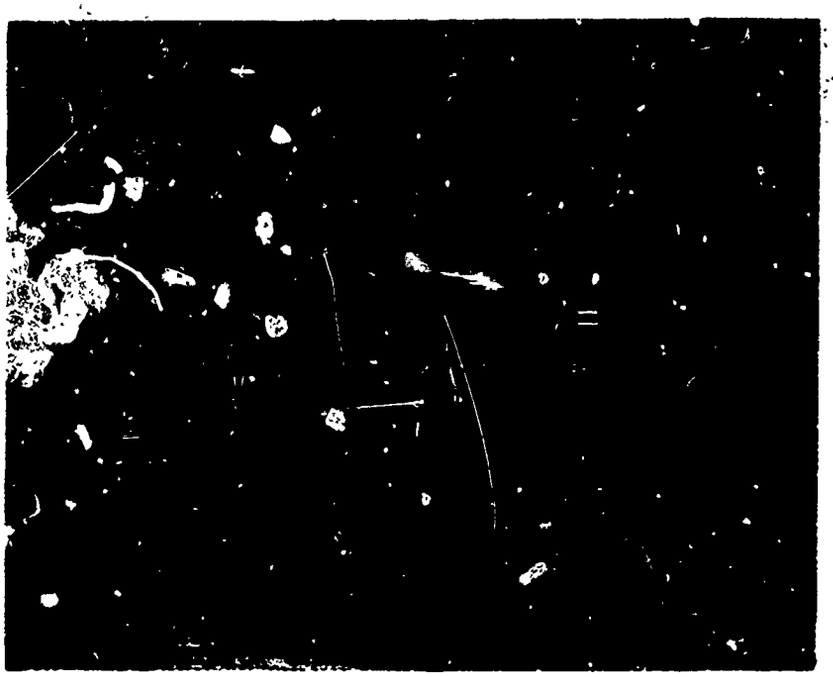

Fig. IV-37 Casting NPC-12 (300 ppm nominal $SrCl_2$) as Cast. Bottom view.

Fig. IV-38 Casting NPC-9 (500 ppm nominal $SrCl_2$) as Cast. Bottom view.

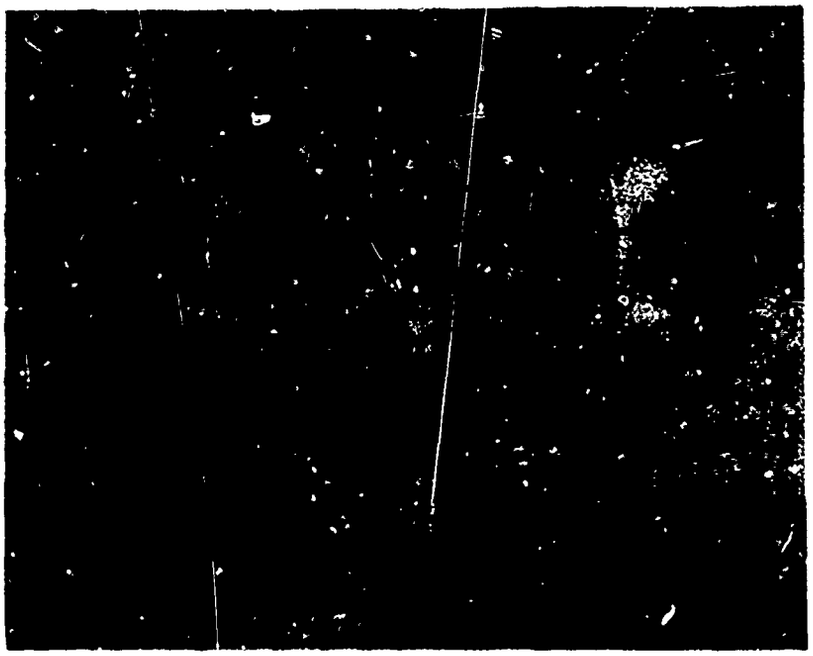

Fig. IV-39 Two Inch Diameter × 1/2 Inch Thick Section of Casting NPC-15 (200 ppm nominal $SrCl_2$).

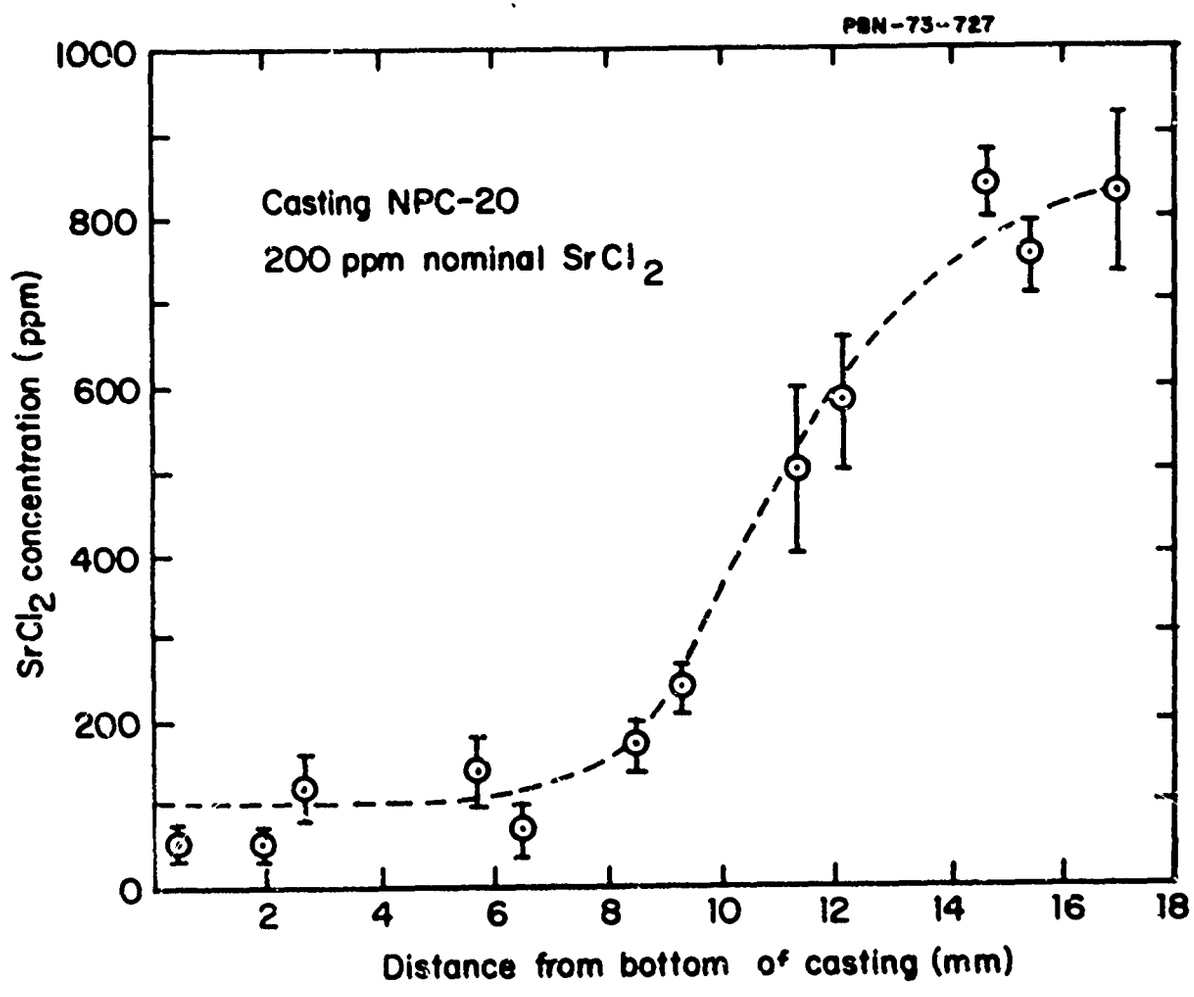

Fig. IV-40 $SrCl_2$ Concentration as Analyzed in Casting NPC-20.

10.6 μm optical properties. The worst effect of this concentration gradient would be a variation of mechanical properties through the thickness of the final window.

c. Microstructure

A typical microstructure of the Sr-doped castings is shown in Fig. IV-41. Little effect of Sr-doping level was actually seen, with grain sizes ranging up to several millimeters. However, the undoped castings were large-grained with grain sizes of about 1 cm, again showing the desirability of doping for grain size reduction.

d. Residual stress

As previously mentioned a major problem in the castings was the high residual strain produced during cooling. While various cooling cycles were developed, none produced a completely strain-free casting. Subsequent handling of the castings has been made difficult by this strain and several have cracked during the removal of the residual grafoil from the casting. Water was generally used and cracking was caused either by the sudden cooling of the surface by the evaporating water or the dissolution of a thin layer of the casting surface. The strain problem is further illustrated in Fig. IV-42 which shows a 1/2 inch thick section of casting NPC-15 as viewed between crossed polarizers, thus revealing the strain pattern. Several cracks which developed during polishing are also shown. Our results indicate that strain-free samples are not the rule and strain is a severe problem which must be still overcome.

The sources of strain appear to be twofold. First, intergranular stresses occur particularly with the large grain size, pure KCl. Frequently, cracking occurs during subsequent cutting and polishing of the ingots even after they have been annealed. This strain is probably the result of the limited number of independent slip systems available in these alkali halides at low temperatures which prevent general deformation of the grains. As the ingot cools down to the vicinity of a few hundred degrees centigrade, only the (110) <110> slip systems are operative. As a result, thermal gradients cause

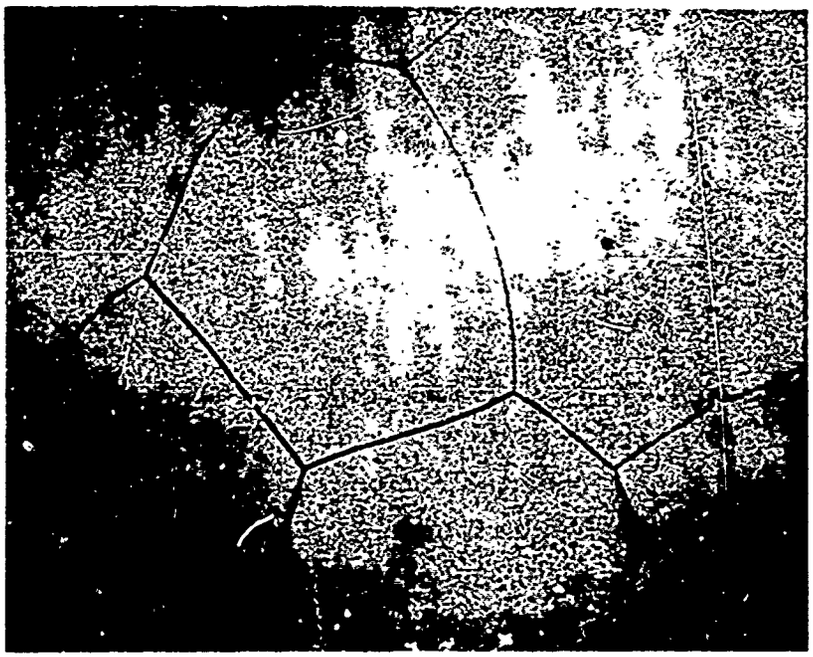

Fig. IV-41 Microstructure in As-Cast Sample NPC-4 (200 ppm nominal $SrCl_2$). 50X.

Fig. IV-41 Microstructure in As-Cast Sample NPC-4 (200 ppm nominal $SrCl_2$). 50X.

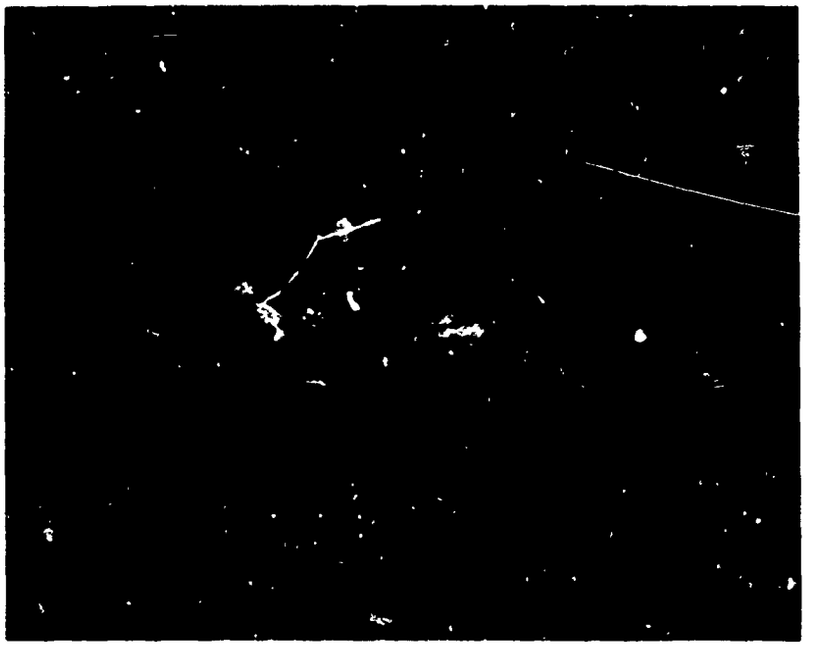

Fig. IV-42 Strain Pattern of Casting NPC-15 (200 ppm nominal $SrCl_2$) as Viewed Through Crossed Polarizers. Three inch diameter sample.

plastic flow and dislocation pileup at grain boundaries. This pileup can then produce a high stress at a boundary. Similarly, during polishing and handling, plastic flow on these limited slip systems will cause pileup at boundaries and cracking. The situation is aggravated in very large grain ingots since the total strain is taken up at only a few grain boundaries causing high stresses. We have observed that in fine grain ingots, intergranular cracking is somewhat less frequent than with large grain ingots although the data is limited. In the case of alloys, a similar situation occurs, but, the grain size in alloys is somewhat smaller and the stress problem is less severe.

In order for casting to be a viable fabrication technique, these casting stresses must be eliminated. We are confident that a proper time-temperature cool down or post-casting annealing can be found to completely eliminate residual stresses so that casting can be used to fabricate high-quality infrared windows.

e. Optical properties

IR transmission spectra were run on the "reagent grade" castings and revealed the variability of impurity levels. Figures IV-43 to IV-45 show the IR spectra for three Sr-doped castings. Figure IV-46 shows the IR spectrum for the undoped KCl casting. All four castings show the NCO^- peak at about 2180 cm^{-1}. The three doped castings show $CO_3^=$ peaks in the 1400 to 1500 cm^{-1} region and $SO_4^=$ peaks in the 1100 to 1200 cm^{-1} region with intensities varying considerably between samples. The undoped sample shows little $CO_3^=$ or $SO_4^=$ but has two strong peaks at 875 and 1050 cm^{-1}. In all four cases, however, 10.6 μm loss is considerable. From the spectra, 10.6 μm absorption coefficients were calculated to be on the order of 0.01 to 0.02 cm^{-1}. With such high absorption coefficients, it was clearly evident that the material was too "dirty" for 10.6 μm calorimetric measurements.

NPC-22 was cast using Merck "suprapure" KCl. To maintain high purity, the furnace with crucibles and grafoil liner was baked at 1350°C three times before adding the melt load. With the "suprapure" KCl loaded, it was vacuum baked at the normal 300° to 400°C. No change in vacuum was noted, indicating no gas evolution which is normally observed with "reagent" grade materials.

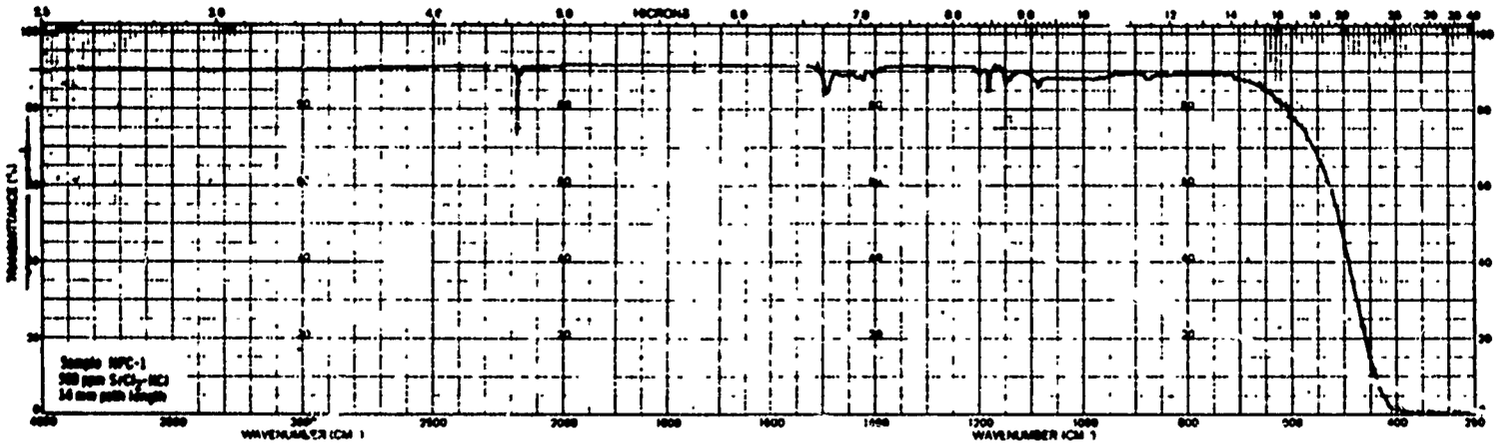

Fig. IV-43 Infrared Transmission Spectrum of Casting NPC-1 (500 ppm nominal $SrCl_2$).

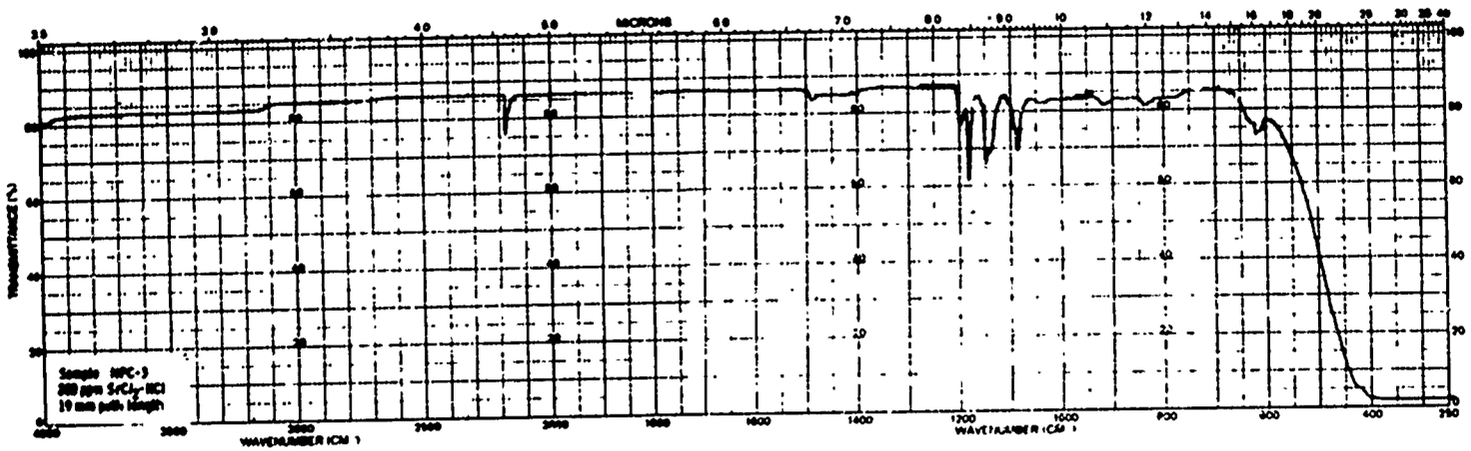

Fig. IV-44 Infrared Transmission Spectrum of Casting NPC-3 (200 ppm nominal $SrCl_2$).

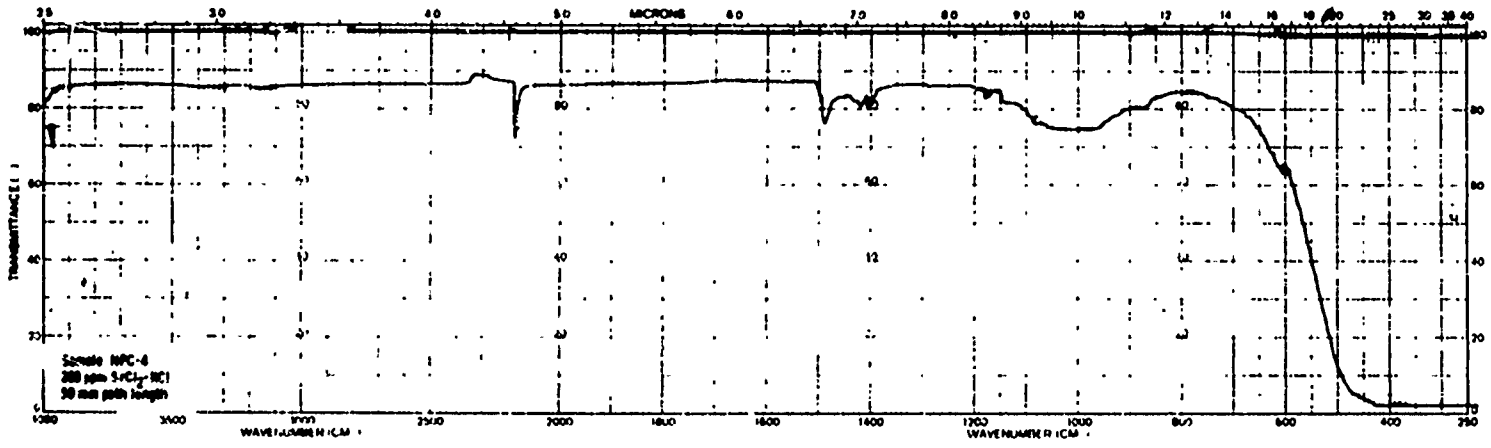

Fig. IV-45 Infrared Transmission Spectrum of Casting NPC-4 (200 ppm nominal $SrCl_2$).

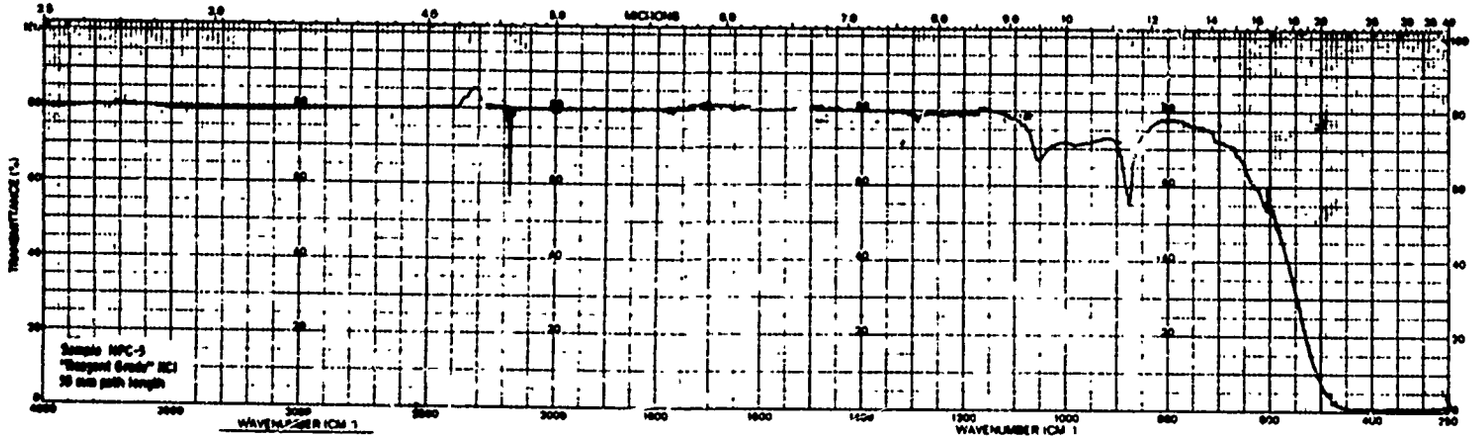

Fig. IV-46 Infrared Transmission Spectrum of Casting NPC-5. "Reagent grade" KCl.

An IR transmission spectrum of the resultant casting (Fig. IV-47) showed none of the impurities present in previous castings and indicated that a high purity casting is obtainable in the new furnace. No dip at 10.6 μm could be detected, indicating a low absorption coefficient. Figure IV-48 plots total absorption at 10.6 μm for the high-purity casting, as measured calorimetrically. The low measured absorption coefficient of $7.8 \times 10^{-4} cm^{-1}$ proves the capability of casting low loss material. This is a particularly significant result for several reasons: First, casting can lead to high purity material; Second, graphite furnace parts can be used without contaminating the material. This means that large crucibles and furnace parts required for scaleup can be made easily and economically from graphite. Third, and most significant, grain boundaries in cast material are clean and do not significantly increase the 10.6 μm absorption.

f. Mechanical properties of castings

Samples for mechanical property measurements were cut from three castings of nominal 500, 300 and 200 ppm $SrCl_2$ ingots. These samples were much larger than the single crystal samples previously discussed which were roughly 0.5 in. × 0.5 in. × 2.25. The test conditions were as described in Sec. III. None of the samples exhibited any yielding before fracture. The resulting fracture strengths are listed in Table IV-5. The reproducibility of the fracture strength suggests that fracture was initiated by plasticity rather than by flaws. The strength does increase with increasing $SrCl_2$ content and the strength of the 500 ppm casting is respectable. These results will be discussed at a later point.

D. Hot Forging

1. Pure KCl

During the first two quarters of this program approximately 38 unconstrained hot forgings of pure KCl single crystals were made to gain familiarity with the technique. Forging temperatures were varied between 160° and 400°C for total strains of 30 to 80 percent. Figure IV-49 shows that the optimum conditions were found to be between 200° and 250°C with 70 to 80 percent strain to produce a small and uniform grain size. For a higher forging temperature or greater strains, a duplex structure indicating secondary grain growth was commonly observed (Fig. IV-50). Figure IV-51 shows a typical hot-forged pure KCl sample.

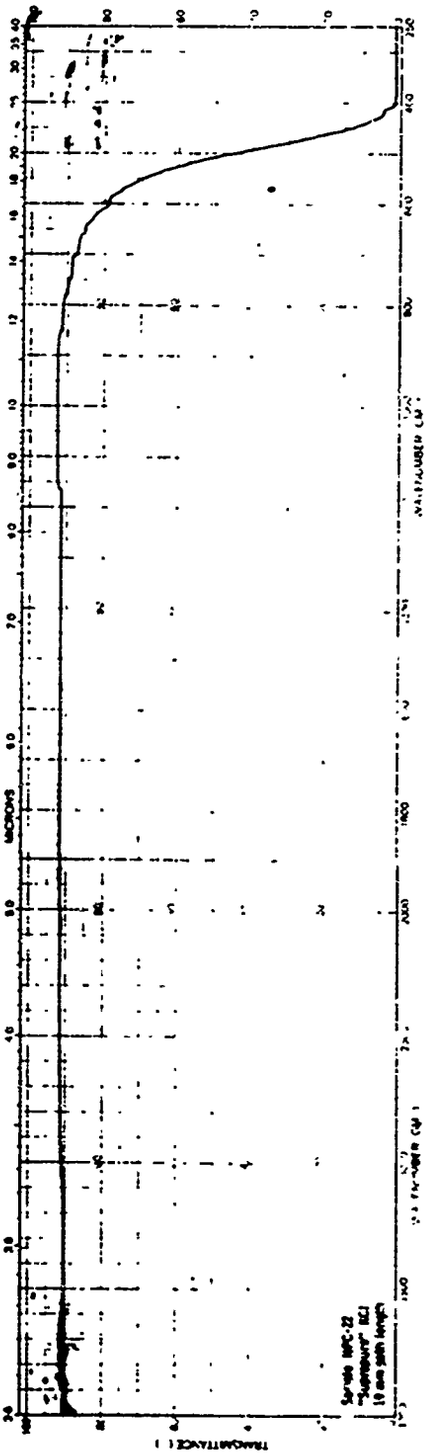

Fig. IV-47 Infrared Transmission Spectrum of Casting NPC-22. Merck starting material.

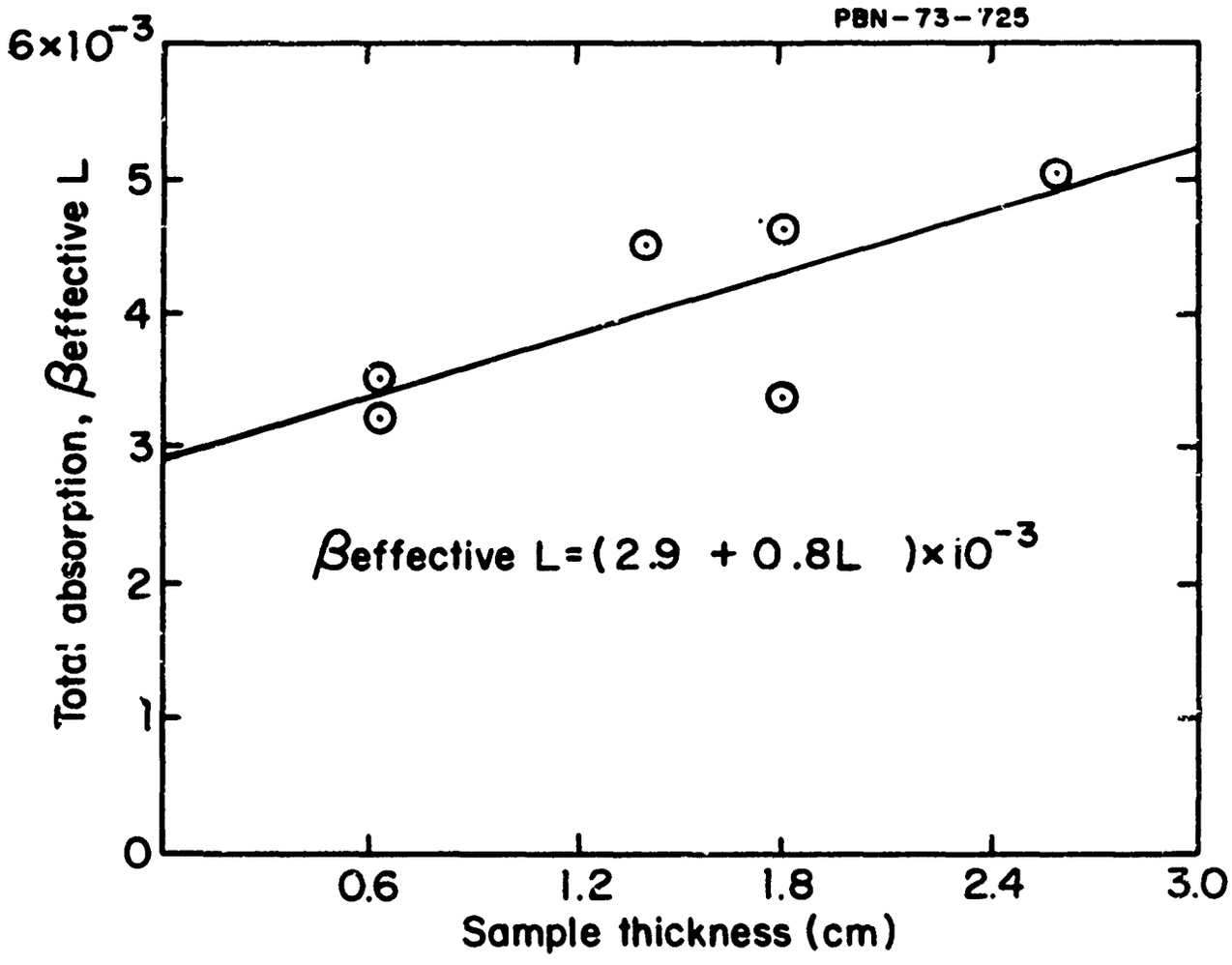

Fig. IV-48 10.6 μm Optical Absorption vs Sample Length for Casting NPC-22. Merck starting material.

TABLE IV-5

MECHANICAL PROPERTIES OF CASTINGS

Casting Number	Nominal $SrCl_2$ (%)	Fracture Strength (psi)
NPC-1	0.05	2189
		2601
		2292
		2055
		Ave. 2284 $^{+317}_{-229}$
NPC-14	0.03	2164
		1528
		1933
		Ave. 1875 $^{+299}_{-347}$
NPC-4	0.02	1573
		1506
		Ave. 1540 ± 34

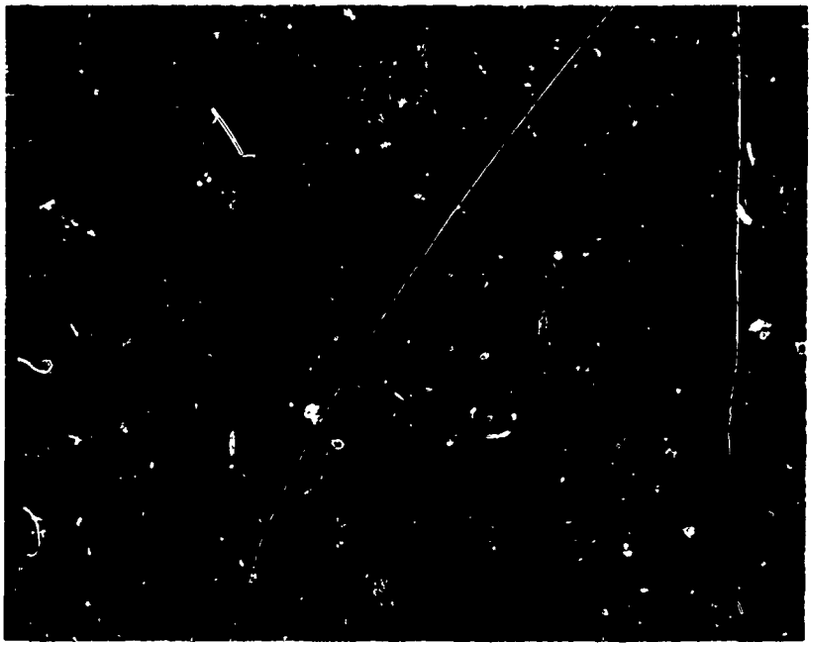

Fig. IV-49 Fine, Equi-Axed Grain Size in an As-Forged Sample. Sample No. HF-12. (Before anneal) 250X.

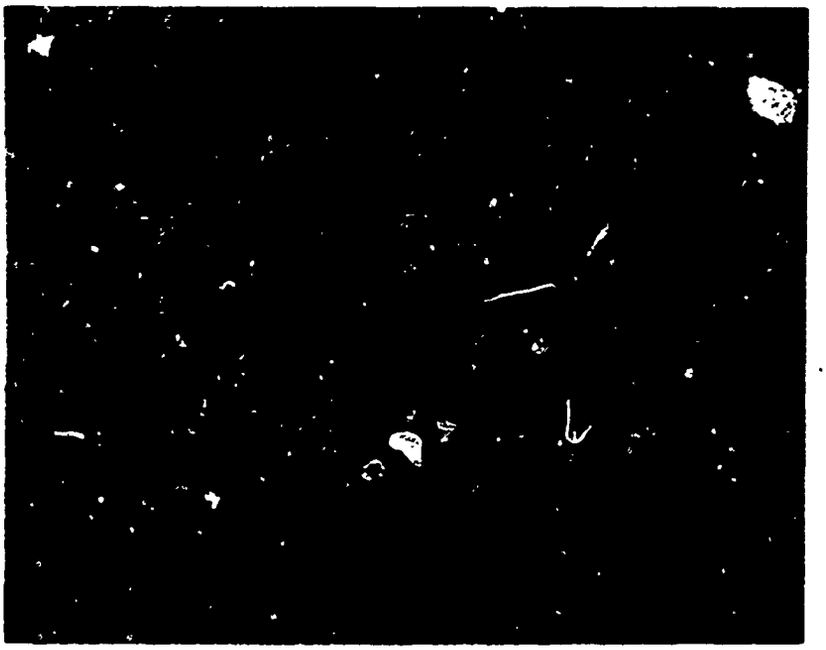

Fig. IV-50 Duplex Partially-Recrystallized Microstructure in Intermediate Anneal Temperature Sample. Sample HN-11. 250X

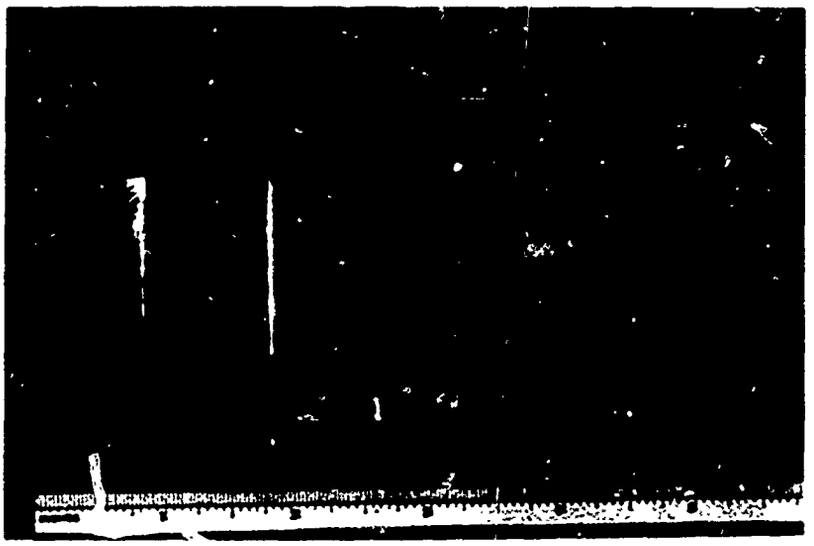

Fig. IV-51 Typical Crack-Free Hot Forged and Recrystallized Pure KCl Crystal.

Annealing was usually found to be necessary to remove residual strain as determined by polarized light examination. Typically, macroscopic strain could not be removed by annealing much below 250°C. However, at these temperatures discontinuous grain growth frequently occurred creating a duplex microstructure.

On the other hand, while annealing at a lower temperature around 100°C prior to the 250°C anneal does not remove the macroscopic strain, it does appear to prevent discontinuous grain growth during subsequent anneals at the elevated temperatures. Presumably, the major driving force for discontinuous grain growth is residual microscopic strain which is removed in the low temperature anneal. By following the two-step annealing procedure, strain-free, fine-grained polycrystalline material can be obtained.

2. $SrCl_2$-KCl alloys

During the fourth quarter, emphasis was placed on hot forging $SrCl_2$-doped crystals and about 45 hot forgings were performed. The purpose was to investigate the effects of temperature, strain, and post-forging annealing on the microstructure and properties of the Sr-doped material. Initially, strains of 35, 50, and 70 percent were chosen, but it was found that the only significant grain-size reduction occurred with the 70 percent strain. Therefore, nominal reductions were increased to 60, 70 and 80 percent. For each composition, three temperatures were chosen for investigation. As the $SrCl_2$ concentration increased, the forging temperature had to be increased in order to obtain a crack-free forging. For example, the 1500 ppm nominal $SrCl_2$-doped crystals could be successfully hot forged as low as 275°C while the one percent crystals could not be forged much below 325°C. Typically, the average grain size, as measured by the linear intercept method, was below thirty micrometers. However, the measurement of grain size in the $SrCl_2$-doped materials proved to be more difficult than in the case of pure KCl. Figure IV- 52 shows a typical hot-forged alloy. As this figure illustrates, not all grain boundaries etch equally as was the case in pure KCl. As a result, it is somewhat unclear as to what are true boundaries. No duplex microstructure was observed in any of these alloys, as with the pure KCl. Only at the very high temperature (500°C) do all of the grain boundaries etch uniformly to a

Fig. IV-52 Hot Forged Microstructure of Hot Forged Sample HF-29. 0.5 Percent $SrCl_2$, 70 Percent Strain, 40°C. 250X.

good, although large, average grain size. The average grain size was not terribly sensitive to either strain or temperature. Nevertheless, grain sizes below ten micrometers could not be obtained with any of the combinations of strain and temperature investigated.

In many cases, precipitation occurs during forging of the more concentrated alloys which doubtlessly affects the final grain size and microstructure. Unfortunately, it is exceedingly difficult to separate the effects of precipitation from the time and temperature effects on the microstructure.

3. $KCl-SrCl_2$-castings

The main effort of hot forging during the last part of the program was directed toward the polycrystalline, cast $SrCl_2$-KCl alloys. Thirty hot forgings were performed on samples of cast material. The castings were nominally doped with 200, 300 and 500 ppm $SrCl_2$. Forging temperatures of 300°, 325° and 400°C were selected for investigation but several other temperatures were also tried. Nominal reductions ranged from 55 to 80 percent. The resultant forged samples generally were about 2 in. diameter.

The average grain size of each hot forging was determined by the linear intercept method. The average grain sizes for the hot forged castings lie in the 20 to 30 micrometer range, and as was found with the Sr-doped single crystals, the average grain size was not particularly sensitive to either the total strain or temperature over the range investigated. The hot forgings of 400°C resulted in good microstructures as shown in Fig. IV-53. Forging at the lower temperatures investigated produced microstructures with areas of ill-defined grain boundaries.

Figures IV-54 and IV-55 show two examples of hot-forged cast material, the former being precipitate-free (200 ppm $SrCl_2$) and the latter showing precipitation (500 ppm $SrCl_2$). The 500 ppm Sr-doped material had precipitated prior to hot forging and any resultant effect on microstructure is unknown.

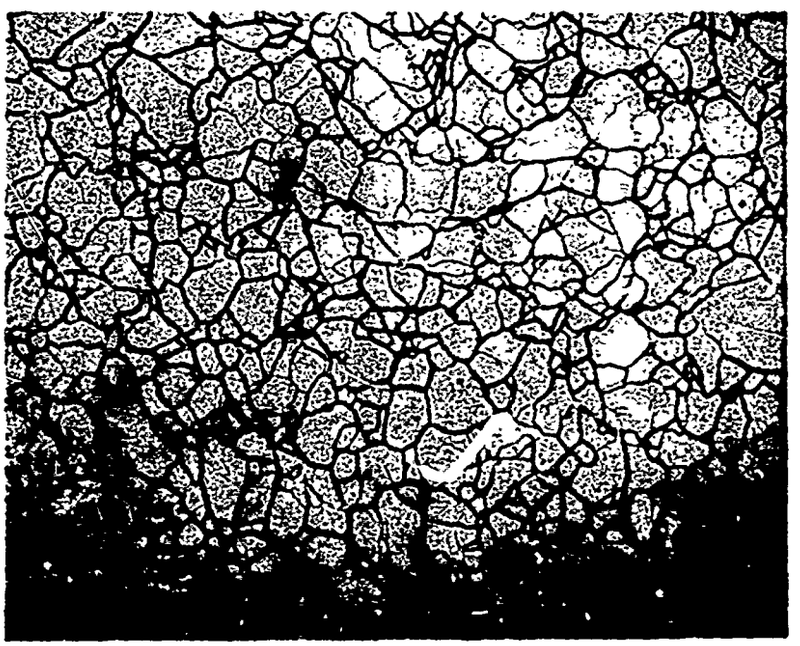

Fig. IV-53 Microstructure of Hot Forged Sample (HF-82) of Casting NPC-14. 400°C Forging Temperature; 69 percent reduction. 250 X.

Fig. IV-54 Typical Crack-Free Hot Forged Sample (HF-90) of Casting NPC-20 (200 ppm nominal $SrCl_2$). Precipitate free.

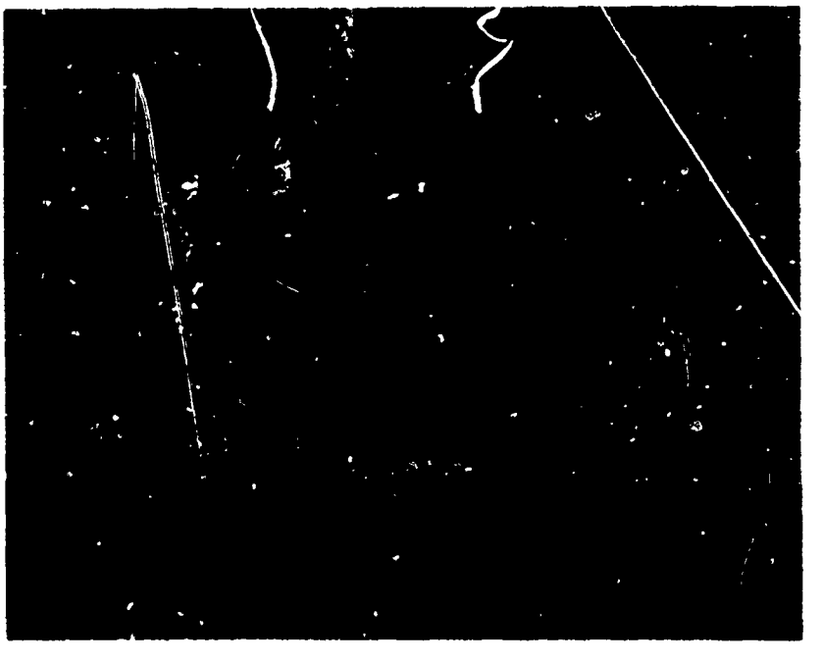

Fig. IV-55 Typical Crack-Free Hot Forged Sample (HF-69) of Casting NPC-1 (500 ppm nominal $SrCl_2$), Showing Precipitate.

4. Mechanical properties of hot forged materials

a. Single crystals

Table IV-6 lists typical yield strengths of various hot-forged single crystals. There is not enough data to draw any conclusions with regard to the effects of grain size on yield strength except that the solution-treated samples have slightly higher yield strengths than comparable single crystals. The non-solution-annealed samples tend to give a lower yield strength than either the solution-treated polycrystalline samples or the single crystal material. This is probably due to precipitation during forging, although as described earlier the effect has not been found consistently with heat-treated single crystals.

TABLE IV-6

YIELD STRENGTH OF HOT FORGED MATERIALS

Sample Number	$SrCl_2$ Concentration, Nominal (percent)	Grain Size (μm)	Yield Strength* (psi)
HF-35	0	7	2262
HF-13	0.1	4-200	1770
HF-11	0.2	20-200	1714
HF-10	0.5	20-2000	2814
HF-12	1.0	20-200	4291
HF-23**	0.5	15	4595
HF-29**	0.5	20	5278
HF-14**	1.0	45	5577
HF-47**	1.0	29	4519

* Average of 3 samples

** Samples solution treated at 700°C for 5 minutes prior to testing. No grain growth observed.

b. Castings

Samples for yield strength determination were cut from hot forgings of castings of nominal 200, 300, and 500 ppm $SrCl_2$. These were again small samples and the results are listed in Table IV-7. As was previously discussed, it was not possible under the conditions used to obtain small grain sizes by hot forging these materials. Forging at lower temperatures usually resulted in cracking. The results with these initially polycrystalline materials are essentially the same as obtained with the $SrCl_2$ - doped, single crystal forgings; namely, grain sizes below 20 μm are difficult to achieve. As a result, the yield strengths are not particularly high.

E. Comparison of Strength of Single Crystals, Forgings, and Castings

Although, there is rather limited data, Fig. IV-56 plots the yield strengths of as-cast, cast-hot-forged, hot-forged single crystal and single crystal alloys versus $SrCl_2$ content. The $SrCl_2$ contents of the single crystals were actually measured, while those of the castings and forgings were estimated from their nominal compositions and the segregation coefficient presented earlier.

The fracture strength of the as-cast material is not much different from yield strength of a doped single crystal of the same composition. This is not unexpected, considering the large grain size of the cast material. The yield strengths of the hot forged cast alloys is roughly a factor of two higher. A significant conclusion therefore, is that cast materials can be hot forged successfully to produce polycrystaliine alloys having yield strengths about a factor of two higher than a single crystal with the same $SrCl_2$ doping. It appears that at low Sr^{2+} concentration, hot forging of both cast and single crystal alloys significantly improves the yield strength. However, at higher alloy contents, forging produces only a modest improvement. This is not a completely fair comparison however, because of the higher alloy contents, precipitation occurs during forging, making it exceedingly difficult to separate the effects of alloying and grain size reduction.

TABLE IV-7

YIELD STRENGTH DATA ON HOT FORGED CASTINGS

Sample	%$SrCl_2$ Nominal	Temp.	% Reduction	Grain Size (μm)	σ_{ys} (psi)	Casting	
HF-77	0.02	325	58	12	-	NPC-3	
-79		325	65	20	3875	NPC-3	
-87		400	61	24	2860	NPC-19	$\overline{\sigma}_{ys} = 3434^{+441}_{-574}$
-88		400	65	20	3479	NPC-20	
-91		400	70	25	3522	NPC-20	
-92		500	65	35	-	NPC-20	
HF-86	0.03	400	55	32	3183	NPC-14	
-81		400	62	35	-	NPC-14	
-82		400	69	23	-	NPC-14	$\overline{\sigma}_{ys} = 3226 \pm 43$
-85		400	77	22	3269	NPC-14	
HF-74	0.05	275	54	21	-	NPC-1	
-73		300	50	30	4368	NPC-1	
-71		300	66	24	4145	NPC-1	$\overline{\sigma}_{ys} = 4149^{+2082}_{-1480}$
-68		325	60	24	6232	NPC-1	
-67		325	65	20	3332	NPC-1	
-70		325	77	25	2669	NPC-1	

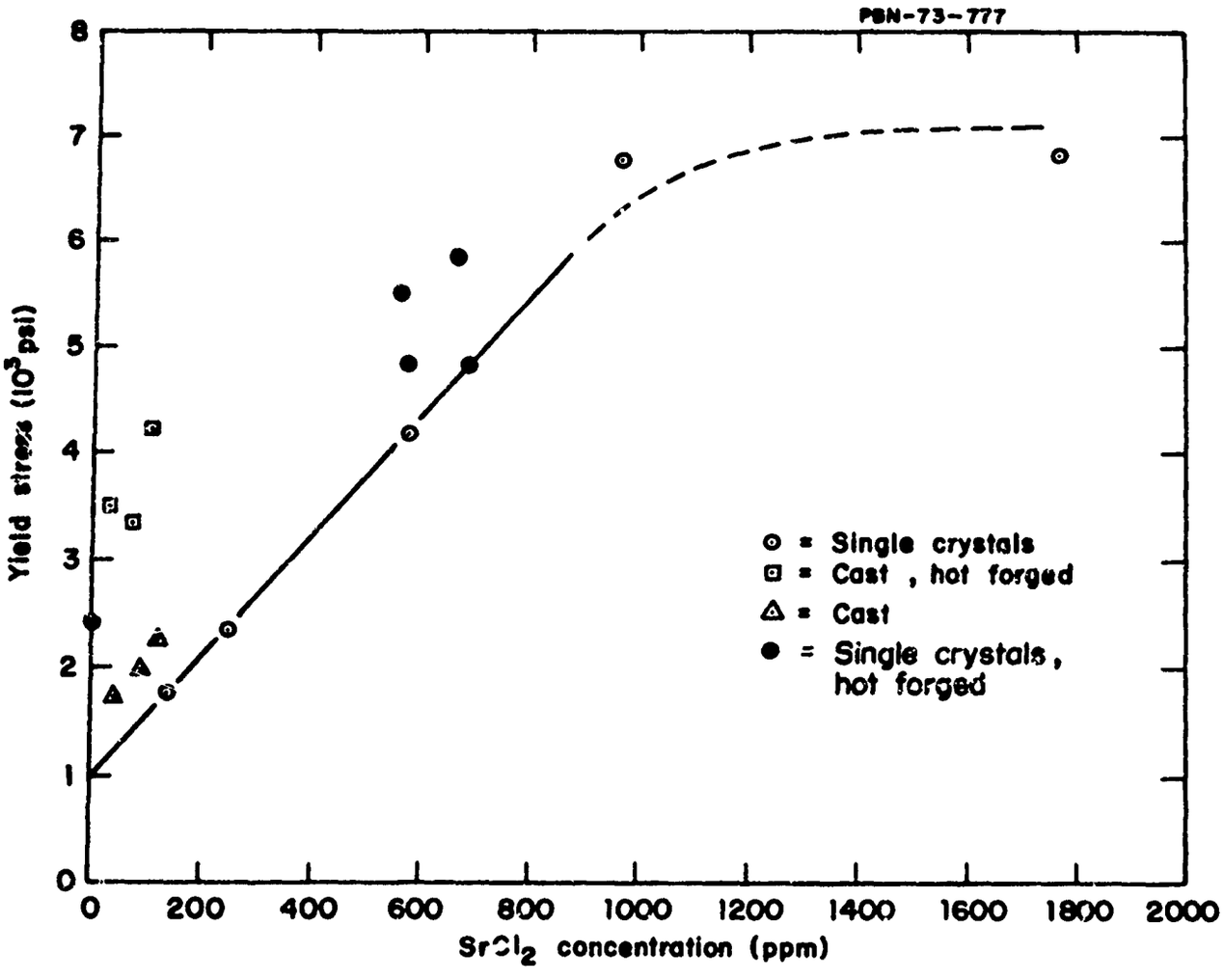

Fig. IV-56 Strength vs $SrCl_2$ Content for Single Crystals, Polycrystalline Cast, and Cast and Hot Forged KCl.

F. Preferred Orientation Studies

The preferred crystallographic orientations were determined by X-ray diffraction of: (1) a hot forged KCl single crystal; (2) a small two furnace, 1500 ppm nominal $SrCl_2$-doped casting; (3) a hot forged, in situ cast small 100 ppm $SrCl_2$-doped casting; (4) a 500 ppm $SrCl_2$ nominal large casting; and (5) a 300 ppm nominal $SrCl_2$ large casting.

The <100> forged single crystal, as expected, was found to have a strong <100> orientation normal to the surface. The half maximum angular spread of the <100> normal was found to be about 15°. This was determined by setting the sample of the Bragg condition for the (100) reflection and then rotating or rocking the sample on its axis.

In a similar fashion, the cast and cast-and hot-forged samples were found to have a surprisingly strong <110> orientation normal to the sample surface or parallel to the freezing direction. The angular dependence of diffracted intensity for the cast sample was not a smooth curve due to the larger grain size, on the order of several hundred micrometers. Nevertheless, the angular spread at half maximum intensity was about 10°. For the cast and hot forged sample the grain size was much smaller and gave a reasonably continuous curve of diffracted intensity as the sample was rocked. Figure IV-57 shows the results. Hot forging did little to decrease the preferred orientation and the half maximum spread in the <110> direction is about seven degrees.

In contrast, both NPC-1 (500 ppm nominal $SrCl_2$) and NPC-14 (300 ppm nominal $SrCl_2$) were found to have very strong <100> orientation parallel to the freezing direction. This apparent difference in preferred orientation between the small and large cast samples is indeed puzzling. It may be a real effect having its origin in the different cooling rates. The large samples were usually solidified over longer periods of time than the smaller samples. On the other hand, it may not be a systematic effect and the degree of preferred orientation may vary from casting to casting. In any event, it certainly seems clear that casting does not provide a random crystallographic texture. The fact that the texture is so strong is doubtlessly due to the directional solidification.

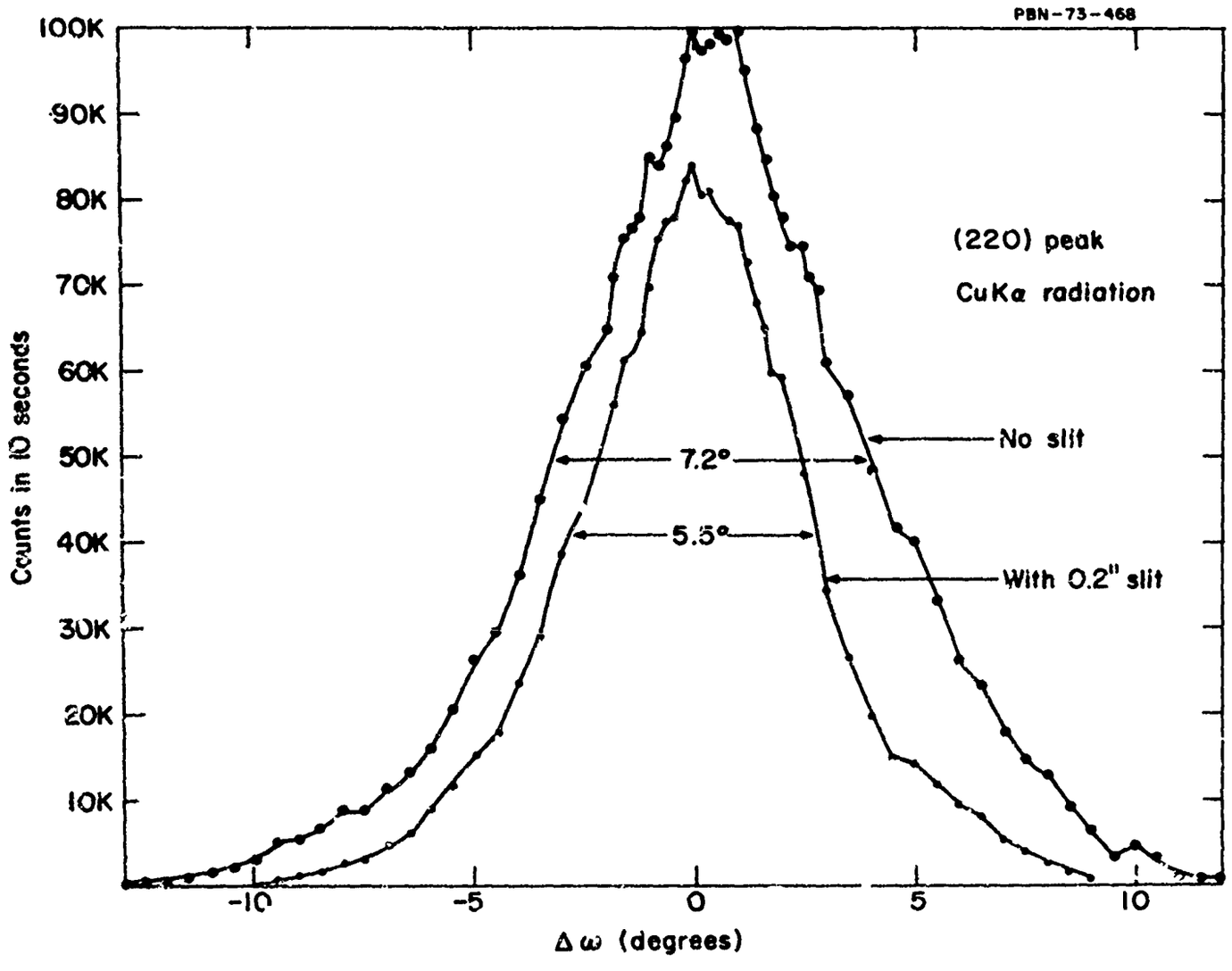

Fig. IV-57 Angular Spread of the <220> Direction Normal to the Sample Surface of a Cast and Hot Forged $SrCl_2$ Doped KCl Ingot.

G. Etch Pit Studies

1. General

We believe that the difficulty encountered with casting and handling large grain alkali halides is probably due to cracks being initiated by dislocation pileup at grain boundaries. The sources of cracking appear to be twofold. First, intergranular cracking occurs particularly with the large grain size, pure KCl. Frequently, this cracking occurs during subsequent cutting and polishing of the ingots even after they have been annealed. This cracking is probably the result of the limited number of independent slip systems available in these alkali halides, at low temperatures, which prevent general deformation of the grains. As the ingot cools down to approximately a few hundred degrees centigrade, only the $\{110\}$ <110> slip systems are operative. As a result, thermal gradients cause plastic flow and dislocation pileup of grain boundaries. This pileup can then produce a sufficiently high stress concentration at a boundary to cause cracking. Similarly, during polishing and handling, plastic flow on these limited slip systems will cause pileup at boundaries and cracking. The situation is aggravated in very large grain ingots since the local strain is taken up only at a few grain boundaries, thus causing high stresses. We have observed that in fine grain and alloy ingots, intergranular cracking is somewhat less than with large grain pure KCl ingots.

With this in mind, we undertook a brief study to develop an etch pit technique which would allow us to observe dislocations. This ability would permit us to examine local plastic strain which could lead to cracking. The availability of a dislocation etch pit technique also permits the observation of other plastic damage such as that introduced by polishing, which may play an important role in optical absorption at the surface.

2. Procedure

Three etchants were tried with equally satisfactory results: $BaBr_2$-methanol-ethanol;[30] $BaBr_2$-absolute ethanol;[31] and pure ethanol. However, most observations were performed after the ethanol etch since it is a simpler procedure. It consists of a two-to-three minute etch while stirring, and blowing dry with dry nitrogen. Figure IV-58 (a and b) shows typical

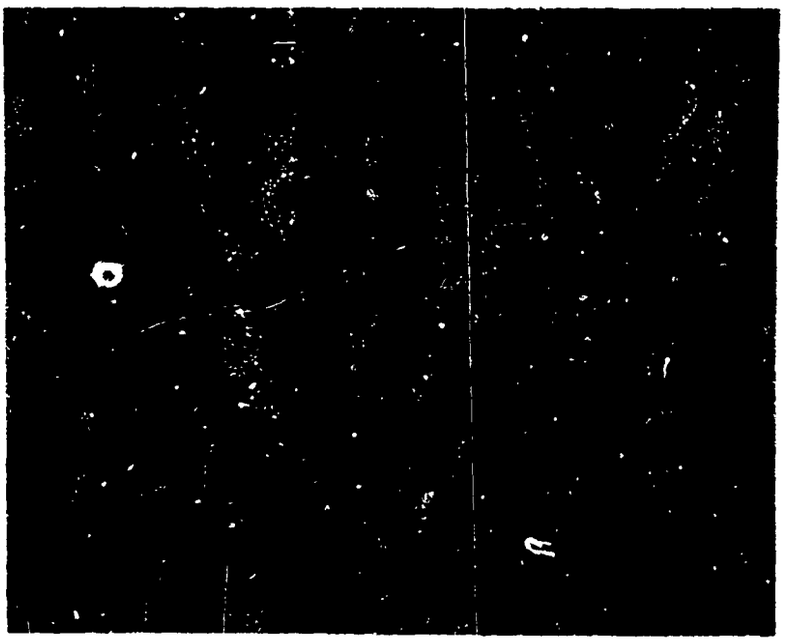

Fig. IV-58A Etched Cleaved Surface of Pure KCl Showing Etch Characteristics. 500X. All etch pit photographs were taken with Nomarski interference contrast illumination.

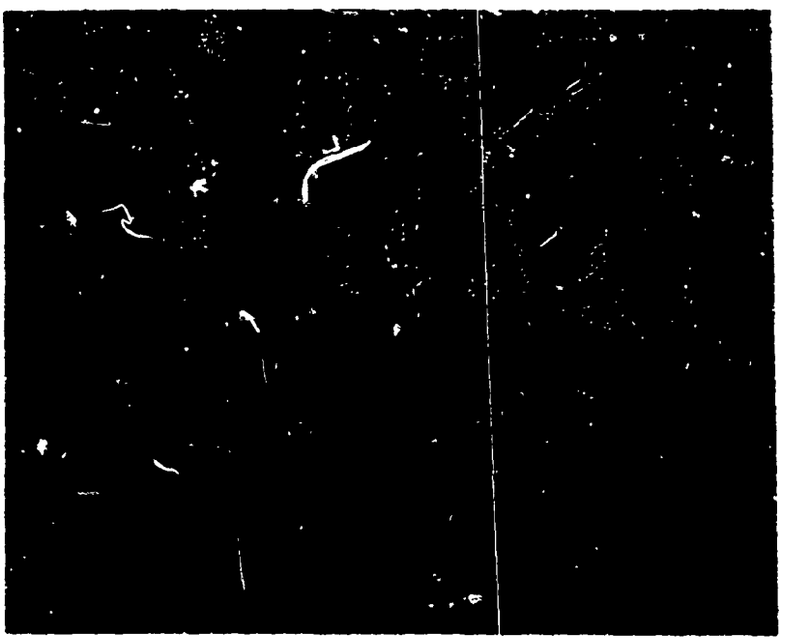

Fig. IV-58B Etched Hardness Indentations in Pure, Cleaved KCl Showing that Both Fresh and Grown-In Dislocations are Etched. 150X.

results. The strain rosettes around hardness indentations and low-angle boundaries are clearly visible and indicate that the etchant is definitely etching dislocations, both as grown and fresh. No attempts were made to correlate etch pits on both faces of a cleavage nor were any attempts made to distinguish between fresh and grown-in, or edge and screw dislocation pit geometries. Figure IV-58 shows that the etch does delineate dislocations associated with plastic flow, thus enabling the detection of damaged regions, which is the purpose of its use in this program.

3. Damage in cast, polycrystalline KCl

Several large-grain, pure KCl crystals which had cracked along grain boundaries were cleaved across several of the large grains and the cleavage face was etched. Two general observations were made that can be seen in Fig. IV-59. First, the etch pit density increases near a grain boundary with slip lines frequently discernible. Second, the density of cleavage steps increases as the boundary is approached, leaving bands of zigzag rows of pits which can be seen running horizontally. The etch pit and cleavage step density, far from the grain boundary, is typical of that shown in Fig. IV-59C Clearly, there is a significantly higher dislocation and cleavage step density near the grain boundaries. The increased cleavage step density and the zigzag or "staircase" bands of etch pits may indicate severe plastic strain during casting near the boundary, resulting in a gradual orientation change within a grain as the boundary is approached. On the other hand, poor cleavage may have been the result of the presence of the grain boundary, and the higher dislocation density the result of the poor cleavage. Therefore, the utility of examining cleaved surfaces for grown-in plastic strain is questionable.

4. Polishing damage

With the availability of the dislocation etch, it was decided to examine the damage produced by polishing in order to: 1) Observe the extent of damage, 2) compare the damage produced by our in-house procedures and those of commercial polishers, and 3) eliminate damage by the $HCl:H_2O$ polish-etch. Figure IV-60 shows the etched, polished surface and the cleavage surface normal to it. There is a significant amount of damage which extends as much as a hundred micrometers below the surface. Note that regions

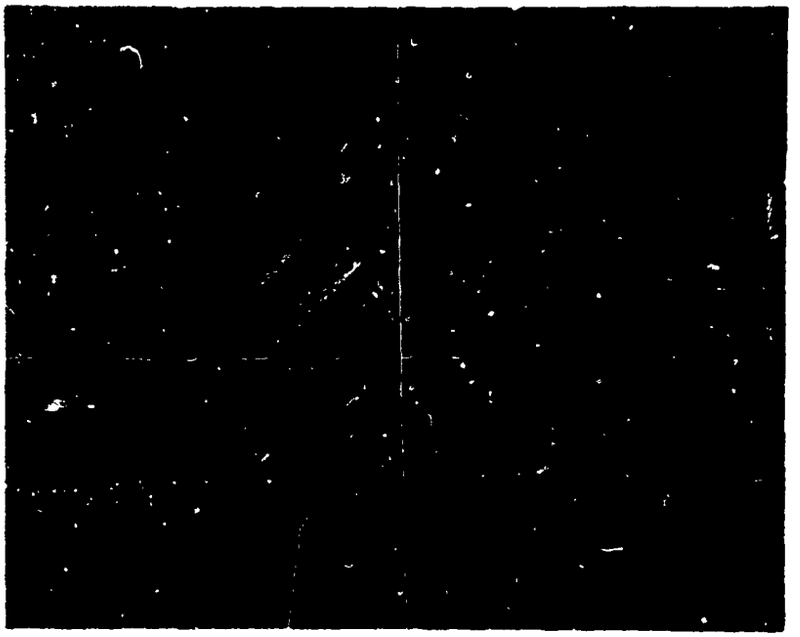

Fig. IV-59A Dislocation Etch Pits and Cleavage Steps Near a Grain Boundary in a Large Grain Cast Pure KCl Sample. The grain boundary is toward the top of the page. 150×

Fig. IV-59B Dislccation Etch Pits and Cleavage Steps Near a Grain Boundary in a Large Grain Cast Pure KCl Sample. The grain boundary is toward the top of the page. 150×

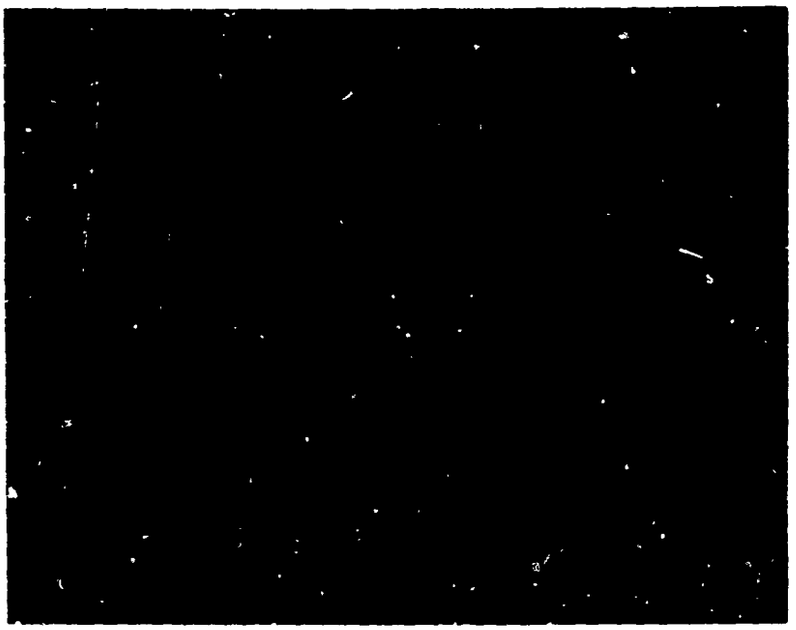

Fig. IV-59C Same as 59A except this is in the Center of a Large Grain far from the Grain Boundary. 150 X.

Fig. IV-60A Etched Polished Surface of Pure Single Crystal KCl. Visually, this etched surface looks like frosted glass. 150X.

Fig. IV-60B Etched Cleaved Surface of the Same Crystal Normal to the Polished Surface. Showing subsurface damage produced by polishing. 150X.

exist in which the damage is deeper than the average such as that just to the left of center. This locally severe damage was probably produced by isolated polishing scratches. It should be pointed out that this was a hand-polished sample. The sample was first rough ground with 600 grit silicon carbide paper with pure isopropyl alcohol as a coolant. Then an initial polish uses a slurry of 0.3 micrometer alumina in isopropyl alcohol on a polishing cloth. Final polishing is performed with a dry polishing cloth. Figure IV-61 compares the damage at the surface of another of our hand-polished crystals to that of a sample polished by a commercial polisher. Certainly, the surface damage is no greater in our hand-polished sample. Since the polishing damage can extend several hundred micrometers below the surface, it is interesting to speculate what effect this might have on the optical absorption of thin polished samples. Unfortunately, the effects of dislocations on 10.6 μm absorption are not known. In any event, it is clear that polished pure KCl single crystals have severely disturbed surface layers which can be highly reactive to the ambient atmosphere.

Figure IV-62 shows the results of etching after partial removal of the polishing damage in the crystal of Fig. IV-61B by chemical polishing in $HCl:H_2O$. An $HCl:H_2O$ ratio of 4:1 was used for about two minutes. The polished surface was blown dry. Figure IV-62A is the cleaved and etched normal surface after polishing. Figure IV-62B shows the polished surface itself and should be contrasted with Fig. IV-60A. Clearly, a large amount of the heavily disturbed polished layer has been removed and the substructure of the base crystal is beginning to become visible. Figure IV-62C is a lower magnification photograph of the polished surface showing regions of deeper damage associated with polishing scratches.

5. Summary of etching studies

A simple dislocation etching procedure has been used to examine damage in pure KCl and some alloys. There is significant damage near grain boundaries in large-grain, cast KCl but it is not clear whether this is a result of the casting or cleaving process. The damage produced by mechanically polishing pure KCl has been observed and shown to be effectively removed by the $HCl:H_2O$ chemical polish.

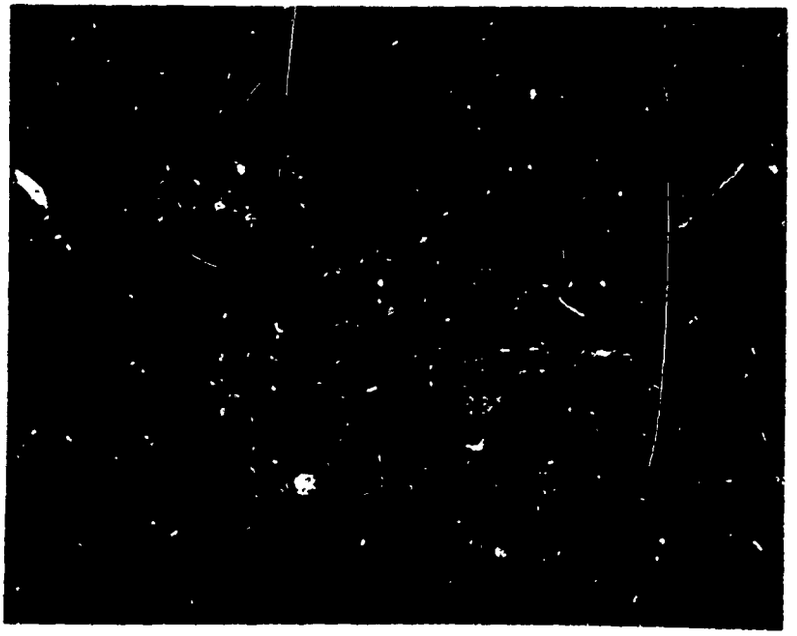

Fig. IV-61A **Polishing Damage at the Surface of a Vendor-Obtained, Optically-Polished, Pure KCl Crystal. 150X.**

Fig. IV-61B **Polishing Damage at the Surface of Another In-House Hand Polished Pure KCl Crystal. 150X.**

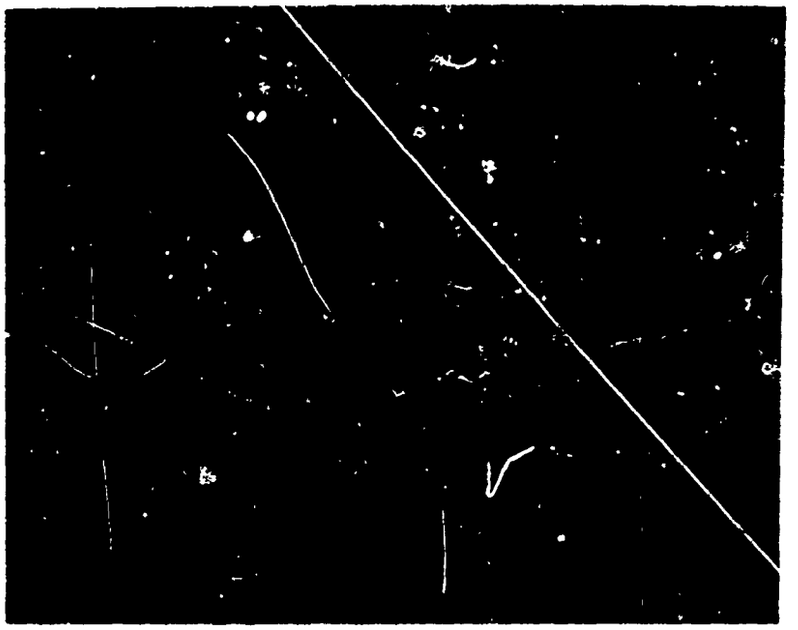

Fig. IV-62A Freshly Cleaved and Etched Surface of the same Crystal as in Fig. IV-61B after 2 min. HC1:H_2O polish of mechanically polished surface. 150 X.

Fig. IV-62B Etched Mechanically Polished Surface of the Same Crystal After HCl:H_2O Chemical Polish. 150X.

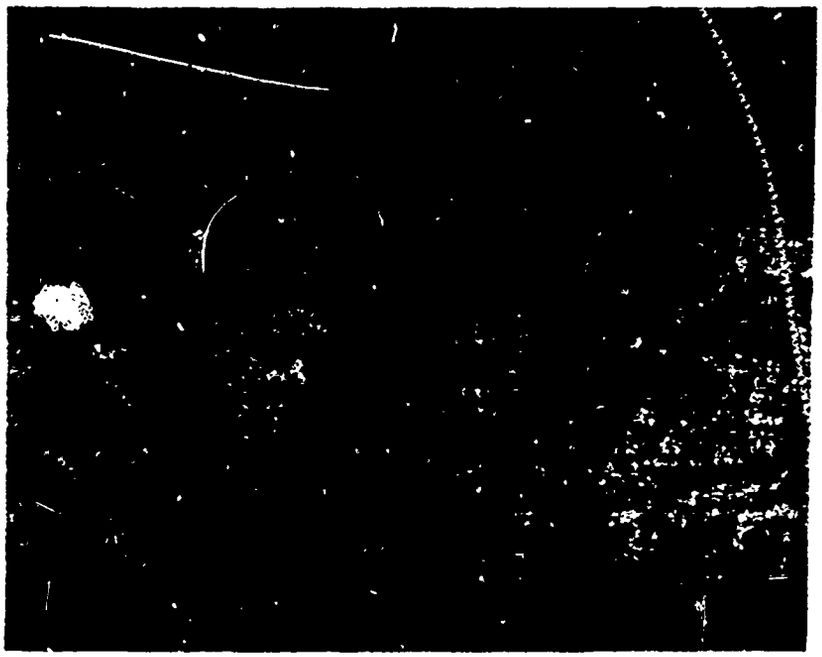

Fig. IV-62C Same as Fig. IV-62B only Lower Magnification Showing Residual, Locally Severe Damage Produced by Polishing Scratches. 50 X.

H. Reactive Atmosphere Treatment of Alkali Halides

The purification of KCl by means of high temperature reactive atmosphere treatment has been well documented. For the present investigation it was sought to learn whether or not such high temperature treatment could be used to reduce 10.6 μm absorption on material already fabricated, i.e., cast or single crystal material, rather than as a pretreatment for purification of starting materials.

A horizontal tube furnace was set up for the annealing experiments. A vycor tube with a gas inlet and outlet on opposite ends was fitted at one end with a ground glass joint for system access. As set up, the system was not a closed one, but rather an open flowing gas system. High purity helium was used as the inert carrier gas and was bubbled through CCl_4 at room temperature. The furnace was maintained at temperatures of 650°, 680° or 725°C. The exiting gases were bubbled through a KOH tower to neutralize possible reaction products. Before annealing runs the system was purged for at least 3 hours with pure helium. IR transmission spectra, run before and after the annealing treatment, were used to analyze the results.

Figures IV-63 to IV-67 illustrate the results of the effect of reactive atmosphere treatment on a single crystal grown from "reagent grade" KCl. Figure IV-63 shows the IR transmission spectrum of the 4.0 cm long crystal (as grown). Note the broadband absorption centered at about 10 μm. The crystal was subsequently cut into four sections of varying thickness. Figures IV-64 and IV-65 show the IR transmission spectra for two of the sections, the 17 mm and 12 mm thick samples, respectively. Figures IV-65 and IV-67 show the IR transmission spectra for the same two samples after having been treated in the He:CCl_4 atmosphere at 680°C for 140 hours. The 10 μm band in each samples has been significantly reduced, indicating a reduced 10.6 μm absorption coefficient. The $CO_3^=$ bands at 1400-1500 cm^{-1} have also been reduced in intensity.

The decrease in 10.6 μm absorption for this sample is shown in Fig. IV-68 which plots total absorption versus sample thickness in both the untreated and treated conditions. The 10.6 μm absorption coefficient has been reduced from 1.06×10^{-2} cm^{-1} to 3.9×10^{-3} by the CCl_4 treatment.

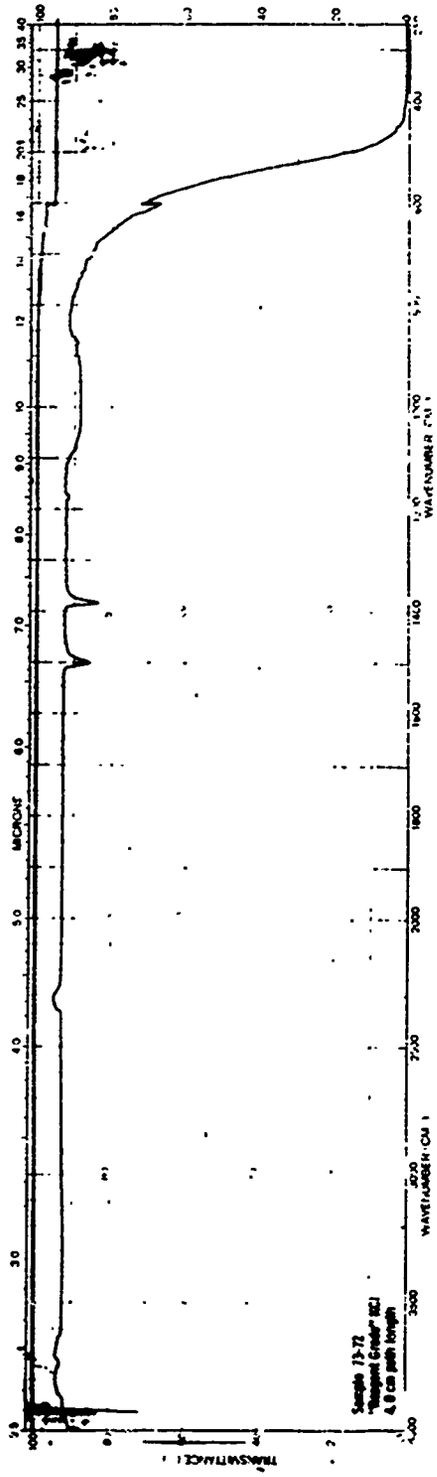

Fig. IV-63 Infrared Transmission Spectrum of Crystal 73-72. "Reagent grade" starting material.

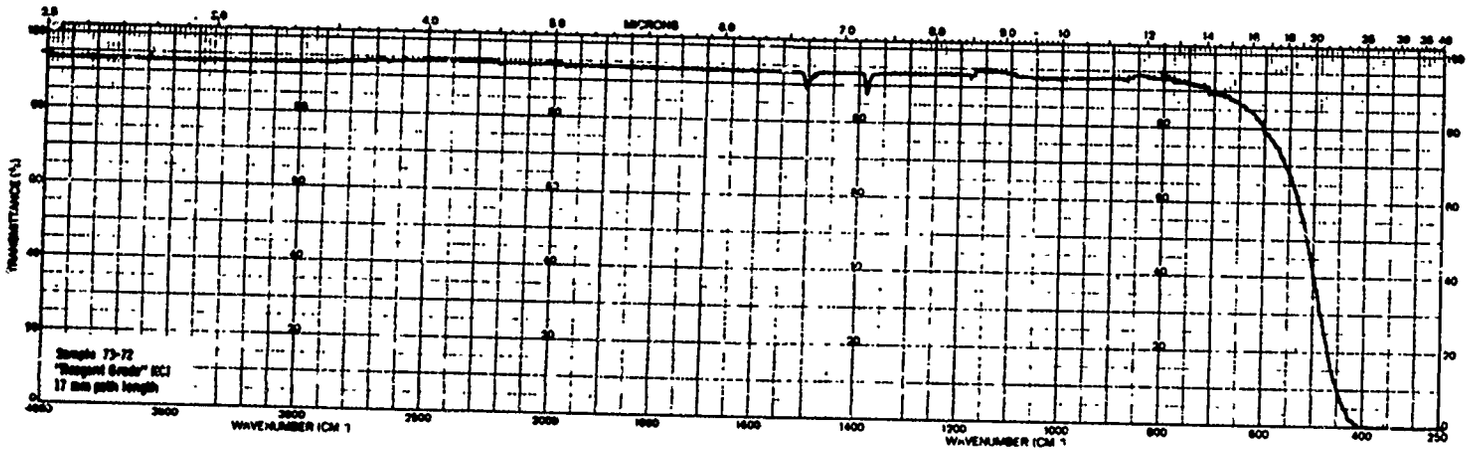

Fig. IV-64 Infrared Transmission Spectrum of Crystal 73-72. "Reagent grade" starting material.

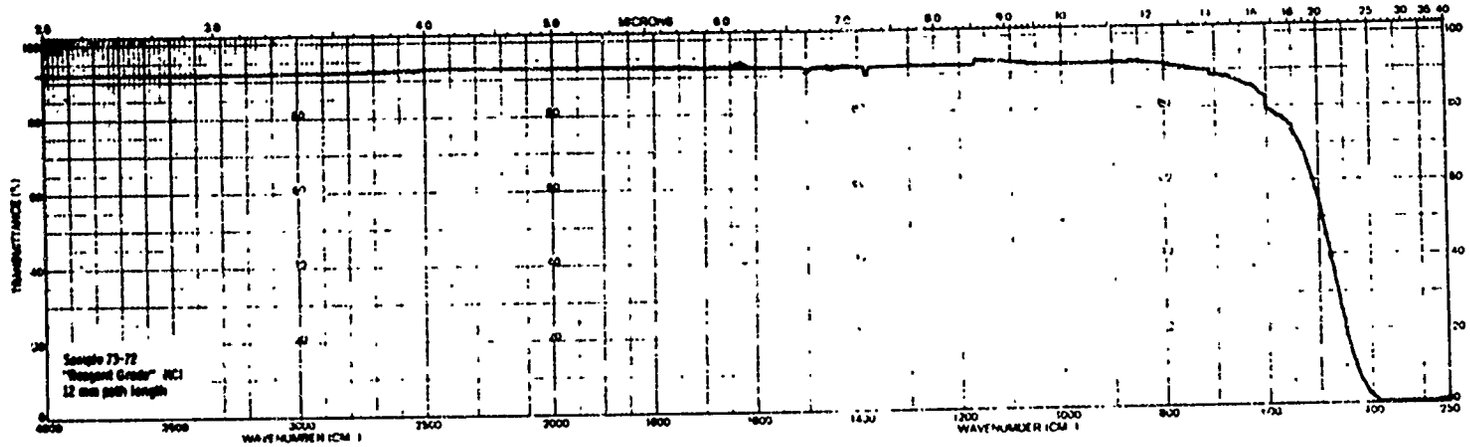

Fig. IV-65 Infrared Transmission Spectrum of Crystal 73-72. "Reagent grade" starting material.

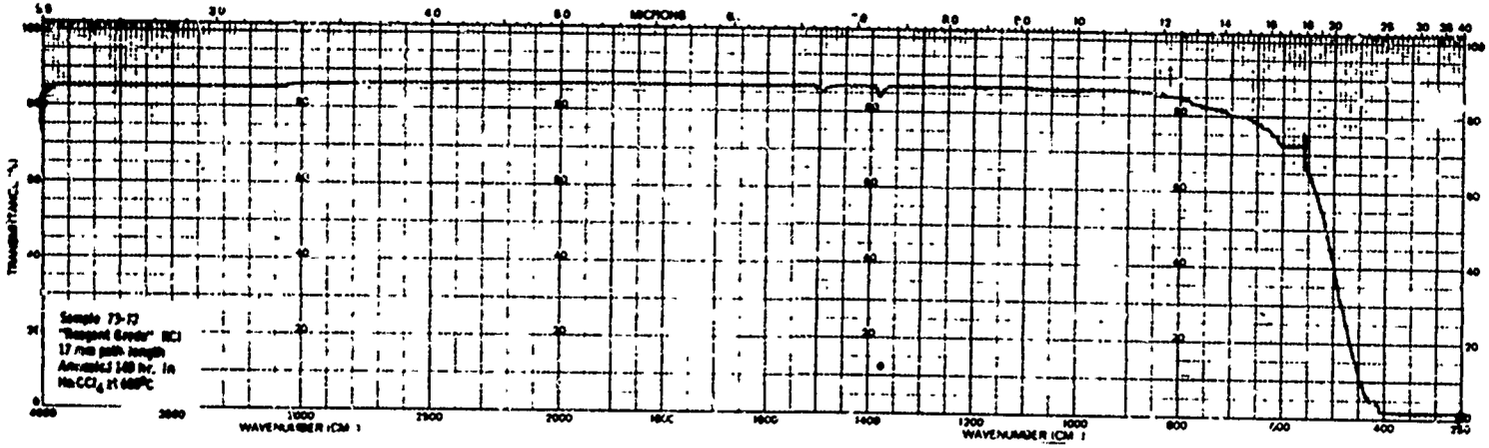

Fig. IV-66 Infrared Transmission Spectrum of Crystal 73-72. "Reagent grade" starting material. Sample annealed 140 hr in He: CCl_4 at 650°C.

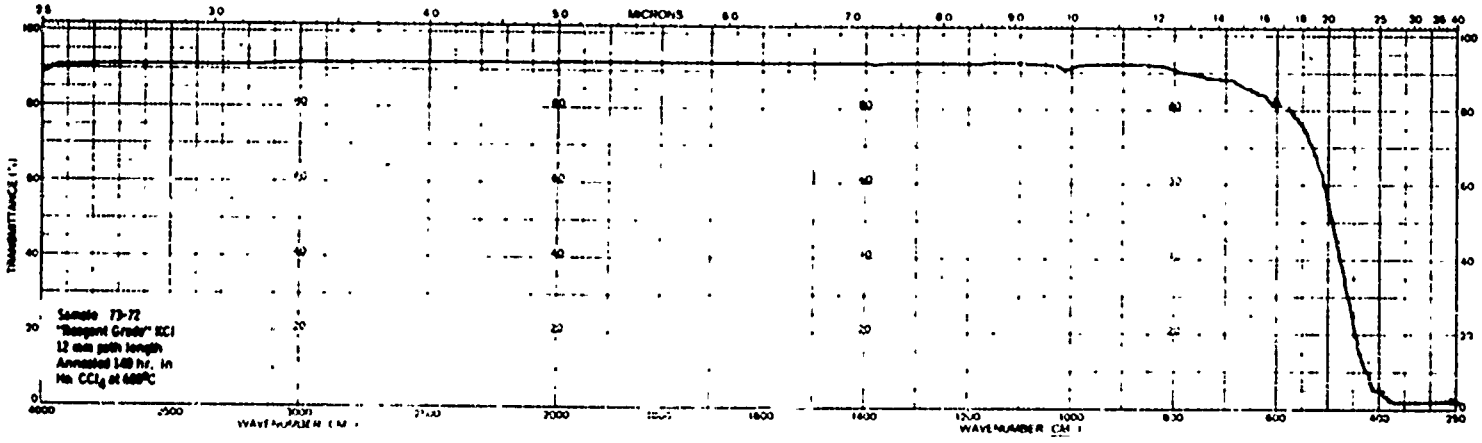

Fig. IV-67 Infrared Transmission Spectrum of Crystal 73-72. "Reagent grade" starting material. Sample annealed 140 hr in He:CCl_4 at 680°C.

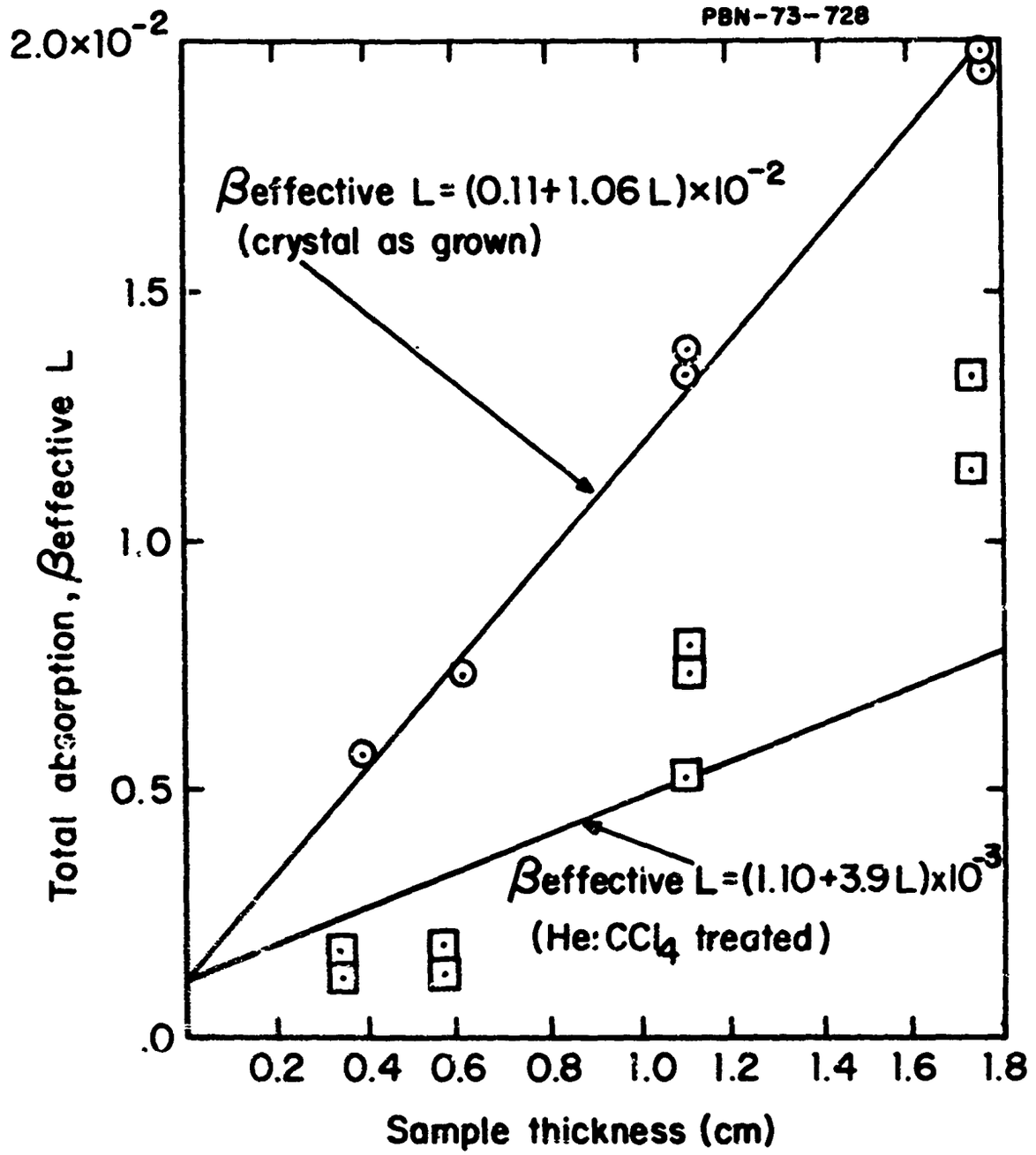

Fig. IV-68 10.6 μm Optical Absorption vs Sample Length for Crystal 73-72. "Reagent grade" starting material. ⊙ as grown crystal ◘ samples annealed 140 hr in He:CCl_4 at 680°C.

Three samples of cast material were also treated. Figure IV-69 shows the IR transmission spectrum for a cast sample (NPC-4) treated for 70 hours at 650°C in the He:CCl_4 atmosphere. Comparing it with the spectrum for the untreated sample (Fig. IV-45), it is possible to see that several things have occurred. The $SO_4^=$ peaks at 1000 to 1200 cm^{-1} have become more defined and show an increase in intensity. The $CO_3^=$ bands at 1400-1500 cm^{-1} have also increased in intensity (noting the difference in path length). Most importantly, the broad band centered at about 10 μm has been reduced significantly.

It was clear from these two experiments that competing reactions were occurring at these high temperatures. At present, we think that the broadband at 10 μm may be due to Cl-O bonds (of which many exist) which may result in no defined structure or IR peaks. At the high temperatures of the reactive treatment, various oxygen-competing reactions may be taking place between the S, C and Cl, resulting in a possible shift of oxygen from the broadband at 10 μm to the $SO_4^=$ or $CO_3^=$ bands.

The necessity of using CCl_4 for these reactions was studied by annealing at the high temperatures in pure helium. Two runs were made. Fig. IV-70 shows the IR transmission spectrum for sample NPC-1 treated for 140 hours at 680°C in pure helium. Comparing it to the corresponding spectrum of the untreated sample (Fig. IV-43), one would conclude no significant change. However, this was not the case for another sample, NPC-3. Figure IV-71 shows the IR transmission spectrum for this sample treated for 140 hours at 680°C in pure helium. Comparing it to the untreated sample, (Fig. IV-44) indicates a decrease in intensity of the $SO_4^=$ peaks while new peaks in the 800 to 1000 cm^{-1} region have appeared. Note however, that sample NPC-3 initially contained more $SO_4^=$ than sample NPC-1.

The results of the high temperature heat treatments have shown the possible shifting of oxygen (the likely cause of 10.6 μm absorption) between competing oxygen components. It is not yet clearly understood what conditions promote such a shift or what role impurities play.

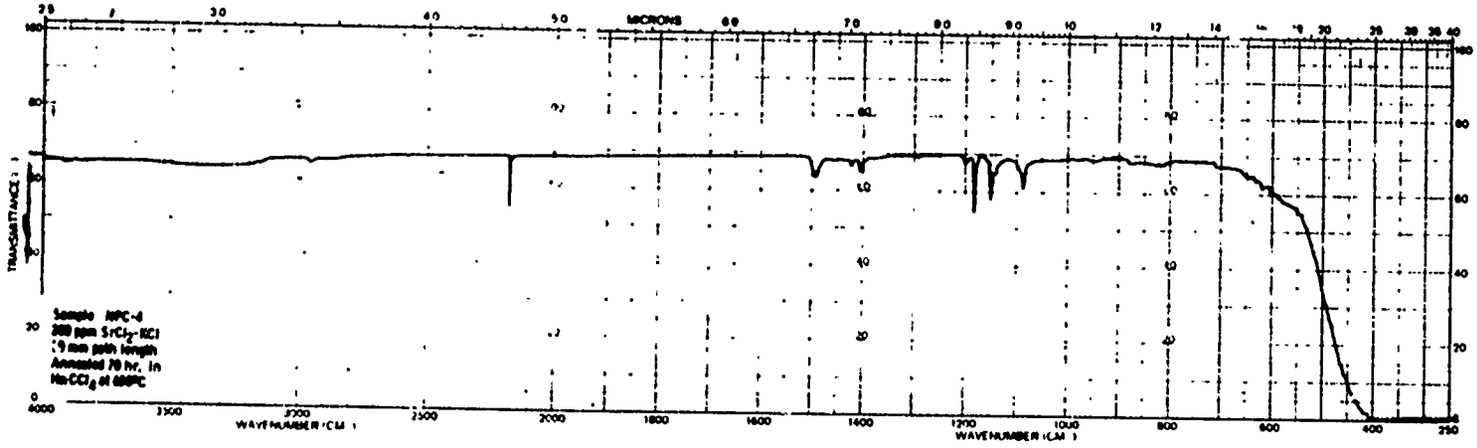

Fig. IV-69 Infrared Transmission Spectrum of Casting NPC-4. Sample annealed 70 hours in He:CCl_4 at 650°C.

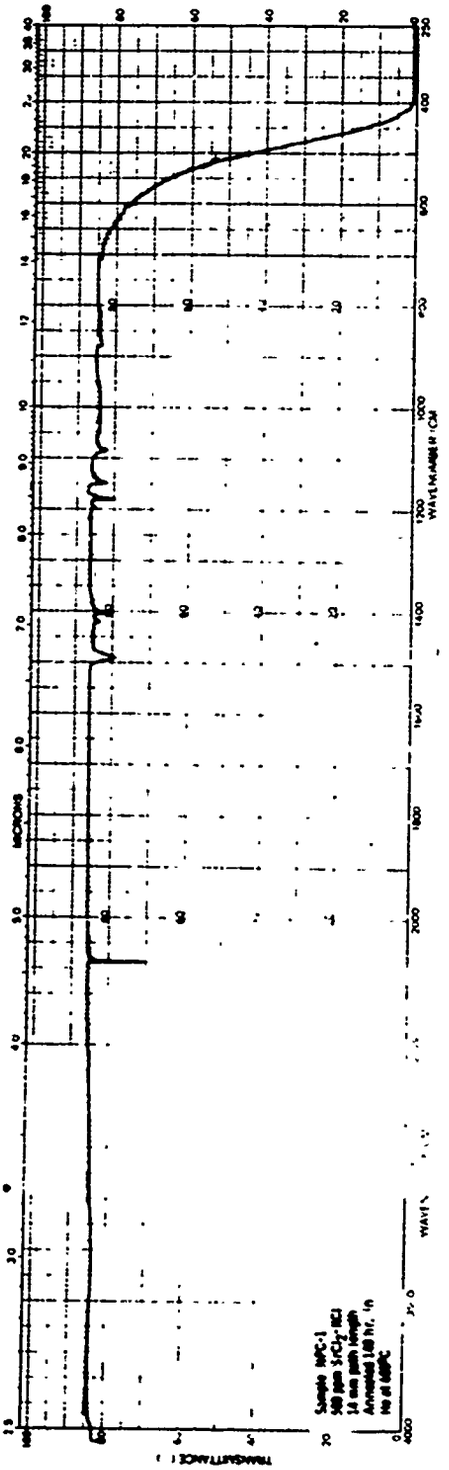

Fig. IV-70 Infrared Transmission Spectrum of Casting NPC-1. Sample annealed 140 hours in He at 680°C.

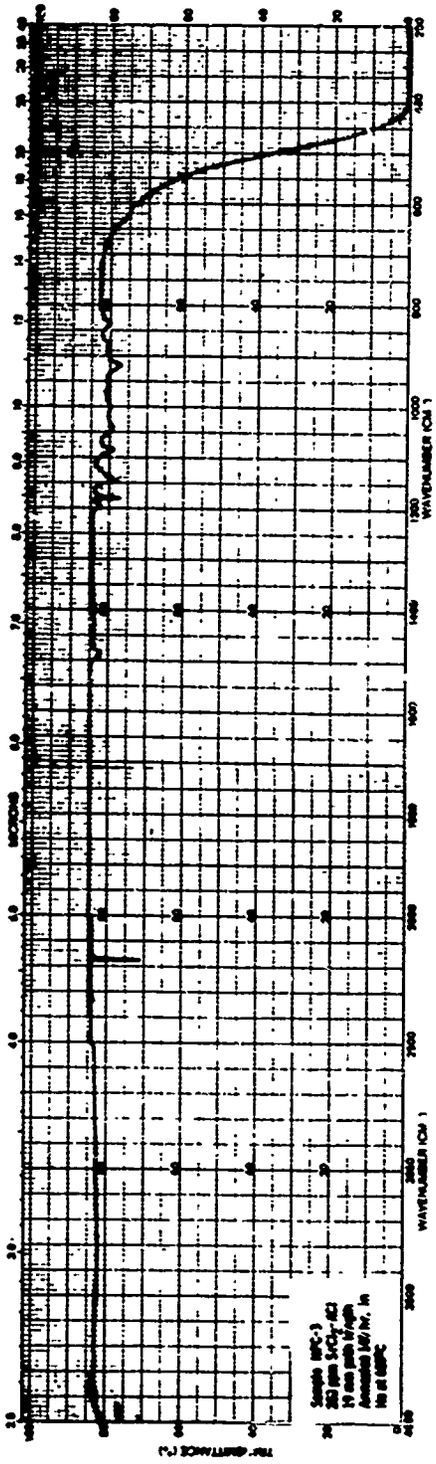

Fig. IV-71 Infrared Transmission Spectrum of Casting NPC-3. Sample annealed 140 hours in He at 680°C.

I. Protective Films

This effort was carried out during the first three quarters of the program. Apart from two exploratory evaporations of cerium fluoride (CeF_3) that resulted in discontinuous films due to microcracks, all evaporations have used As_2S_3 as the film material and KCl as the substrate. The object was to determine the 10.6 μm loss coefficient in As_2S_3 films and to determine its dependence on evaporation and substrate conditions. All evaporations were carried out in an Edwards system (Fig. IV-72) housed in a clean room facility.

Most of the calorimetric measurements on our films were made on a system using a 5-10 watt laser in a fixed source-sample configurations. In the course of our study however, a new system (Fig. IV-73) was built with both a higher power (50 watt) source and a more flexible vacuum chamber and sample mounting system that allows the sample to be moved through the 10.6 μm laser beam, whose position can be determined by an overlapping visible laser beam. These improvements were designed both to increase the system sensitivity, and to increase the relative accuracy of measurements made on different samples. The data on bulk loss in our polycrystalline halide materials were also obtained using this system.

Calorimetric data were reduced by computer and interpreted using the relationship valid for low loss, thick or resonant samples, namely

$$P_{abs}/P_{trans} = \beta L \frac{1+\eta^2}{2\eta}$$

where P_{abs} is the laser power absorbed in a sample of length L with loss coefficient $\beta\,cm^{-1}$ and refractive index η. P_{trans} is the transmitted power. This formula is adequate for measurement on coated substrates provided that the coating loss dominates, and provided that the film faces away from the laser source. A small correction should be made for nonresonant films, but in our experimental case, this would be only a few percent for films less than $\lambda/2$, and progressively less for thicker films.

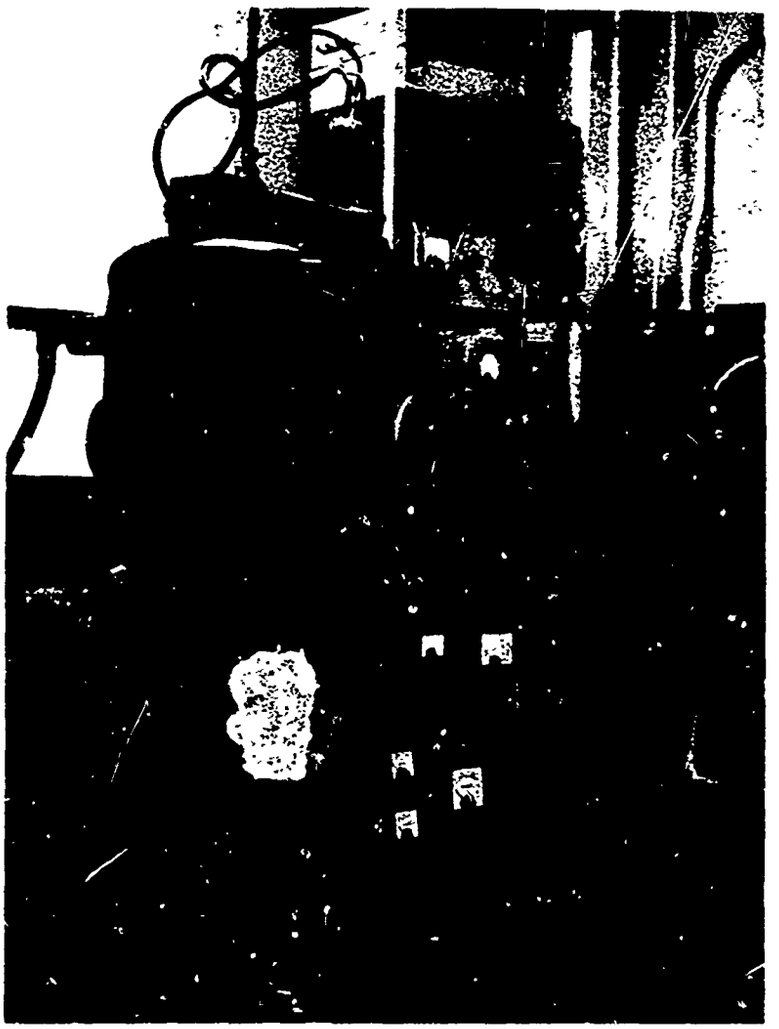

Fig. IV-72 Edward Vacuum Station used for As_2S_3 Thin Film Evaporation.

Fig. IV-73 Laser Calorimeter with a 20- to 50-watt Laser Source and X-Y Sample Translation.

In order to minimize the surface preparation steps likely to lead to contamination we have used cleaved substrates of single-crystal KCl for most of these evaporations. While simple, this procedure has the drawback of variability in the density of cleavage steps across the surface. These steps lead to the possibility of surface scatter, particularly when the surface is replicated by a high-index film. This factor introduces some ambiguity in the interpretation of calorimetric loss measurements at 10.6 μm, particularly in samples whose bulk absorption coefficient is low. The substrate material was usually an Optovac crystal with a bulk loss coefficient of approximately 3×10^{-3} cm^{-1}.

Our evaporations of CeF_3 were carried out using Poly Research CeF_3 powder as the source. The charge was outgassed at 10^{-5} torr prior to the evaporation which took place with background pressures between 0.8 and 2×10^{-5} torr. The KCl substrate temperature rose to 115°C during evaporation due to heating from the source enclosure. A 5 minute evaporation produced a 2 μm thick film. On subsequent examination, this film showed excessive scatter at visible wavelengths, and an apparent 0.01 loss factor at 10.6 μm. The latter may have been largely due to lateral scatter and subsequent absorption. The scatter was produced by intergranular cracks in the film indicating a high-stress deposit.

In evaporation of As_2S_3, our basic practice was to use Poly Research broken glass as a source. This was outgassed for 6 hours at pressures between 4×10^{-6} and 10^{-5} torr. The KCl substrate was heated for 1 hour at 150°C prior to evaporation. The background pressure immediately before evaporation was usually 8×10^{-7} torr. During evaporation the pressure rose to between 1 and 6×10^{-5} torr depending on the evaporation rate. Evaporation times have ranged from 10 to 35 minutes. Originally, the substrate temperature varied from 35°C to 67°C during evaporation. In the latter case, the sample became heated during the long source bakeout and the film was unusually thin, and rough in texture. It appeared that re-evaporation had taken place, similar to the effect noted in the work at the University of Arizona. Accordingly, a water-cooled stage was built to maintain substrate temperature during evaporation at or near 35°C. As for film adherence, a scotch-tape test on As_2S_3 films on KCl crystals showed film degradation at the substrate edge due to fracture of the KCl, but no film removal as such.

The first experiments were made by completely covering individual substrates to a film thickness of approximately 2 μm. These films showed loss factors near 0.005. However, variations in apparent loss factor for different substrates made the accurate measurement of film loss difficult. To improve this technique, we made two-step depositions on a single substrate (Fig. IV-74) leaving part of the material uncoated. Calorimetric loss measurements on the substrate prior to evaporation showed no significant difference in apparent loss factor in the three areas. This technique gave some improvements in consistency, and the evaporation of much thicker films up to 10 μm permitted us more dependable measurement of film loss coefficient. Film thickness has been measured both mechanically, by crystal monitors, and by observing interference fringes in the infrared (Fig. IV-75). These two measurements gave inconsistent results, but we consider the interferometric technique the more reliable. In any case, the interferometric measurement is the one most appropriate for use in a multilayer film design because the more important length is the optical path itself. Typical bulk absorption coefficients ranged from near $7cm^{-1}$ to $3cm^{-1}$ (Figs. IV-76 and IV-77). This is to be compared to the published value near 1.4 cm^{-1} measured in bulk glass.

In a related experiment, we prepared an As_2S_3 evaporation source following a procedure used at the University of Arizona, namely the heating of the original glass in air at 400°C until approximately half of the material has distilled off. Preliminary measurements of loss in films evaporated with this pretreated material, however, did not seem to differ from those of films made from the original source material, although difficulties with the calorimeter system during these measurements may have influenced the data. A second attempt was made to establish the usefulness of predistillation by setting up a two-source evaporation and by making a two-thickness evaporation on each of two KCl substrates. The data (Fig. IV-78) are internally inconsistent, but the most likely interpretation is that the predistillation has no effect, and that the loss coefficient of each film was near 2.6 cm^{-1}.

The final experiments on As_2S_3 coatings used a polished substrate and a source of untreated glass. A movable shutter slot above the substrate was displaced progressively during evaporation, and resulted in the formation of four different thicknesses of film. The data (Fig. IV-79) shows a satisfactory consistency, although a repeat of the two measurements after a three day interval indicated an increase insurface loss. The corresponding bulk loss factor is 1.5 cm^{-1}, close to the intrinsic bulk value.

PBN-72-960

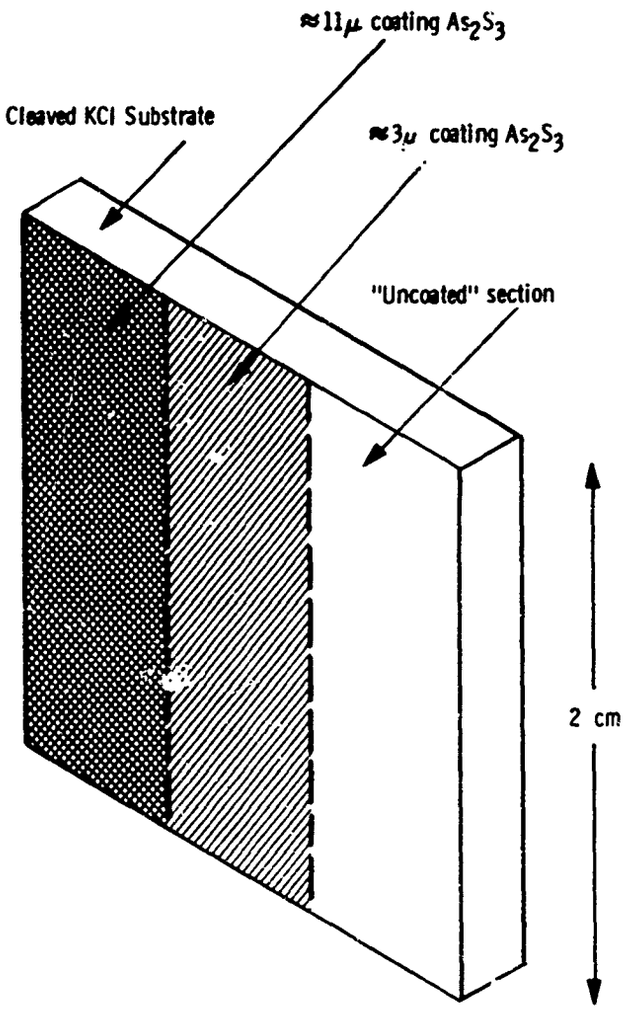

Fig. IV-74 Calorimeter Sample Configuration with Multiple Evaporations.

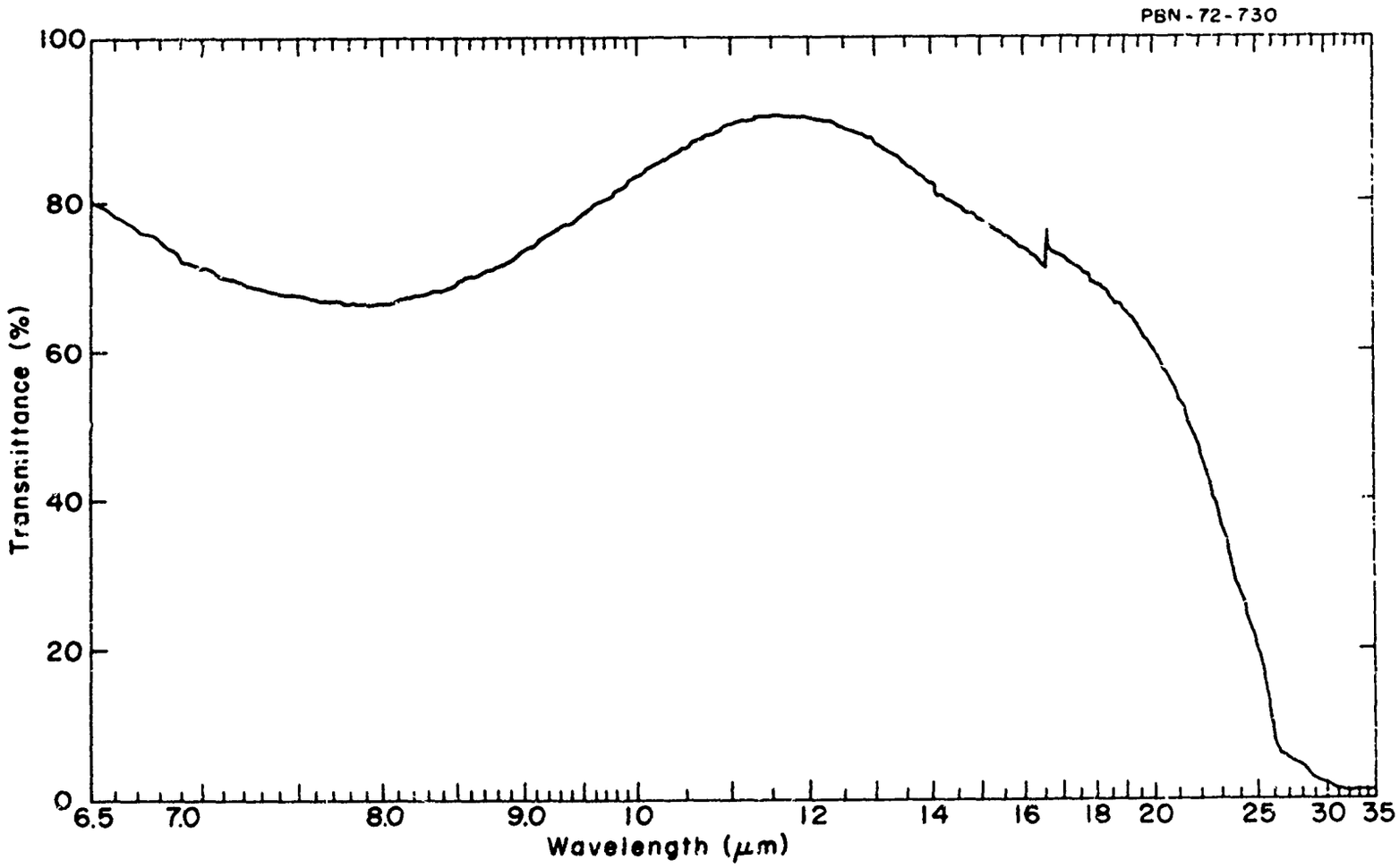

Fig. IV-75. Transmission Spectrum of KCl Sample with a Single-Sided As_2S_3 Coating. Note interference fringe used in thickness determination.

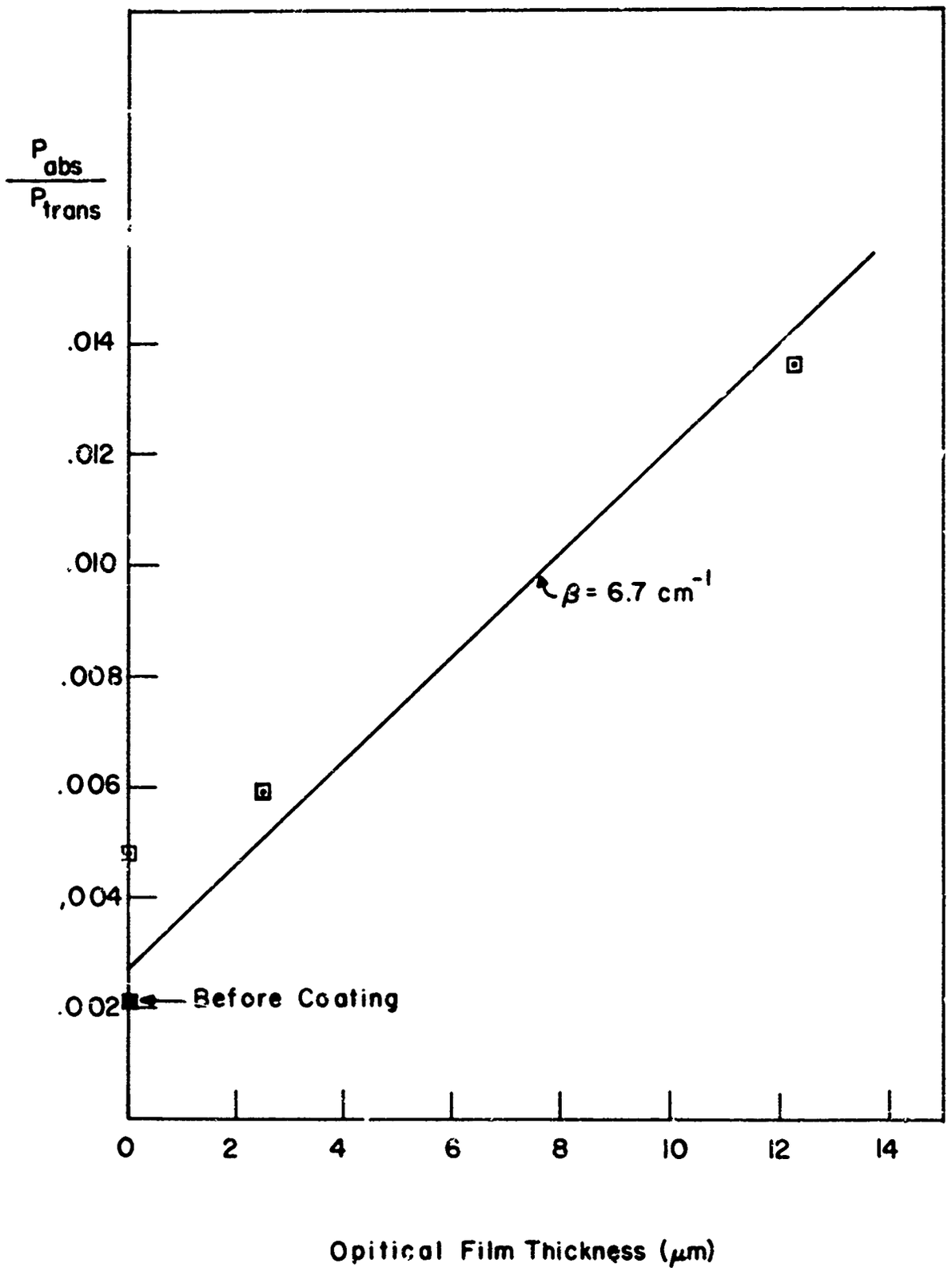

Fig. IV-76 Fractional Power Absorption versus Film Thickness for an Early As_2S_3 Film on Cleaved KCl.

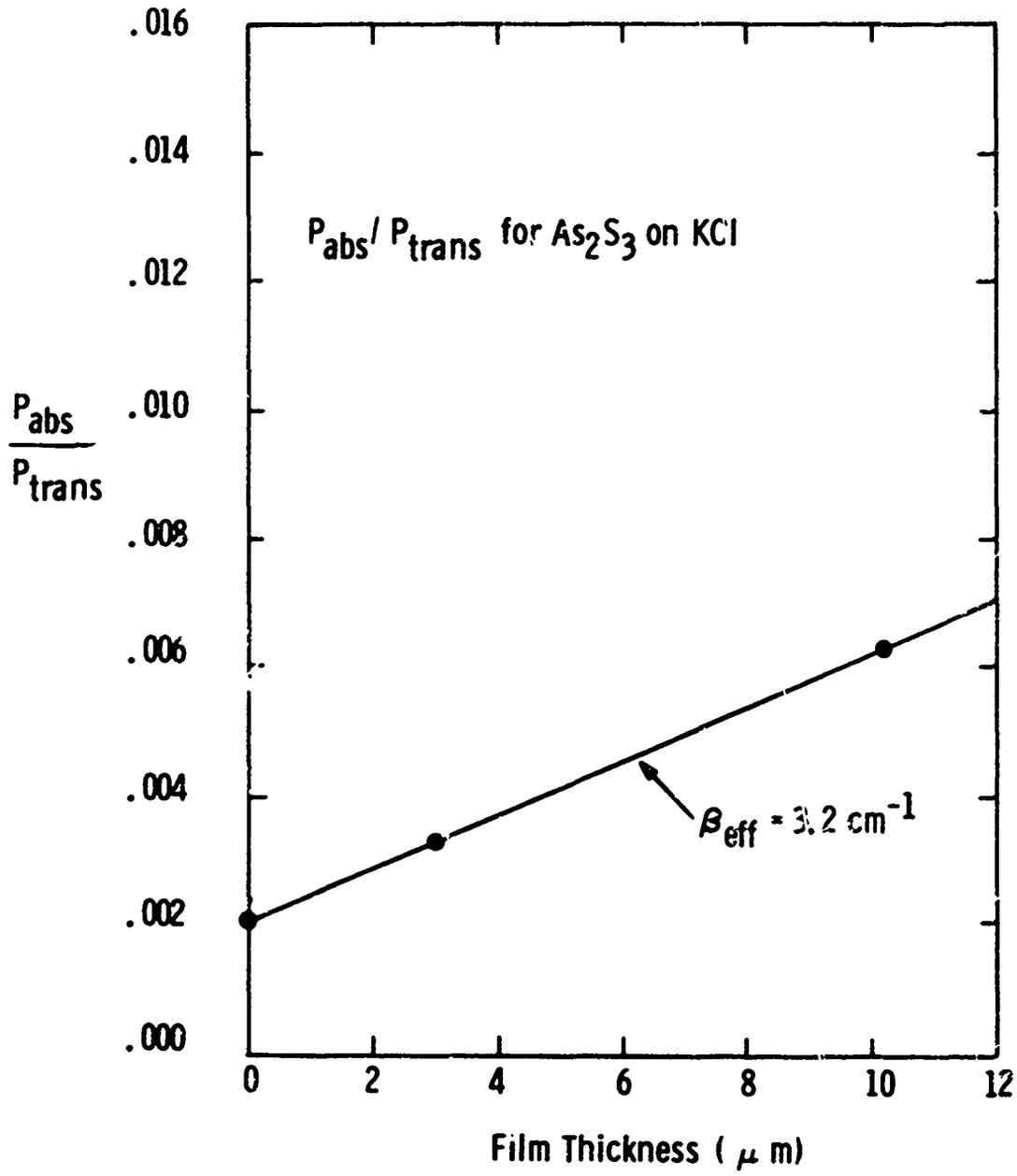

Fig. IV-77 Optical Absorption of Evaporated As_2S_3 Films of Varying Thickness Deposited During a Single Evaporation.

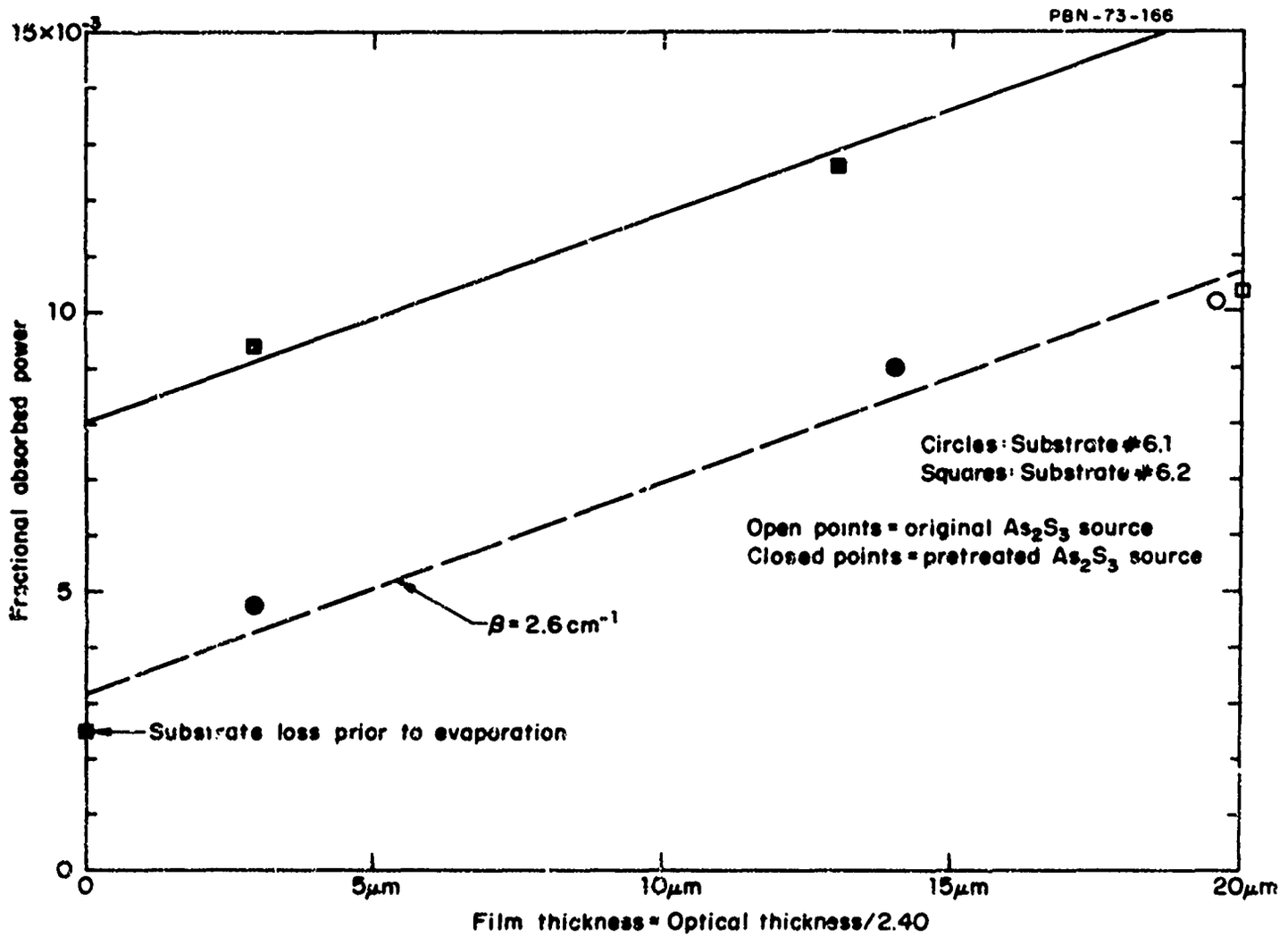

Fig. IV-78 Experimental Data for Loss in Films Made for Original As_2S_3 Glass and from Pretreated glass Sources.

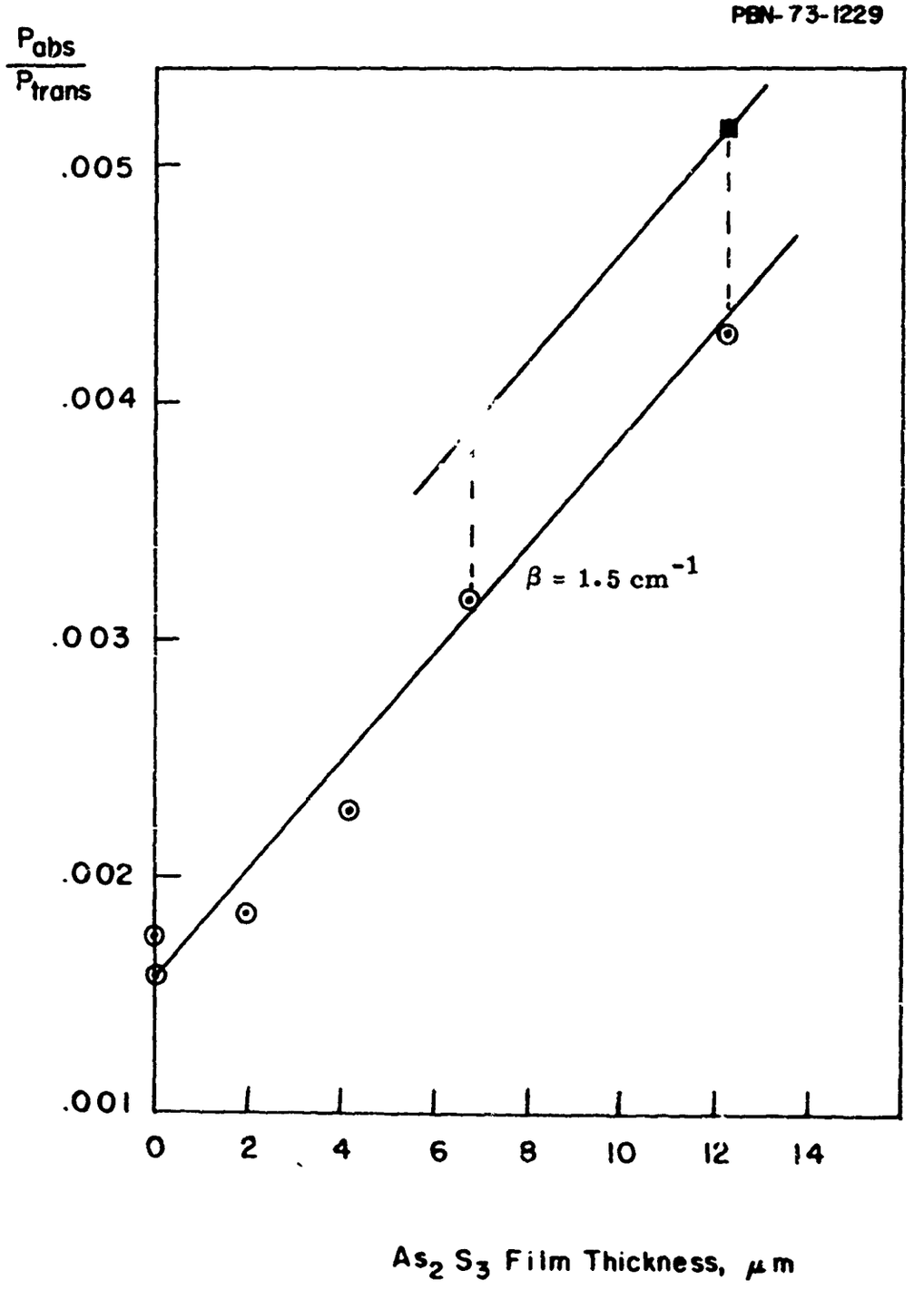

Fig. IV-79 Fractional Power Absorption versus Film Thickness for and As_2S_3 Film on Polished KCl. Solid points indicate increase of surface loss with time.

To summarize, we observed a progressive decrease in the apparent absorption coefficient of the evaporated films, but one that depended for the most part on repetition rather than an explicit change of technique. It is probably significant, however, that the best film was deposited on a polished substrate. In any event the film loss coefficients approached the normal value in bulk samples, and were certainly low enough to be incorporated in a double layer design with a loss factor less than 10^{-3}.

As the AFWL-funded program at Hughes Aircraft Co. began producing more extensive data on As_2S_3/ThF_2 films and other related combinations, further efforts in this area were discontinued in favor of a concentration of our resources on the development of the halide materials themselves. It is important to emphasize, however, that low-loss, high-quality As_2S_3 films were produced with relatively little effort. This finding is consistent with the original observations on the relatively high resistance of As_2S_3 films to laser damage. While commercial coating houses profess a dislike for the use of As_2S_3 films in wideband infrared coatings, it would seem appropriate for laser coating manufacturers to review this situation.

5. SUMMARY AND CONCLUSIONS

A. Alloy Systems

Essentially three alloy types have been examined, namely the KCl-KBr, KCl-KI and the KCl-$SrCl_2$ systems. The major effort has been devoted to the $SrCl_2$-KCl system. Work on both the KCl-KBr and KCl-KI systems was held to a minimum since these alloys were extremely difficult to handle. They both exhibited very low thermal conductivity and hardness no higher than the KCl-$SrCl_2$ alloys.

B. Solid Solution Strengthening in the KCl-$SrCl_2$ System

The hardness and yield strength of KCl-$SrCl_2$ solid solutions were determined on single crystals up to almost 2000 ppm actual $SrCl_2$ content. With these concentrations, a factor of 2.5 increase in hardness was achieved and roughly a factor of 30 in yield strength. With appropriate heat treatment, yield strengths of 9000 psi were obtained, a value which is the highest reported to date in a KCl-based system. Actual $SrCl_2$ contents were measured using X-ray fluorescence and the segregation coefficient of $SrCl_2$ in KCl crystals was determined.

C. Precipitation in the KCl-$SrCl_2$ System

1. Mechanical properties

The effects of heat treatment and the attendant precipitation in KCl-$SrCl_2$ alloys were investigated. The yield strength of alloys with less than about 600 ppm at $SrCl_2$ in solution is temperature insensitive. At higher $SrCl_2$ contents, precipitation occurs at temperatures between 200° and 425°C with a decrease in yield strength. Finally, heat treatment of the 1762 ppm $SrCl_2$ alloy at 500°C produces the highest strength in a KCl-based system to date with a yield stress above 9000 psi. Although precipitation leads to a lower yield stress in this system, ductility increases with precipitation and the yield stress can be maintained in the 4500-5000 psi range with little difficulty.

2. Optical properties

Another important goal of the program was to investigate the effect of optical scattering from precipitates on the IR transmission or absorption coefficient of 10.6μm. It was postulated that if the precipitate particle size could be kept small compared to the wavelength, the scattering loss would be low. The data obtained indicate that the actual precipitate particles do not present a problem for 10.6μm scatter, although there may very well be other larger scatter centers introduced during fabrication that will be important at 10.6μm.

D. Starting Materials and Purification

10.6μm absorption coefficients have been shown to be strongly dependent on starting material. By growing single crystals with high-purity KCl, absorption coefficients of 6×10^{-4} cm^{-1} have been obtained. Initial experiments indicated that the addition of $SrCl_2$ did not degrade the optical absorption. Recently we have obtained an absorption coefficient as low as 3×10^{-4} on a heavily-doped (one percent $SrCl_2$-doped) alloy. This is to be compared to the intrinsic KCl loss of approximately 1×10^{-4} cm^{-1}

E. Casting KCl Alloys

1. Casting facilities

Initially, two-inch diameter, directionally-solidified castings of pure and $SrCl_2$-doped KCl were successfully prepared, pore and crack free. A larger, eight inch diameter capability furnace was designed and delivered at the end of the first year of this program. This new furnace allowed us to obtain better control over directional solidification of much larger ingots. These larger ingots permitted evaluation of microstructure, compositional uniformity and mechanical and optical properties.

2. Optical properties

Optical evaluation has not been completed, but using high-purity starting

material we have obtained 10.6μm absorption coefficients in the 7×10^{-4} cm^{-1} range. Also, the IR transmission of a polycrystalline casting shows none of the characteristic absorption bands associated with carbonate, sulphate, etc. which are usually observed when lower purity, "reagent grade" starting material is used. This is an important result in that contamination is not introduced during casting by the furnace, graphite crucible or mold. It also strongly suggests that with reasonably clean material, grain boundaries in castings do not contribute to 10.6μm absorption.

3. Mechanical properties

Mechanical strengths of as-cast samples with large grains (average sizes of several hundred micrometers) and low $SrCl_2$ doping have exceeded 2000 psi, a value comparable to the yield strengths of single crystals with the same strontium content.

4. Crystallographic texture

The crystallographic orientation in the large, essentially in-situ, castings has been found to have strong <100> texture. That is, the <100> axes of the columnar grains lie parallel to the freezing direction. This is in contrast to a strong <110> texture found in poured, two inch diameter castings.

5. Alloying and grain size

A large decrease in as-cast grain size was obtained with increasing $SrCl_2$ for poured castings.

6. Residual strain

The most severe remaining problem with the cast alloys is that of the high residual stresses found in the ingots. These stresses are high enough to cause cracking in some cases, and have led to the development of cracking during subsequent cutting and polishing in others. These stresses

are doubtlessly introduced during the cooling cycle due to temperature gradients within the ingot while some regions are more plastic than others. We are confident that a cooling or annealing cycle can be found which will eliminate residual stress.

F. Hot Forging

The technique of hot forging single crystals of both pure and doped KCl has been investigated. Our primary interest in hot forging has been to use it as a secondary fabrication process to refine the grain size of cast polycrystalline materials. Grain sizes below ten micrometers have been achieved in pure KCl single crystals with yield strengths on the order of 3000 psi. An important point is that cast material has been successfully hot forged.

G. Protective Films

Amorphous films of arsenic trisulphide were successfully deposited onto KCl single crystal substrates. A film on a polished substrate exhibited a loss coefficient at 10.6μm of 1.5 cm^{-1}, very close to the level found in bulk samples of As_2S_3 glass.

H. Etching Studies

An etching technique was developed which was used to delineate dislocations produced during polishing and at grain boundaries during cooling. This etching technique is useful for examining the sources of residual stress in the cast alloys.

I. Reactive Gas Processing

Heat treatment of both single and polycrystalline KCl in a reactive gas (CCl_4) atmosphere has been shown to affect the 10.6μm absorption. However, the effect of the heat treatment is modified by the presence of various complex anion groups such as sulphates and carbonates.

6. ACKNOWLEDGMENTS

B. Bryant assisted with the castings, prepared samples and made property measurements. C. Snider and P. Roman made the strength measurements. C. Snider and W. Finch performed hot forgings. The calorimetric absorption coefficient measurements were made by J. DeCastro under the direction of Dr. T. Kohane. X-ray fluorescence data were supplied by D. Howe. Dr. Otto Guentert provided the preferred orientation analysis. F. Taylor was responsible for the single crystal growth.

7. REFERENCES

1. F.A. Horrigan, R.I. Rudko, Final Report, "Materials for High-Power CO_2 Lasers, "Contract No. DAAH01-69-C-0038, Sept. 1969, AD693311.

2. F.A. Horrigan, T. Deutsch, Final Report, "Research in Optical Materials and Structures for High-Power Lasers, "Contract No. DAAH01-70-C-1251, Sept. 1971, AD888788L.

3. F.A. Horrigan and T.F. Deutsch, Proc. Conf. on High Power IR Laser Window Materials, AFCRL Special Report No. 127 (1972).

4. M. Sparks, The Rand Corp., WN-7243-PR, April 1971.

5. M. Sparks, The Rand Corp., WN-7296-PR, April 1971.

6. M. Suszynska and J. Pozniak, "Effect of Ionizing Radiation and Sr^{2+} Concentration on Hardening of KCl Crystals (II), "Phys. Stat. Sol. (A), 6, 79 (1971).

7. R.L. Fleischer, "Solution Hardening by Tetragonal Distortions: Application to Irradiation Hardening in F.C.C. Crystals, "Acta. Met. 10, 835 (1962).

8. P.L. Pratt, R. Chang and C. W.A. Newey, "Effect of Divalent Metal Impurity Distribution, Quenching Rate and Annealing Temperature on Flow Stress in Ionic Crystals (NaCl, LiF), "Appl. Phys. Lett. 3, 83 (1963).

9. R.G. Wolfson, W. Kobes and M.E. Fine, "Precipitation in NaCl-KCl Mixed Crystals," J. Appl. Phys. 37, 704 (1966).

10. R.J. Stokes and C.H. Li, "The Sodium Chloride-Silver Chloride Alloy System," Acta. Met. 10, 535 (1962).

11. E.M. Levin, C.R. Robbins and H.F. McMurdie, Phase Diagrams for Ceramists, (The Am. Ceram. Soc., Columbus), 1964.

12. S.K. Dickinson, Jr., "Ionic, Covalent, and Metallic Radii of the Chemical Elements, "Report No. AFCRL-70-0727, Dec. 1, 1970

13. J.S. Dryden, S. Morimoto and J.S. Cook, "The Hardness of Alkali Halide Crystals Containing Divalent Ion Impurities, "Phil. Mag. 12, 379 (1965.

REFERENCES (Cont)

14. C.S. Sahagian and C.A. Pitha, "Compendium on High Power Infrared Laser Window Materials," Report No. AFCRL-72-0170, Special Report No. 135, March 9, 1972.

15. T.L. Lukmanova and Ya. E. Vil'nyanskii, "Solubility of Some Gases in Molten Metallic Chlorides, "Izv. Vyssh. Ucheb. Zaved., Khim. Tekhnol. 9, (4) 537 (1966).

16. D. Bratland, et al., "Solubility of Carbon Dioxide in Molten Alkali Halides," Acta. Chem. Scand. 20, 1811 (1966).

17. C.T. Butler, et al., "Growth and Evaluation of High-Purity KCl Crystals," J. Chem. Phys. 45, 968 (1967).

18. P.A. Young, "Thin Films for Use on NaCl Components of CO_2 Lasers," Thin Solid Films 6, 423 (1970).

19. J.T. Cox and G. Hass, "Antireflection Coatings for Optical and Infrared Optical Materials," Physics of Thin Films 2, 239, Hass and Thun, eds., Academic Press, New York, (1964).

20. P.H. Berning, "Theory and Calculations of Optical Thin Films," Physics of Thin Films, 1, 69, G.Hass, ed., Academic Press, N.Y., (1963).

21. P.H. Berning, "Use of Equivalent Films in the Design of Infrared Multilayer Antireflection Coatings," J. Opt. Sci. Am. 52, 431 (1962).

22. J.S. Loomis, "Antireflection Coating Designs for 10.6 μm Window Materials," Tech. Rept. AFWL-TR-72-180 Jan. (1973).

23. M. Braunstein, A.I. Braunstein, J.E. Rudisill. "Optical Coatings for High Energy I.R. Laser Windows," AFCRL Spec. Rpt. #162 Jan 1973.

24. "High Energy Laser Windows," Semiannual Report No. 1, ARPA Order 2031, Naval Research Laboratory, June 30, 1972.

25. T.F. Deutsch and R.I. Rudko, "Research in Optical Materials and Structures for High-Power Lasers," Final Report, ARPA Order No. 1180, January 1973.

26. G.Y. Chin, et al., "Strengthening of Alkali Halides by Divalent Ion Additions," J. Am. Ceram. Soc. 53, (7), 369 (1973).

27. T. Deutsch, private communication.

28. M. Kerker, "The Scattering of Light," (Academic Press, N.Y.) (1969).

29. W. Heller, "Theoretical Investigations on the Light Scattering of Spheres. XV The Wavelength Exponents at Small α Values," J. Chem. Phys, 40, (9) 2700 (1964).

30. P.R. Moran, "Dislocation Etch Techniques for Some Alkali Halide Crystals," J. Appl. Phys. 29, 1768, (1958).

31. Glen A. Slack, "Thermal Conductivity of Potassium Chloride Crystals Containing Calcium," Phys. Rev. 105, 834 (1957).

☆ U S GOVERNMENT PRINTING OFFICE · 1974-704-296/6E